(6)

THERMOSTRUCTURAL RESPONSE OF ALUMINUM ANNULI.

Physics International Company
2700 Merced Street
San Leandro, California 94577

(12) 12 p.

(12) 162 P.

(11) Mar[redacted]78 (10) V. Buck, J. Shea

(9) Final Report, [redacted] Mar[redacted]76—Sep[redacted]77,

(14) PIFR-930-2 (15) CONTRACT No DNA 001-76-C-0246

APPROVED FOR PUBLIC RELEASE;
DISTRIBUTION UNLIMITED.

THIS WORK SPONSORED BY THE DEFENSE NUCLEAR AGENCY
UNDER RDT&E RMSS CODE B342076464 N99QAXAA12115 H2590D.

(16) (17) A121

Prepared for
Director
DEFENSE NUCLEAR AGENCY
Washington, D. C. 20305

Destroy this report when it is no longer needed. Do not return to sender.

UNCLASSIFIED

SECURITY CLASSIFICATION OF THIS PAGE (When Data Entered)

REPORT DOCUMENTATION PAGE		READ INSTRUCTIONS BEFORE COMPLETING FORM
1. REPORT NUMBER DNA 4480F	2. GOVT ACCESSION NO.	3. RECIPIENT'S CATALOG NUMBER
4. TITLE (and Subtitle) THERMOSTRUCTURAL RESPONSE OF ALUMINUM ANNULI		5. TYPE OF REPORT & PERIOD COVERED Final Report for Period Mar 76 - Sep 77 6. PERFORMING ORG. REPORT NUMBER PIFR-930-2
7. AUTHOR(s) V. Buck and J. Shea		8. CONTRACT OR GRANT NUMBER(s) DNA 001-76-C-0246
9. PERFORMING ORGANIZATION NAME AND ADDRESS Physics International Company 2700 Merced Street San Leandro, California 94577		10. PROGRAM ELEMENT, PROJECT, TASK AREA & WORK UNIT NUMBERS Subtask N99QAXAA121-15
11. CONTROLLING OFFICE NAME AND ADDRESS Director Defense Nuclear Agency Washington, D.C. 20305		12. REPORT DATE March 1978 13. NUMBER OF PAGES 162
14. MONITORING AGENCY NAME & ADDRESS(if different from Controlling Office)		15. SECURITY CLASS (of this report) UNCLASSIFIED 15a. DECLASSIFICATION/DOWNGRADING SCHEDULE

16. DISTRIBUTION STATEMENT (of this Report)

Approved for public release; distribution unlimited.

17. DISTRIBUTION STATEMENT (of the abstract entered in Block 20, if different from Report)

18. SUPPLEMENTARY NOTES

This work sponsored by the Defense Nuclear Agency under RDT&E RMSS Code B342076464 N99QAXAA12115 H2590D.

19. KEY WORDS (Continue on reverse side if necessary and identify by block number)

Thermostructural Response
Radiation Heating
Electron Beams
Aluminum Annuli
Strain Guage
Quartz Guage

20. ABSTRACT (Continue on reverse side if necessary and identify by block number)

The thermostructural response of aluminum annuli subjected to sudden radiation heating was experimentally investigated using pulsed electron beams. The DNA OWL II generator, operating at a nominal mean voltage of 1.0 MeV, provided the radiation environment. Transport of the electron beam from the diode to the target was achieved using a longitudinal magnetic field. The aluminum annuli had a 22.9-cm (9 inch) inner diameter, a 27.9-cm

DD FORM 1 JAN 73 1473 EDITION OF 1 NOV 65 IS OBSOLETE

→ next page

UNCLASSIFIED

SECURITY CLASSIFICATION OF THIS PAGE (When Data Entered)

20. ABSTRACT (Continued)

(11 inch) outer diameter, and had thicknesses of 0.254-cm 0.1-inch) or 0.381-cm (0.15-inch). The annuli were suspended at three points on the inner diameter. The annuli were irradiated uniformly on one side. Circumferential strain data were obtained on the outer diameter of the annuli at two locations 90 degrees apart. Problems with strain gauge survivability were encountered and a new strain guage design was developed especially for these experiments. Quartz guage stresstime measurements were performed on flat aluminum specimens simultaneously with the annulus experiments. The response was also observed with fast motion pictures (7000 frames/sec). Data were obtained at fluences that varied between 3 cal/cm^2 (elastic response) and 15 cal/cm^2 (elastic-plastic response).

PREFACE

The work described in this report was performed by Physics International Company for the Defense Nuclear Agency under contract DNA001-76-C-0246. The principal investigator at Physics International was Mr. E. V. Buck, who was assisted by Mr. B. Burgess, Mr. B. Chao, Mr. A. D'Agostino, Mr. C. Felts, and Mr. A. York. The project supervisor was Dr. James Shea. The efforts were coordinated with Dr. A. O. Burford of Lockheed Missiles and Space Company. The project monitor was Mr. Donald Kohler, DNA, SPAS Division.

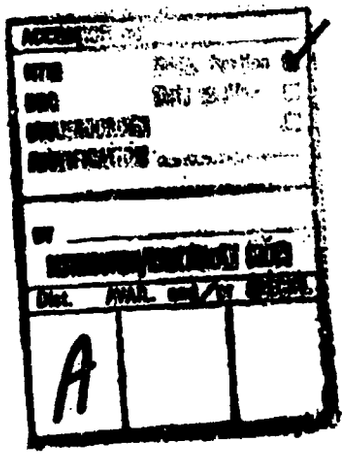

Conversion factors for U.S. customary to metric (SI) units of measurement.

To Convert From	To	Multiply By
angstrom	meters (m)	1.000 000 X E -10
atmosphere (normal)	kilo pascal (kPa)	1.013 25 X E +2
bar	kilo pascal (kPa)	1.000 000 X E +2
barn	meter^2 (m^2)	1.000 000 X E -28
British thermal unit (thermochemical)	joule (J)	1.054 350 X E +3
calorie (thermochemical)	joule (J)	4.184 000
cal (thermochemical)/cm^2	mega joule/m^2 (MJ/m^2)	4.184 000 X E -2
curie	*giga becquerel (GBq)	3.700 000 X E +1
degree (angle)	radian (rad)	1.745 329 X E -2
degree Fahrenheit	degree kelvin (K)	$t_K = (t°f + 459.67)/1.8$
electron volt	joule (J)	1.602 19 X E -19
erg	joule (J)	1.000 000 X E -7
erg/second	watt (W)	1.000 000 X E -7
foot	meter (m)	3.048 000 X E -1
foot-pound-force	joule (J)	1.355 818
gallon (U.S. liquid)	meter^3 (m^3)	3.785 412 X E -3
inch	meter (m)	2.540 000 X E -2
jerk	joule (J)	1.000 000 X E +9
joule/kilogram (J/kg) (radiation dose absorbed)	Gray (Gy)	1.000 000
kilotons	terajoules	4.183
kip (1000 lbf)	newton (N)	4.448 222 X E +3
kip/inch^2 (ksi)	kilo pascal (kPa)	6.894 757 X E +3
ktap	newton-second/m^2 ($N-s/m.^1$)	1.000 000 X E +2
micron	meter (m)	1 000 000 X E -6
mil	meter (m)	2.540 000 X E -5
mile (international)	meter (m)	1.609 344 X E +3
ounce	kilogram (kg)	2.834 952 X E -2
pound-force (lbs avoirdupois)	newton (N)	4.448 222
pound-force inch	newton-meter (N·m)	1.129 848 X E -1
pound-force/inch	newton/meter (N/m)	1.751 268 X E +2
pound-force/foot^2	kilo pascal (kPa)	4.788 026 X E -2
pound-force/inch^2 (psi)	kilo pascal (kPa)	6.894 757
pound-mass (lbm avoirdupois)	kilogram (kg)	4.535 924 X E -1
pound-mass-foot^2 (moment of inertia)	kilogram-meter^2 ($kg·m^2$)	4.214 011 X E -2
pound-mass/foot^3	kilogram/meter^3 (kg/m^3)	1.601 846 X E +1
rad (radiation dose absorbed)	**Gray (Gy)	1.000 000 X E -2
roentgen	coulomb/kilogram (C/kg)	2.579 760 X E -4
shake	second (s)	1.000 000 X E -8
slug	kilogram (kg)	1.459 390 X E +1
torr (mm Hg, 0° C)	kilo pascal (kPa)	1.333 22 X E -1

*The becquerel (Bq) is the SI unit of radioactivity; 1 Bq = 1 event/s.
**The Gray (Gy) is the SI unit of absorbed radiation.

A more complete listing of conversions may be found in "Metric Practice Guide E 380-74," American Society for Testing and Materials.

CONTENTS

ILLUSTRATIONS

SECTION 1

INTRODUCTION

This report describes thermostructural response testing performed for the Defense Nuclear Agency (DNA) using pulsed electron beams to induce thermal loads in aluminum annuli. The pulsed electron beams were generated by the DNA OWL II facility at Physics International Company. The aluminum annuli had an inner diameter of 22.9 cm (9 in.), an outer diameter of 27.9 cm (11 in.), and a thickness of 2.54 mm (0.100 in.) or 3.81 mm (0.150 in.). The annuli were irradiated uniformly on one side.

The primary response data consisted of measurements of dynamic strain in the circumferential direction at the outer edge of the annuli. A special strain gauge which better withstands the shock waves produced by rapid heating was developed for this program. Measurements were successfully obtained over a range of dose levels that spanned the threshold for permanent deformation of the annuli. Some problems with strain gauge survivability remain, however.

The structural response data collected in this program will be used by Lockheed Missiles and Space Company (LMSC) for modeling studies and comparison with computer code predictions under Contract DNA001-76-C-0246. Lockheed personnel (Dr. A. O. Burford, E. Olson, R. Walz, et al.) participated in the design of the experiment and selection of test conditions. Test specimens were provided by LMSC.

Descriptions of the experimental apparatus, techniques and procedures are presented in Section 2. The experimental results are described in Section 3, and the conclusions and recommendations are given in Section 4.

SECTION 2

EXPERIMENTAL APPARATUS AND TECHNIQUES

2.1 EXPERIMENTAL CONFIGURATION

The OWL II electron beam generator was used to produce rapid thermal loading of the aluminum annuli. The accelerator is a pulse charged system, consisting of an oil-immersed 1/3 MJ Marx generator and a water-insulated coaxial transmission line pulse transformer, which provides the pulse-forming network (Reference 1). The accelerator configuration employed for the testing reported here utilized a 120-ns pulse forming line, a 1.8-ohm output impedance transformer, and a 22.9-cm (9 in..) diameter circular cathode (Reference 2).

The electron beam test geometry is shown schematically in Figure 1. The apparatus is a modification of hardware used in previous structural response experiments on rings and cantilevered beams (References 3, 4, and 5). The electron beam is generated by a field emission cathode and passes through a transmission anode (0.013-mm-thick titanium) into the experimental chamber. A graphite aperture with a 20.3 cm (8-in.) inside diameter and a second 0.013-mm-thick titanium foil are located just behind the anode. The graphite absorbed the intense portion of the beam that originates at the perimeter of the cathode and effectively prevented anode material from reaching the test specimen. A magnetic lens was used to control and transport the electron beam from the cathode emission surface to the target. This produces an electron beam that retains the cross-sectional shape

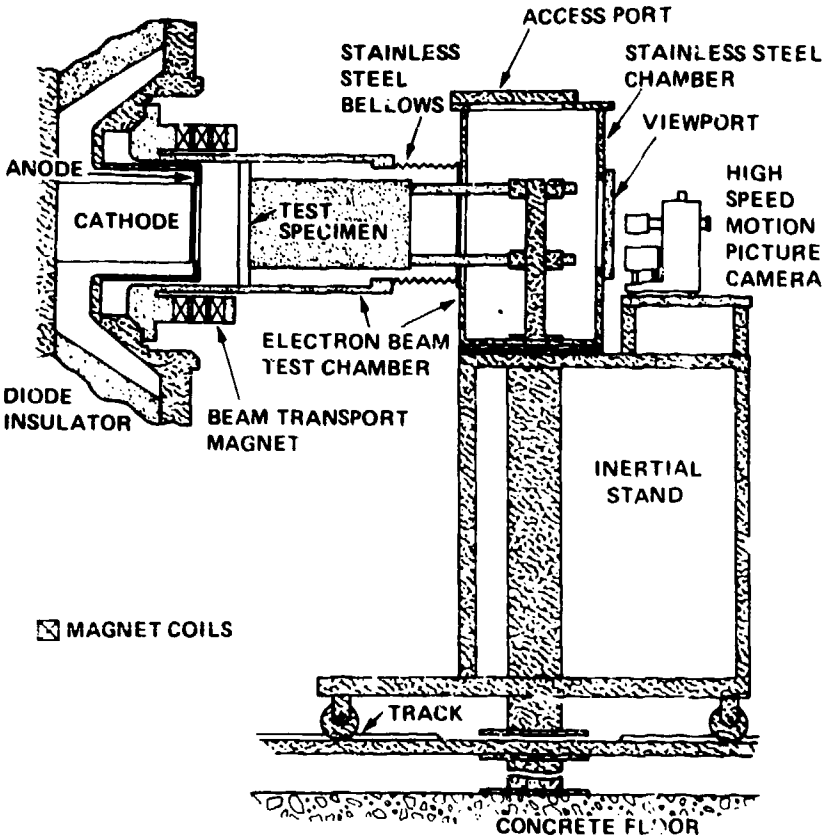

Figure 1 Electron beam test geometry.

of the cathode, but the area of the beam varies inversely with the magnetic lens ratio; hence the beam fluence is directly proportional to the magnetic lens ratio. Fluence uniformity is controlled to first order by dishing the cathode to compensate for the bow of the anode produced by the 1-torr gas pressure in the test chamber.

The target holder apparatus is shown in Figures 2 and 3. Details of the instrumentation are shown in Figures 4 and 5. The annulus was suspended at three points from small clips attached to elastic bands. The clips contacted the annuli on its inner edge. Tension of the bands was adjusted by pegs located behind the outer ring of calorimeter blocks. The entire target apparatus was mounted on an inertial stand bolted to the concrete floor. This arrangement is necessary to prevent shock waves generated in the machine from affecting the experiment.

The pulsed magnetic field used for beam control exerts a considerable force on the annulus. The direction of the force is such that the annulus is pushed into the target holder. To restrain the annulus, rubber bumpers were placed between it and the holder apparatus. When the electron beam fires, the magnetic field intensity will have reached a maximum; hence the force on the annulus is at a minimum. The strain records show that the strain caused by the magnetic field just prior to the beam fire, in the worst case, was less than 10 percent of the measured peak strain. Most records show much less strain. Thus the effect of the magnetic field on the dynamic strain measurements is not significant.

The strain gauge packages were located on the top (0 degree) and left (90 degree) sectors of the annulus. The gauge packages

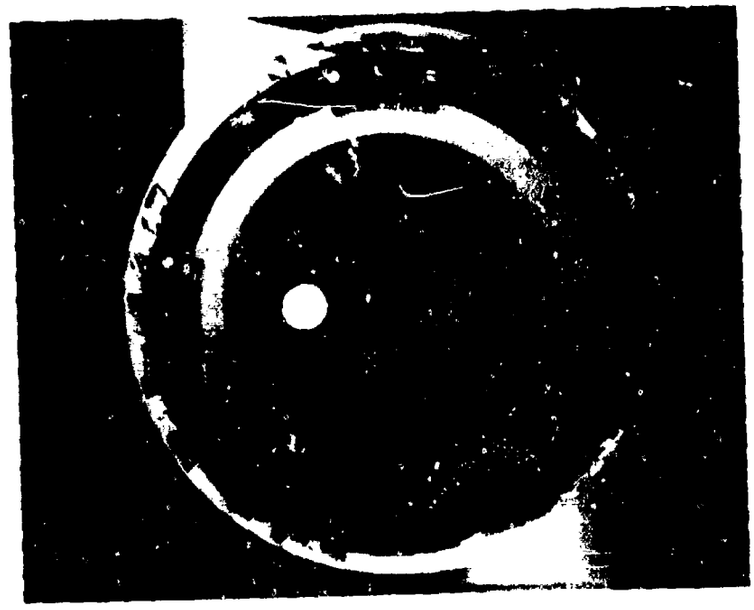

Figure 2 Front view of annulus holder. Strain gauge packages at top and left behind shields. Quartz pressure transducer at left of center. Shield for mirrors at center with viewing slots extending to right and bottom.

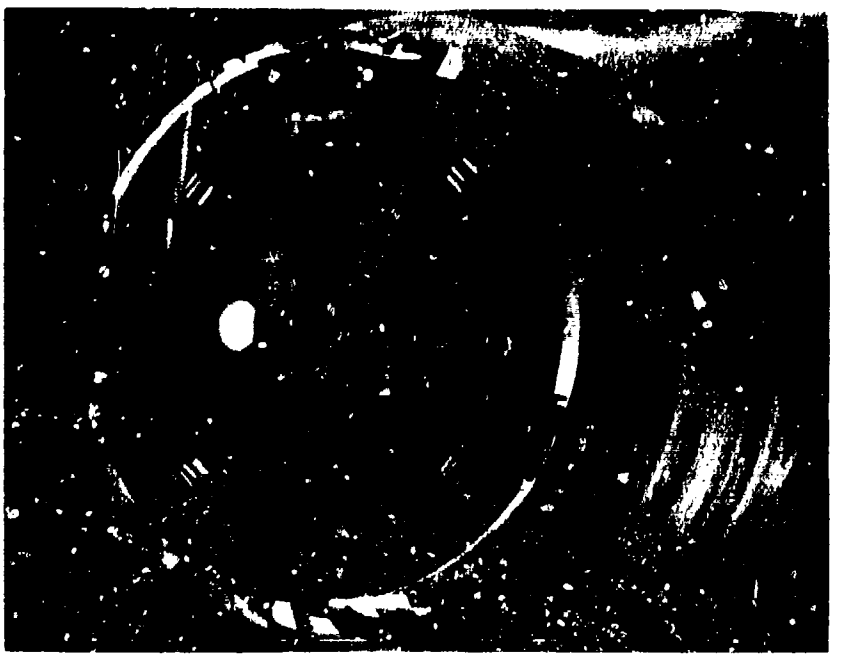

Figure 3 Annulus holder with annulus removed, showing rubber bumpers and three retaining clips.

Figure 4 Strain gauge package with shield removed. Signal leads enter pipe at left center.

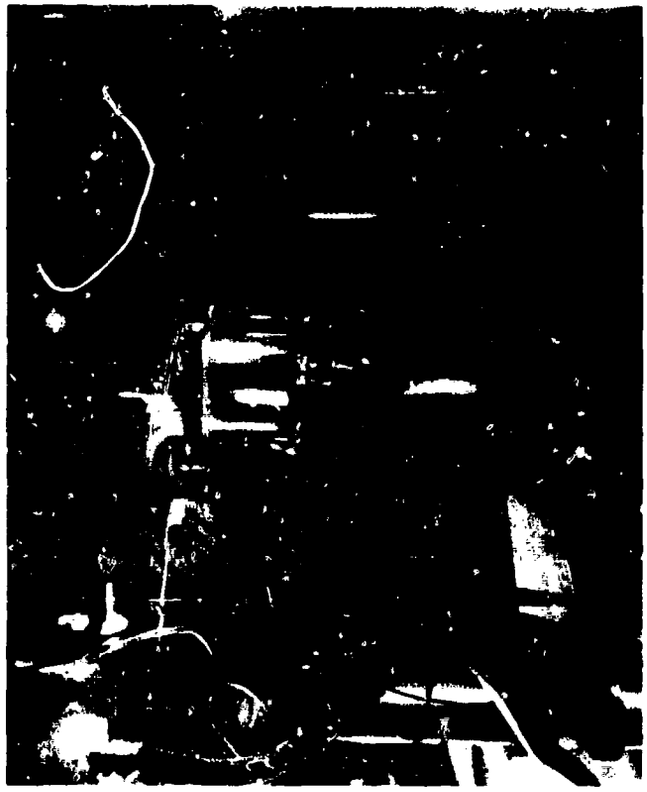

Figure 5 Rear side of annulus holder. Quartz pressure transducer at center with mirrors immediately to the left. Lamp assembly in left foreground. Thermocouple leads visible at bottom and left.

were protected by a graphite shield that extended approximately 2.5 mm over the annulus. On some tests the shield was extended to 5.0 mm or 7.5 mm in an effort to improve gauge survivability.

Calorimeter blocks were arranged in rings inside and outside the annulus. The blocks enable the simultaneous measurement of fluence and structural response data. A coupon of the test material with a quartz pressure transducer bonded to the rear surface was mounted inside the inner ring of calorimeter blocks. The quartz pressure transducer provides simultaneous measurement of the stress-time history of the annulus. Finally, a pair of mirrors were mounted in a protective graphite housing in the center of the apparatus. The mirrors provided views of the right and bottom cross sections of the annulus for a high-speed motion picture camera.

2.2 ELECTRON BEAM DIAGNOSTICS

Diagnostics used in characterization of the electron beam were employed both in the diode and at the target location. The diode diagnostics consisted of a voltage monitor, a set of $\dot{B}$ probes, and a set of current monitors. The voltage monitor is a capacitive voltage divider embedded in the diode insulator. The $\dot{B}$ probes are magnetic field sensors and have an output proportional to the time rate of change of the magnetic field associated with the diode current. The diode current monitors consist of Rogowski coil segments that are $\dot{B}$ probes with built-in integrators so that the output is directly proportional to diode current. Four B probes and two Rogowski coil segments were on the anode plate located on a diameter just inboard of the inside diameter of the diode insulator. Two full Rogowski coils surrounded the cathode: one was in the anode plate and the other was in the anode extension near the cathode tip.

The diode diagnostics were recorded with fast oscilloscopes (typically 150-MHz bandwidth). The oscilloscope data were digitized and analyzed on the Physics International Interactive Data Reduction Facility. The facility includes a digitizing tablet, a keyboard and graphics display unit, a hard copy unit, a 64K word mini-computer, and a code which interactively receives, analyzes, and plots the data. The data analysis includes correction of the input data for any RC and L/R slumps inherent in the monitors, calculation of the accelerator voltage, and calculation of quantities such as the total beam energy and mean electron energy. The accelerator voltage, V_{acc}, was determined from the equation:

$$V_{acc} = V_{monitor} - L \frac{dI}{dt}$$

or

$$V_{acc} = V_{monitor} - L \times \left(\text{constant} \times \frac{dB}{dt}\right)$$

where

$V_{monitor}$ is the voltage measured by the voltage monitor after correction for RC slump

L is the diode inductance

I is the diode current

and the constant is the ratio I/B at the location of the $\dot{B}$ probe. The product L x constant was determined by comparing $V_{monitor}$ to the $\dot{B}$ probe when the cathode was shorted to the anode (i.e., $V_{acc} = 0$).

The acceleration voltage and diode current waveforms were used directly in the PIEID Monte Carlo Code (Reference 6) to calculate electron beam energy deposition profiles for correlation with measurements.

The beam diagnostics used at the target location consisted of fluence and deposition profile calorimeters. On data shots the primary diagnostic used at target location was the peripheral calorimeter array (Figure 2). A separate calorimeter array, shown in Figures 6 and 7, in which a third ring of calorimeter blocks replaced the annulus was used for initial fluence mapping and determining fluence uniformity. The calorimeters are constructed of ATJ graphite blocks mounted on fiberglass boards with aluminum screws. Each block was instrumented with an iron-constantan thermocouple. The thermocouple signals were recorded by a scanning digital voltmeter. Fluences were calculated with a PI mini-computer program, using polynomial fits to handbook enthalpy curves for ATJ graphite and aluminum (Reference 7).

The electron beam energy deposition profile was investigated with a graphite foil stack calorimeter, visible from the rear in Figure 7. Two foil stack calorimeters were used simultaneously. One was located at a radius corresponding to the average radius of the annulus. The second was located at a radius corresponding to the position of the quartz pressure transducer. The two calorimeters provided a measurement of the variation of deposition profile with radius. The foils were 0.5-mm-thick ATJ graphite foils held in position by polyethylene blocks. The foils were instrumented with iron-constantan thermocouples, which were clamped against a copper tab attached to an edge of each foil. The thermocouple signals were read out with the same scanning digital voltmeter system described previously. The deposition profiles were calculated with a PI mini-computer program using polynomial fits to the enthalpy curves for ATJ graphite and copper.

Figure 6 Front view of calorimeter. Fluence calorimeter blocks are in three concentric rings. Apertures for foil stack calorimeter at 10 o'clock position.

Figure 7 Rear view of calorimeter showing thermocouple attachments and foil stacks.

2.3 STRUCTURAL RESPONSE DIAGNOSTICS

Structural response induced by pulsed electron beam irradiation of the aluminum rings was measured using strain gauges and high-speed motion pictures. The strain gauge data acquisition system was essentially the same as used during previous experiments on aluminum rings (Reference 5). The system is capable of handling six channels. A block diagram of one channel of this system is shown in Figure 8. A schematic of the basic bridge circuit is shown in Figure 9. A common dc power supply was used to set up and balance each bridge circuit; individual pulsed power supplies were used during data collection. Considerable attention was paid to noise reduction. Double shielding was used wherever possible, with the inner shield of each channel single-point grounded to the amplifier chassis. The outer shield, which enclosed all six channels, extended from the annulus itself to the electronics rack.

A set of small magnetic field compensation loops located close to the annulus were used to tune out signals induced by the pulse magnetic beam guide. These tuning loops were enclosed in a Faraday cage that was designed to shield the electrical noise from the electron beam but remain transparent to the magntic beam guide. This is feasible because the relevant frequencies differ by at least five orders of magnitude (hence the skin depths differ by more than two orders of magnitude).

The recording instrumentation consisted of Preston Model 8300XWB-B differential amplifiers, a Bell & Howell Model 5-134 oscillograph, and an Ampex Model FR-2000 FM tape recorder. The strain gauge signals were recorded on magnetic tape at a speed of 305 cm/s (120 ips). The signals were simultaneously recorded

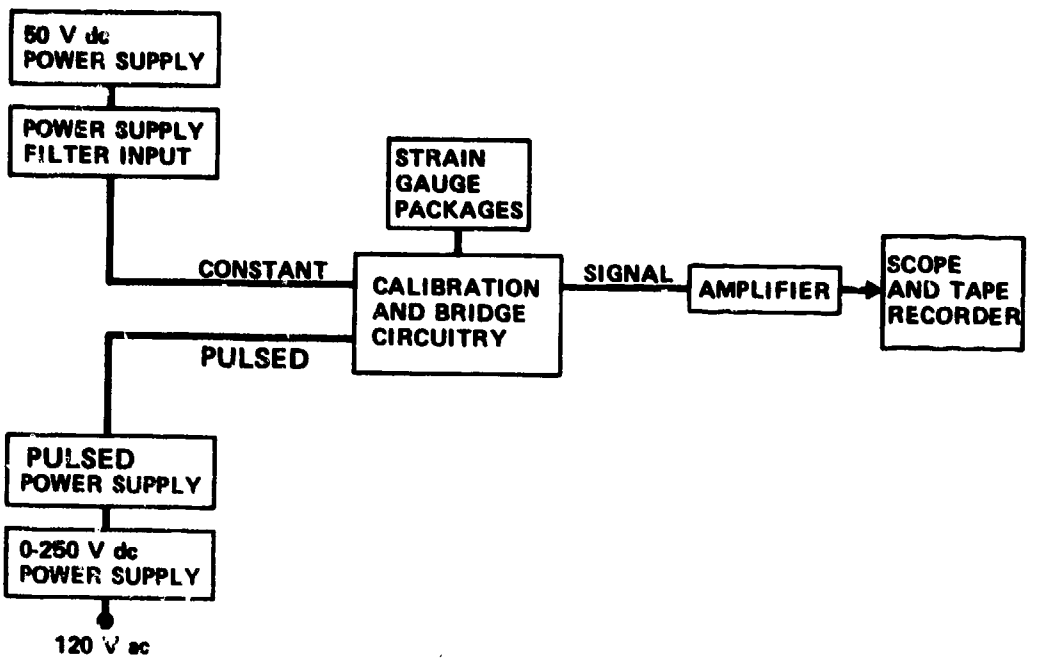

Figure 8 Block diagram of strain gauge instrumentation.

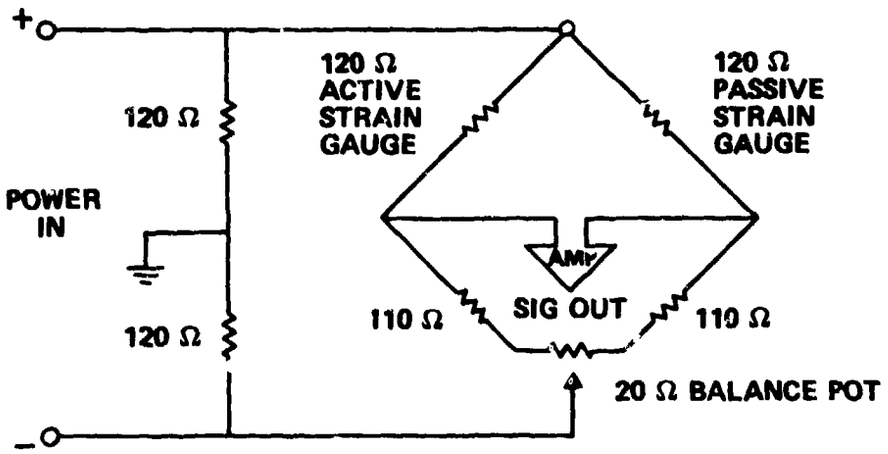

Figure 9 Bridge circuit schematic.

on the oscillograph at a paper speed of 254 cm/s (100 ips). The oscillograph records provided an on-line check of system performance and a preliminary comparison of strain data with predictions. At a later date, the magnetic tape was played back at a tape speed of 9.5 cm/s (3-3/4 ips) and the reproduced signals recorded on the oscillograph at a paper speed of 254 cm/s (100 ips). The time scale on these oscillograph records was thus expanded by a factor of 32. These records will be used by LMSC for detailed analysis of the strain data. The bandwidth of the system was limited to 100 kHz by the Preston amplifiers.

Strain gauge packages were located at two positions 90 degrees apart along the outer circumference of the annulus. Three different gauge configurations were employed in the course of the experiment. They will be denoted Configuration I, II, and III, respectively. At the 0 degree, or top, position, Configuration I had three Micromeasurements Type EA13-031DE-120 (31 mil wide) guage, one Micromeasurement Type EA13-062-DF-120 (62 mil wide) gauges, and one Micromeasurement Type EA13-125AV-120 (option B64) (125-mil-wide "long lead") gauges. At the 90 degree (or left) position, two 31-mil gauges were employed. The gauge placement for Configuration I is illustrated in Figure 10. For Configuration II, two 125-mil-long lead gauges were employed at both the 0-degree and 90-degree positions. Configuration II is illustrated in Figure 11. For Configuration III, two BLH type FAE-18-12-S13-1 (25-mil-wide "long lead") gauges and one Micromeasurements 125-mil-long lead gauge were employed at both the 0-degree and 90-degree positions. Configuration III is illustrated in Figure 12. The BLH gauges were designed and fabricated especially for this experiment. The details of the grid pattern for this gauge are shown in Figure 13.

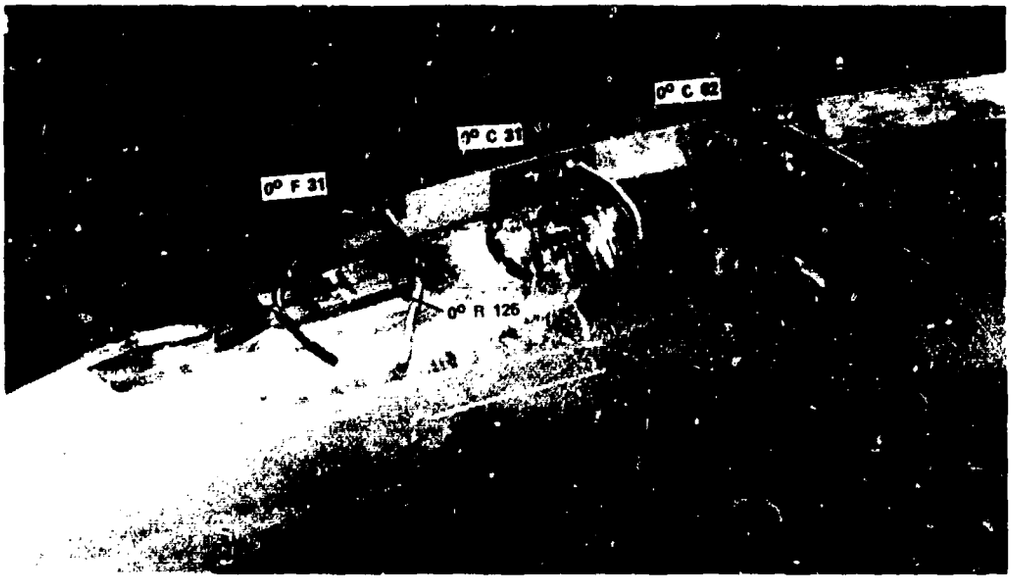

Figure 10a

Figure 10b

Figure 10 Strain gauge placements for Configuration I.

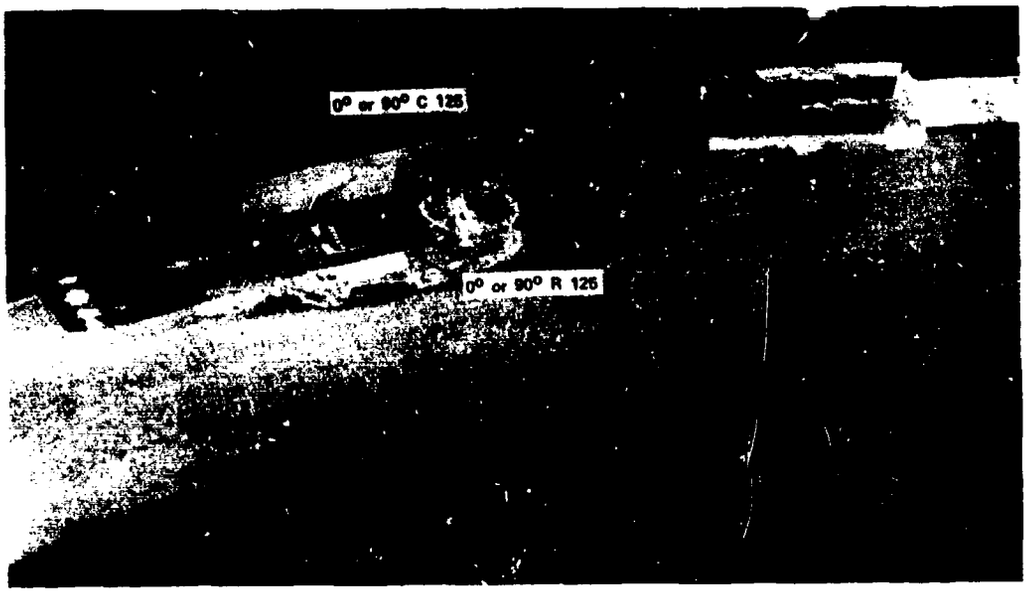

Figure 11 Strain gauge placements for Configuration II.

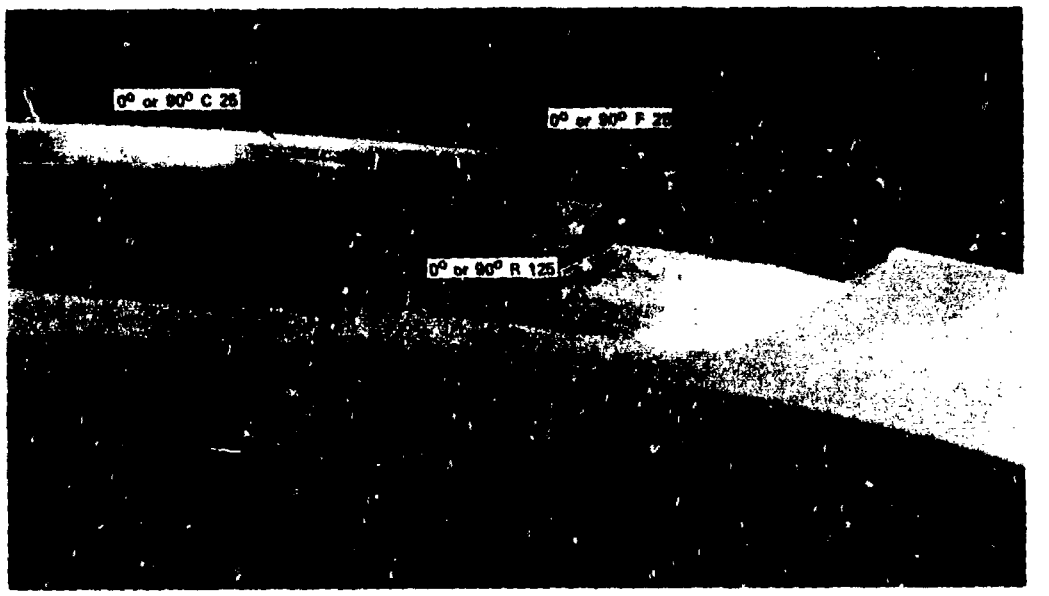

Figure 12 Strain gauge placements for Configuration III.

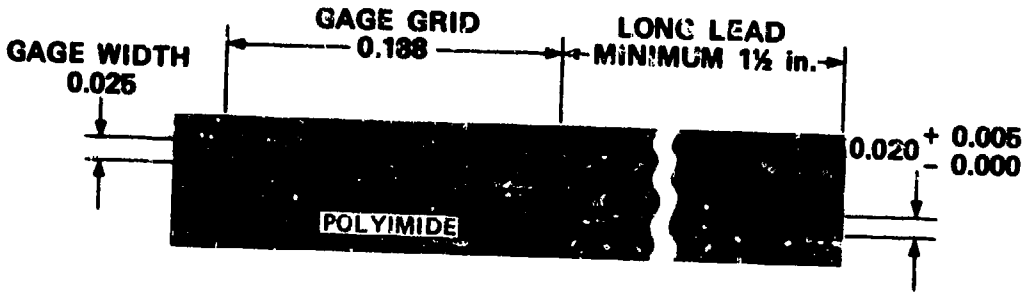

GENERAL INFORMATION:

1. CONSTANTAN FOIL
2. POLYIMIDE FILM BACKING
3. RESISTANCE 120 OHMS
4. OPEN FACE CONSTRUCTION

Figure 13 25 mil wide strain gauge with long integral leads.

Each strain gauge channel consisted of two gauges, an active gauge bonded to the annulus and a passive gauge mounted directly above the active gauge, mechanically decoupled from the annulus with a foam pad. The passive gauge comprised one leg of the bridge circuit and served to cancel spurious signals induced in the active gauge by the pulsed magnetic field used to guide the beam and the pulsed electron beam itself. A complete gauge package is shown in Figure 14. The entire package was covered by copper foil for additional noise shielding.

Gauges were bonded to the rings with Micromeasurements Type M-Bond 610 adhesive. The cure cycle employed was approximately 45 minutes warmup, followed by approximately 60 minutes at 420°K, followed by approximately 45 minutes cooldown.

Motion of the front region of the ring was recorded with a high-speed motion picture system mounted at the rear of the test chamber. The photographic record was taken with a Red Lakes Lab Model 1C 2051E "Hycam" operating at a framing rate of about 7000 frames per second. The camera was enclosed by a 2.5-cm-thick lead box in order to minimize X-ray fogging of the high-speed film.

Figure 14 Completed gauge package with passive gauges attached to annulus by a foam pad.

SECTION 3

EXPERIMENTAL RESULTS

3.1 ELECTRON BEAM DATA

Data were collected during two sessions at the OWL II facility. The first session occurred in February 1977, and the second session occurred in August 1977. The data for both sessions are summarized in Table 1. The fluences tabulated are the averages for each of the three rings of calorimeter blocks. The mean square deviations indicate the degree of fluence uniformity obtained around the circumference of the annulus. The uniformity in the radial direction can be assessed by comparing the average fluence for the inner, middle, and outer rings of calorimeter blocks for a particular pulse. For those experiments in which the apparatus was closer than 34 cm from the cathode, the outer ring of blocks was not fully illuminated, and therefore these data are not tabulated. Also tabulated in Table 1 are the normalized peak dose measured by the outer foil stack, the mean energy per electron and the total beam energy, calculated from diode diagnostics, and the cathode to target distance.

The fluence maps obtained for this program are presented in Appendix A-1. Since the blocks used in the fluence calorimeter arrays for this experiment are relatively large, fluence variations over a smaller scale would not be detected. To investigate this possibility, data were obtained on two pulses, 3839 and 3840, with an array of blocks of dimensions 0.5 cm by 0.5 cm. The array was positioned in the center of the electron beam. Results of these experiments are shown in Appendix A-2.

TABLE 1 OVERALL DATA SUMMARY

Pulse Number	Cathode-Target Distance (cm)	Target[1]	Average Fluence: Inner Ring (cal/cm²)	M.S.D. (cal/cm²)	Middle Ring (cal/cm²)	M.S.D. (cal/cm²)	Outer Ring (cal/cm²)	M.S.D. (cal/cm²)	Normalized Peak Dose Outer Foil Stack (cal/gm / cal/cm²)	Total Diode Energy (kilojoules)	Mean Electron Energy (MeV)
Session I:											
3477	36.8	C	5.38	0.29	5.03	0.28	4.86	0.30	3.14	50	0.87
3478	36.8	C	5.40	0.32	4.88	0.34	4.73	0.63	3.06	49	0.91
3479	36.8	M								52	0.96
3480	36.8	M								50	0.95
3481	36.8	A	1.75	0.17			1.54	0.20		17.8	0.92
3482	36.8	A	5.39	0.46			5.61	0.54		52	0.97
3483	36.8	C	5.45	0.69	4.91	0.26	4.28	0.55	2.99	50	0.98
3484	36.8	C	3.80	0.78	3.82	0.49	4.01	0.42	2.82	42	1.00
3485	36.8	C	4.23	0.31	4.04	0.35	3.85	0.55	2.90	40	0.93
3486	36.8	A	5.31	0.51			5.34	0.41		49	0.91
3487	36.8	A	5.37	0.45			5.37	0.61		52	0.96
3488	36.0	C	3.38	0.71	3.89	0.69	3.88	0.65	2.89	42	0.96
3489	36.8	A	5.44	0.69			5.01	0.95		51	1.00
3490	36.8	A	5.31	0.63			5.02	0.46		49	0.93
3492	30.5	C	8.55	0.86	8.51	0.78			3.04	48	0.93
3493	30.5	C	7.83	0.94	7.97	1.50			3.03	48	1.00
3494	30.5	A	7.60	1.13						49	0.96
3495	30.5	C	8.83	1.09	8.45	0.94			—[3]	49	0.91
3497	30.5	C	8.53	1.35	8.67	0.64			2.82	51	0.99
Session II:											
3824	36.8	C	1.22	0.14	1.18	0.11	1.16	0.11	3.56	18.8	0.69
3825	36.8	C	4.90	0.44	4.64	0.31	4.59	0.20	3.22	—[4]	
3826	36.8	C	4.83	0.40	4.69	0.25	4.71	0.23	3.04	56	0.90
3827	36.8	M								58	0.87
3828	36.8	A	4.70	0.29			4.74	0.33		—[4]	
3829	36.8	C	4.97	0.25	4.56	0.28	4.34	0.15	2.86	56	0.92
3830	36.8	A	2.36	0.10			2.16	0.13		29.7	0.99
3831	30.5	A	7.61	0.69						57	0.93
3832	25.4	C	9.97	0.38	8.53	1.22			3.21	55	0.78
3835	29.2	C	15.9	0.8	14.7	0.8			2.93	103	0.96
3836	29.2	A	16.0	0.6						—[4]	
3837	29.2	C	17.0	0.8	15.2	0.7			3.24	99	0.91

TABLE 1 OVERALL DATA SUMMARY (CONT.)

Pulse Number	Cathode-Target Distance (cm)	Target[1]	Inner Ring (cal/cm^2)	M.S.D. (cal/cm^2)	Middle Ring (cal/cm^2)	M.S.D. (cal/cm^2)	Outer Ring (cal/cm^2)	M.S.D. (cal/cm^2)	Normalized Peak Dose Outer Foil Stack $\left(\frac{cal/cal}{gm/cm^2}\right)$	Total Diode Energy (kilojoules)	Mean Electron Energy (MeV)
3838	29.2	C	18.6	0.5	17.4	0.5			2.96	109	0.93
3839	29.2	H	5.73[2]	0.33						42	0.96
3840	29.2	H	11.1[2]	0.9						64	0.85
3841	29.2	A	12.9	0.7						86	0.84
3842	29.2	C	16.1	0.2	14.6	0.6			3.16	98	0.87
3843	30.5	C	4.80	0.20	4.46	0.19			3.13	42	0.78
3844	30.5	C	3.42	0.32	3.32	0.27			3.30	--[4]	
3845	30.5	C	14.2	0.5	12.9	0.5			3.47	88	0.83
3846	34.3	C	11.4	0.8	9.83	0.72	9.07	0.74	3.22	87	0.81
3847	34.3	A	3.07	0.19			2.97	0.37		27.9	0.70
3848	34.3	C	9.50	0.40	8.68	0.31	8.00	0.45	3.32	86	0.76
3849	34.3	A	10.3	0.8			9.34	0.88		87	0.83

[1] A - annulus, C - calorimetry, N - noise test, H - high resolution fluence calorimeter (see text).

[2] Measured at center of beam.

[3] Foil stack data not obtained.

[4] Diode diagnostic data not obtained.

The mean square deviations were 6 and 8 percent, respectively, for the two pulses, showing good uniformity to the limit of resolution of this calorimeter. Additional information on fluence uniformity, obtained from previous experiments with similar apparatus, may be found in Reference 6.

The electron beam energy deposition profile measurements are shown in Appendix B. These data for the outer foil stack are compared to electron beam energy deposition profiles calculated from the acceleration voltage and current waveforms (Appendix B-1). The calculations assume a normal angle of incidence. Albedo suppression was not considered for these calculations since only 3 to 4 percent of the incident energy is reflected for this beam condition. Measurements by the inner foil stack are shown in Appendix B-2. The profiles measured by the inner and outer foil stacks are very similar. Deposition profile calculations for the annulus experiments are presented in Appendix C. These were calculated in the same manner as for Appendix B.

3.2 STRUCTURAL RESPONSE DATA

The structural response data pulses are summarized in Table 2. The fluence levels indicated were estimated from data of the surrounding calorimeter blocks. The table also indicates the success of failure of data recovery for the strain gauges, the quartz pressure transducer, and the film records. It was found that the 31- and 62-mil strain gauges of Configuration I failed at all but the lowest fluence levels. The failure mode was a debonding of the gauge solder tab and consequent loss of electrical contact. The debonding was evidently caused by the initial shock wave induced in the annulus by the electron beam. The long lead gauges in widths of 125 and 25 mils had a

significantly higher survival rate, although some failures occurred with these gauge types also. The failure mode was usually a tearing of the long lead at its point of departure from the annulus surface.

The oscillograph records of dynamic strain obtained on-line are reproduced in Appendix D. The data are in general of excellent quality. Some of the records show an apparent baseline shift at the time of beam fire. This might be caused by a stretching or partial tearing of the long lead by the initial shock wave. The expanded time scale oscillograph records obtained from play back of the magnetic tape have been forwarded to LMSC under separate cover for detailed analysis.

Quartz pressure transducer records of excellent quality were obtained for all but two of the annulus experiments. The two failures were due to oscilloscope problems. The transducer records are reproduced in Appendix E. The film records obtained from Session I turned out to be severely underexposed and are of little use. An improved lighting system was employed for Session II. These films turned out well and should provide quantitative structural response data. A portion of the film record for pulse 3849 is reproduced in Figure 15. The transducer records and films have been forwarded to LMSC.

Measurements of the permanent distortion induced in the annuli are presented in Table 3. The method of measurement is illustrated in Figure 16. Two modes of distortion were observed. The first is bending of the annulus into a cone shape (Figure 17). The second is bending of the entire annulus into a saddle shape (Figure 18). The degree of coning as a function of fluence is plotted in Figure 19. The threshold for permanent deformation appears to be 5 to 6 cal/cm^2 for the electron energy used in this experiment.

TABLE 2 SUMMARY OF STRUCTURAL RESPONSE DATA

Pulse	Thickness of Annulus (mm)	Fluence (cal/cm^2)	Strain Gauge Configuration	Strain Gauge Data[1]						Quartz Pressure Transducer	High Speed Movie
				Channel 1	Channel 2	Channel 3	Channel 4	Channel 5	Channel 6		
3481	2.54	1.7	I	F	F	F	F	F	F	F	N
3482	2.54	5.5	I	F	N	N	N	N	N	F	N
3486	2.54	5.3	I	F[2]	N[2]	N[2]	F[2]	N[2]	N[2]	F	N
3487	3.81	5.4	II	O	F[2]	F[2]	F[2]	F[2]	O	F	N
3489	3.81	5.2	II	O	F[2]	F[2]	O	F	P	F	N
3490	3.81	5.2	I	F[3]	N[3]	N[3]	F[3]	N[3]	N[3]	F	N
3494	3.81	7.6	II	O	F[2]	F[2]	O	F[2]	F[2]	F	N
3828	2.54	4.7	III	F	F	F	F	P	F	N	F
3830	2.54	2.2	III	F	F	F	F	F	F		F
3831	2.54	7.4	III	N	P	F	F	F	F	F	F
3836	2.54	15.0	III	F	F	F	F	F	F	N	F
3841	2.54	12.0	III	F	F	F	F	F	F	F	F
3847	2.54	3.0	III	F	F	F	F	P	F	F	F
3849	2.54	10.0	III	P	P	F	P	P	F	F	F

1. Key: F - Full data recovery
P - Partial recovery
N - Not recovered
O - Channel not used

2. 5-mm graphite shield instead of 2.5 mm

3. 7.5-mm graphite shield

TABLE 3 POST-IRRADIATION DISTORTION MEASUREMENTS

Pulse	Thickness of Annulus (mm)	Fluence (cal/cm^2)	Distortion			
			Position 1 (mm)	Position 2 (mm)	Position 3 (mm)	Position 4 (mm)
3481	2.54	1.7	0.03	0.03	0.03	0.03
3482	2.54	5.5	0	0.10	0.10	0.08
3486	2.54	5.3	0.10	0.10	0.10	0.13
3487	3.81	5.4	0.05	0.10	0.08	0.08
3489	3.81	5.2	0.08	0.08	0.08	0.10
3490	3.81	5.2	0	0	0.03	0.05
3494	3.81	7.6	0.71	0.66	0.76	0.99
3828	2.54	4.7	0	0	0	0
3830	2.54	2.2	0	0	0	0
3831	2.54	7.4	1.93	1.93	1.07	1.07
3836	2.54	15.0	19.94	19.94	6.73	6.73
3841	2.54	12.0	19.53	19.53	6.48	6.48
3847	2.54	3.0	0	0	0	0
3849	2.54	10.0	4.14	4.14	2.41	2.41

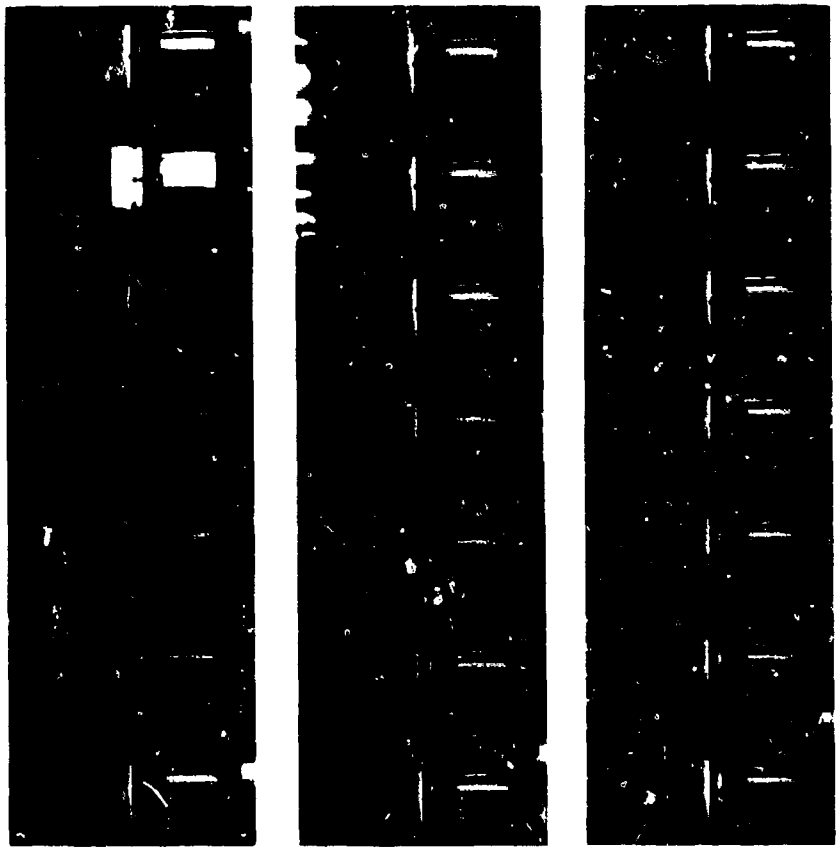

a b c

Figure 15 Movie frames from pulse 3849. Electron beam fires in second frame. 2.54-mm reference pin appears in right (270 degrees) view of annulus. Film speed 6800 frames/sec.

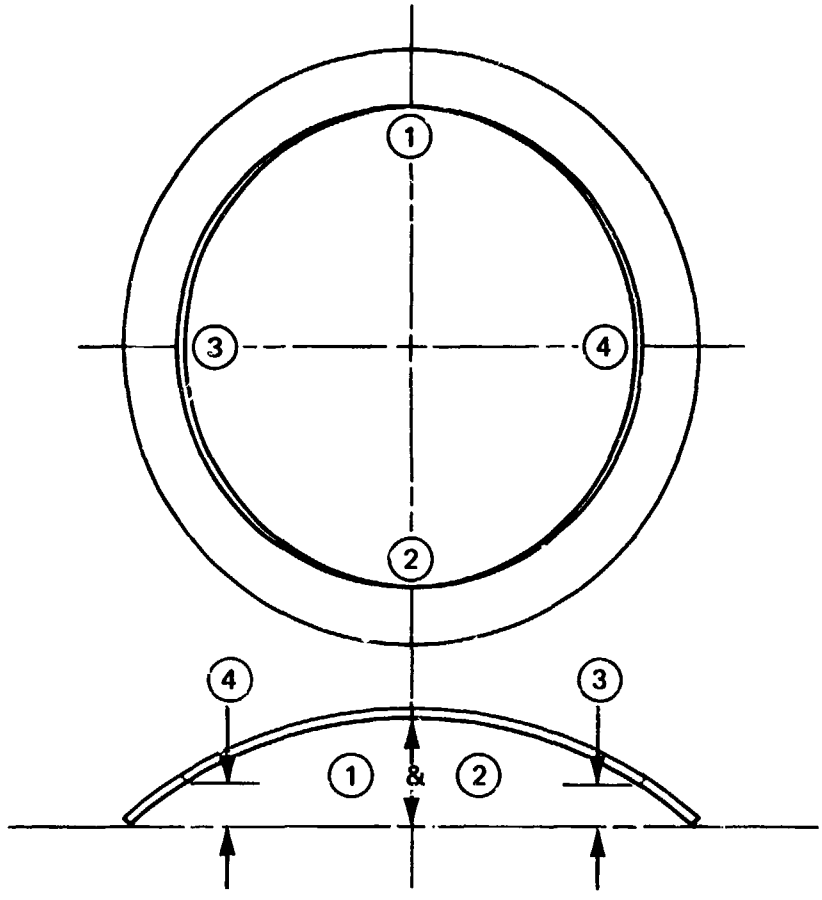

Figure 16 Locations of distortion measurements.

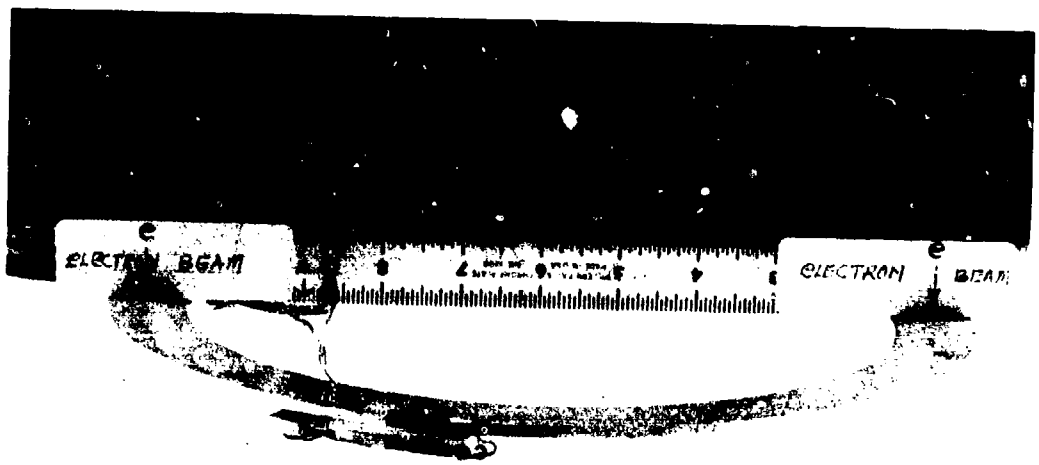

Figure 17 Coning deformation in 3.81-mm annulus, pulse 3494.

Figure 18 Saddle deformation in 2.54-mm annulus, pulse 3836.

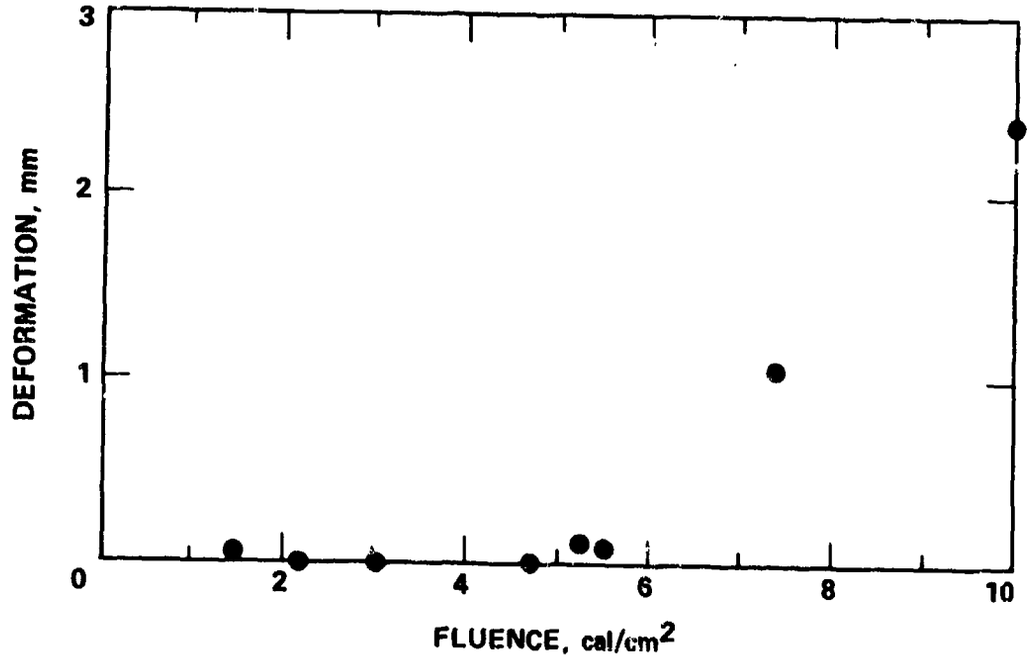

Figure 19 Coning deformation versus fluence for 2.54-mm annuli.

SECTION 4

CONCLUSIONS AND RECOMMENDATIONS

Dynamic strain gauge data and high-speed motion pictures were successfully obtained on aluminum annuli irradiated by an electron beam. Substantial permanent deformations were induced at the higher fluence levels. Measurements of the stress pulse were obtained concurrently with a quartz pressure transducer bonded to a coupon of the test material. The electron beam was diagnosed with diode monitors, peripheral graphite block calorimeters, and graphite foil stack calorimeters.

The advantages of electron beams for structural response experiments have been demonstrated by this program. Unanticipated problems with strain gauge survivability were uncovered and appropriate solutions were found. This information will be useful in designing underground test experiments, as well as future electron beam experiments. This program has provided a substantial data base in a geometry which has not previously been investigated. These data, combined with existing data for rings and cantilevered beams, will enable continued progress in theoretical modeling of structural response. To further this end, we recommend future experiments with more complex geometries and advanced materials.

REFERENCES

1. K. Nielsen, G. Frazier, and P. Spence, OWL II Generator Enhancement and Electron Beam Characterization (Unpublished) Physics International Company, San Leandro, CA.

2. K. Childers and C. Stallings, OWL II Diode Study, PIFR-788 (Draft), Physics International Company, San Leandro, CA.

3. K. Childers, V. Buck, and J. Shea, Carbon-Carbon Thermal Structural Response Testing, AFWL-TR-74-330, Air Force Weapons Laboratory, Kirtland Air Force Base, NM, October 1975.

4. K. Childers, V. Buck, and J. Shea, Thermostructural Response of Cantilevered Titanium Alloy Beams Subjected to Pulsed Radiation Heating, PIFR-836, Physics International Company, San Leandro, CA, February 1976.

5. V. Buck and J. Shea, Aluminum Ring Thermostructural Response Study, PIFR-930-1, Physics International Company, October 1976.

6. J. Reaugh and L. Behrmann, Documentation of the Physics International Monte Carlo Electron Transport Computer Code, PIIR-9-71, Physics International Company, San Leandro, CA, January 1971.

7. A. Mazzella, Graphite Calorimeter Calibrations, PIIR-22-68-V, Physics International Company, 1968.

APPENDIX A-1

FLUENCE MAPS
(NORMAL RESOLUTION)

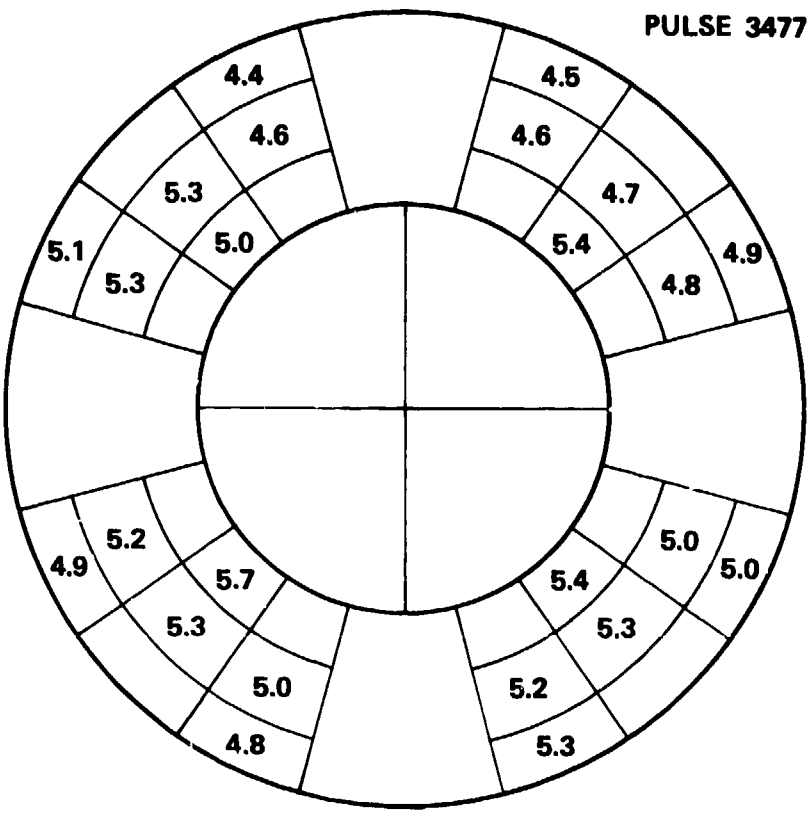
PULSE 3477
4.4
4.6
5.3
5.0
5.1
5.3
4.5
4.6
4.7
5.4
4.9
4.8
5.2
4.9
5.7
5.3
5.0
4.8
5.0
5.4
5.0
5.3
5.2
5.3

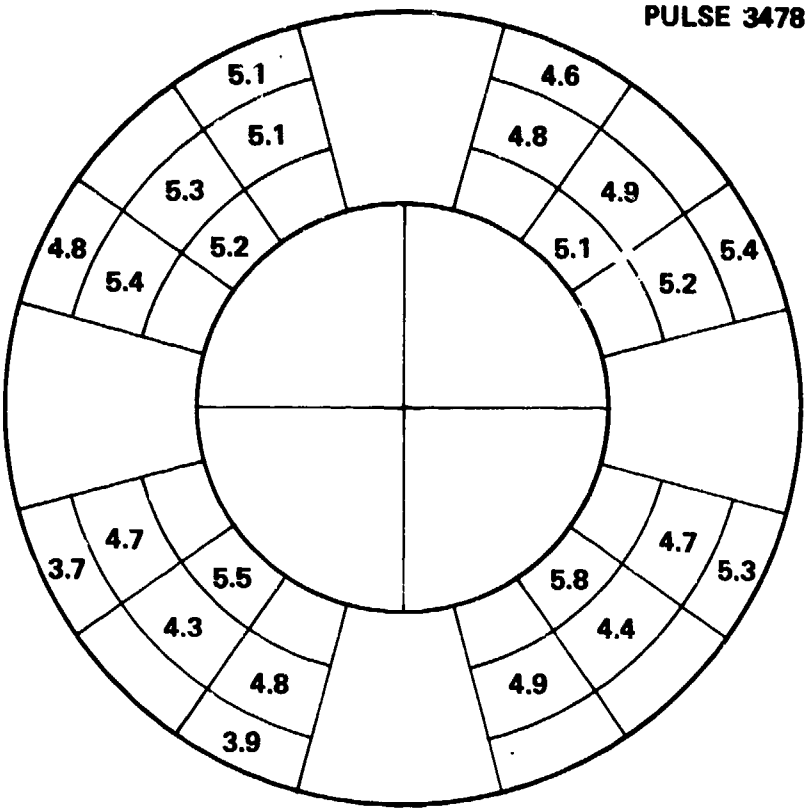
PULSE 3478
5.1
5.1
5.3
5.2
4.8
5.4
4.6
4.8
4.9
5.1
5.2
5.4
4.7
3.7
5.5
4.3
4.8
3.9
4.7
5.8
4.4
4.9
5.3

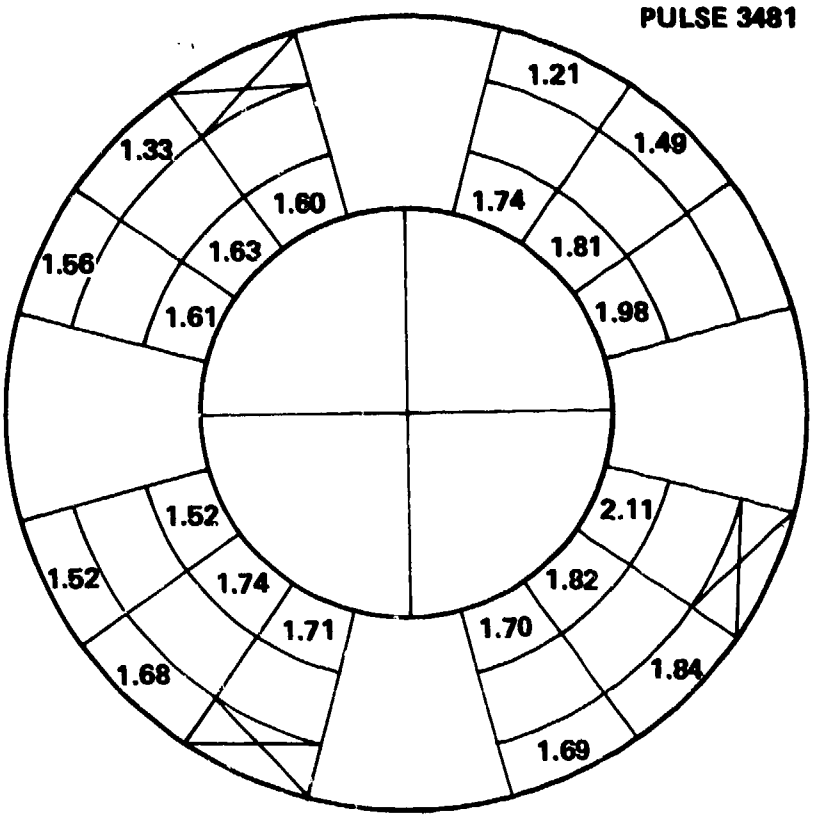
PULSE 3481
1.21
1.49
1.74
1.81
1.98
1.60
1.33
1.63
1.56
1.61
2.11
1.82
1.70
1.84
1.69
1.52
1.52
1.74
1.71
1.68

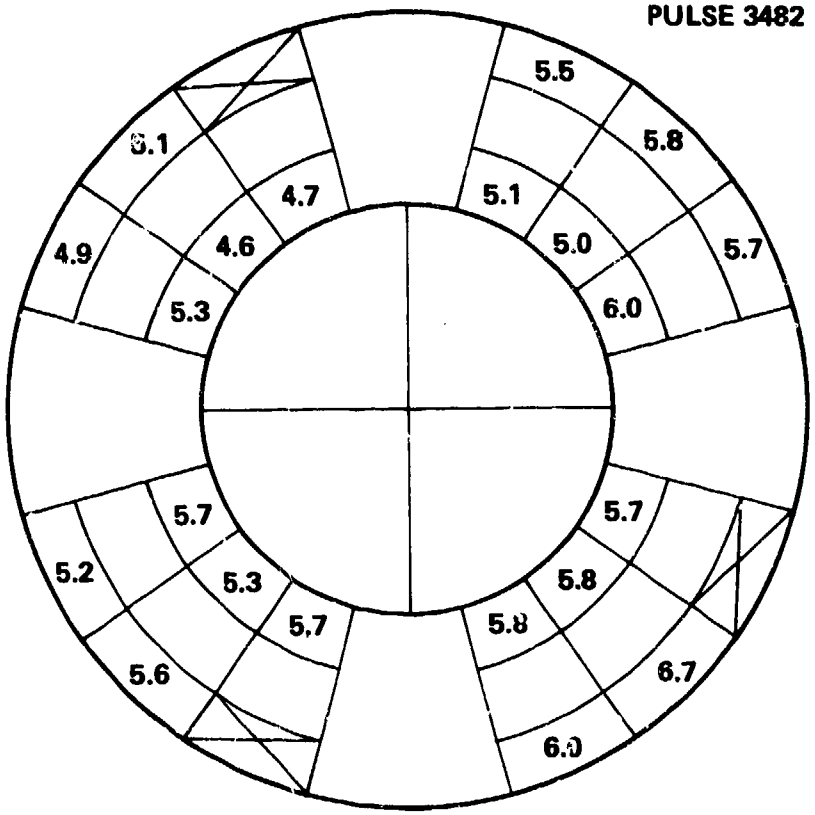
PULSE 3482
5.5
5.8
5.1
5.0
5.7
6.0
4.7
4.6
4.9
5.3
5.7
5.2
5.3
5.7
5.6
5.7
5.8
5.8
6.7
6.0

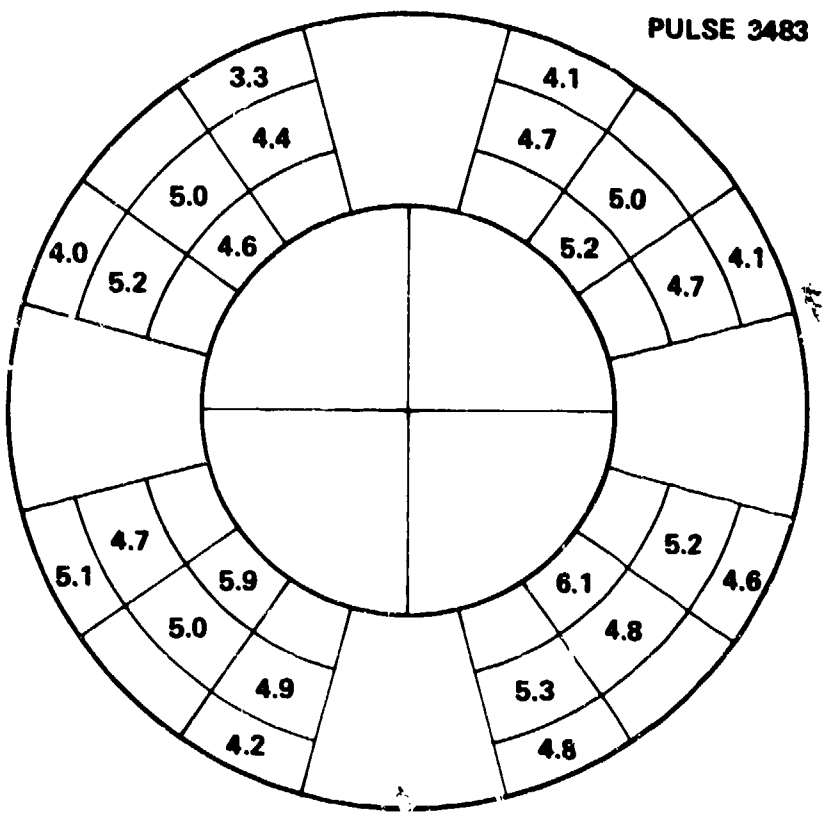
PULSE 3483
3.3
4.4
5.0
4.6
4.0
5.2
4.1
4.7
5.0
5.2
4.7
4.1
5.1
4.7
5.9
5.0
4.9
4.2
6.1
5.2
4.6
4.8
5.3
4.8

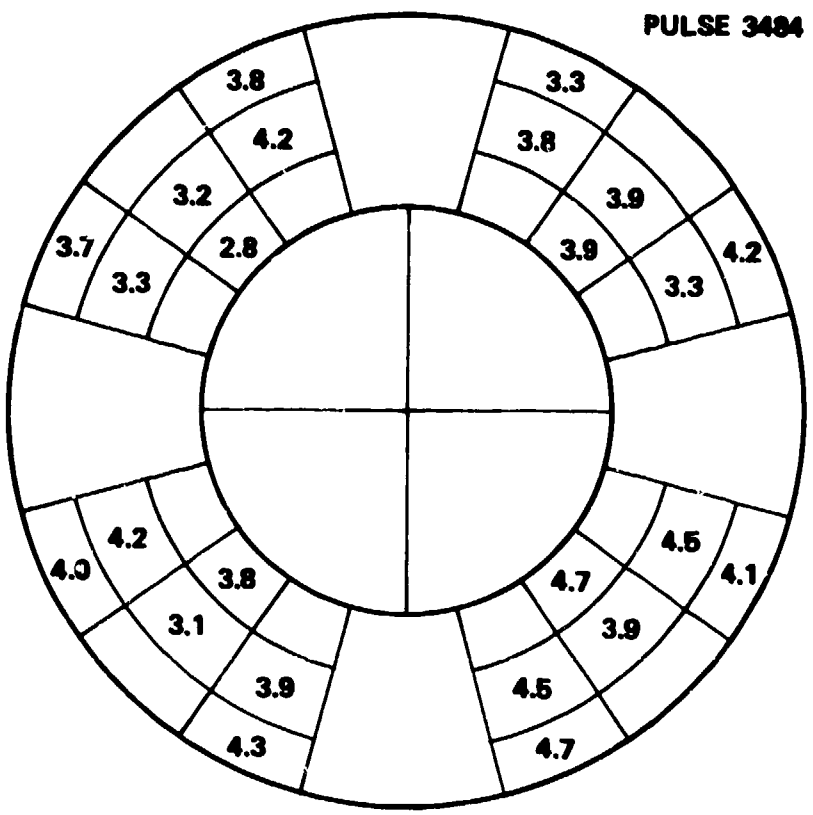
PULSE 3484
3.8
4.2
3.2
2.8
3.7
3.3
3.3
3.8
3.9
3.9
3.3
4.2
4.0
4.2
3.8
3.1
3.9
4.3
4.5
4.7
4.7
3.9
4.5
4.1

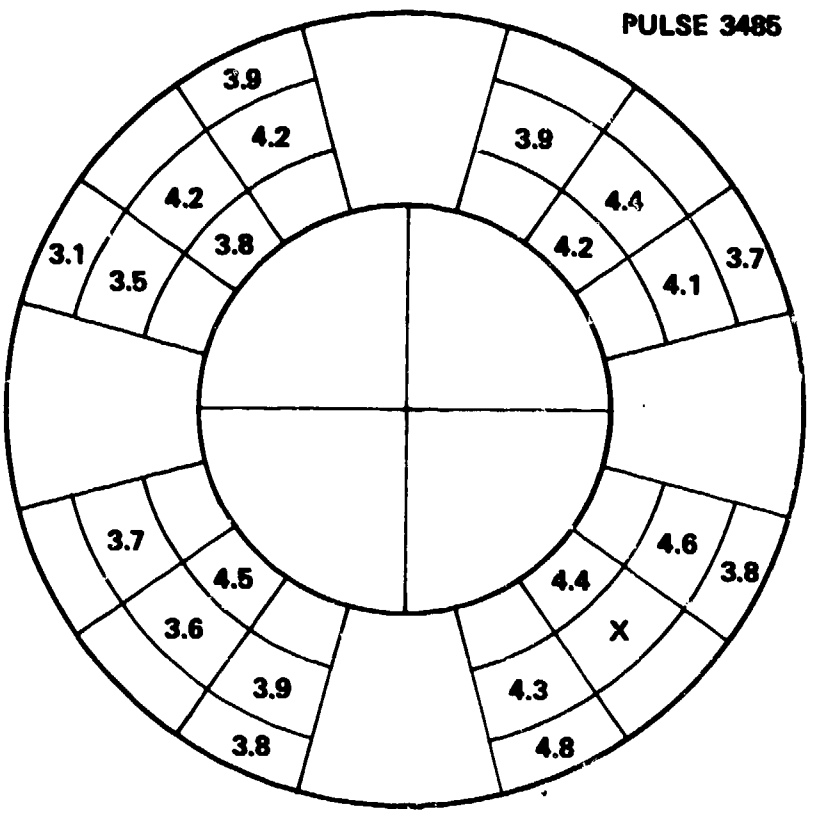
PULSE 3485
3.9
4.2
4.2
3.8
3.1
3.5
3.9
4.4
4.2
4.1
3.7
3.7
4.5
3.6
3.9
3.8
4.6
3.8
4.4
X
4.3
4.8

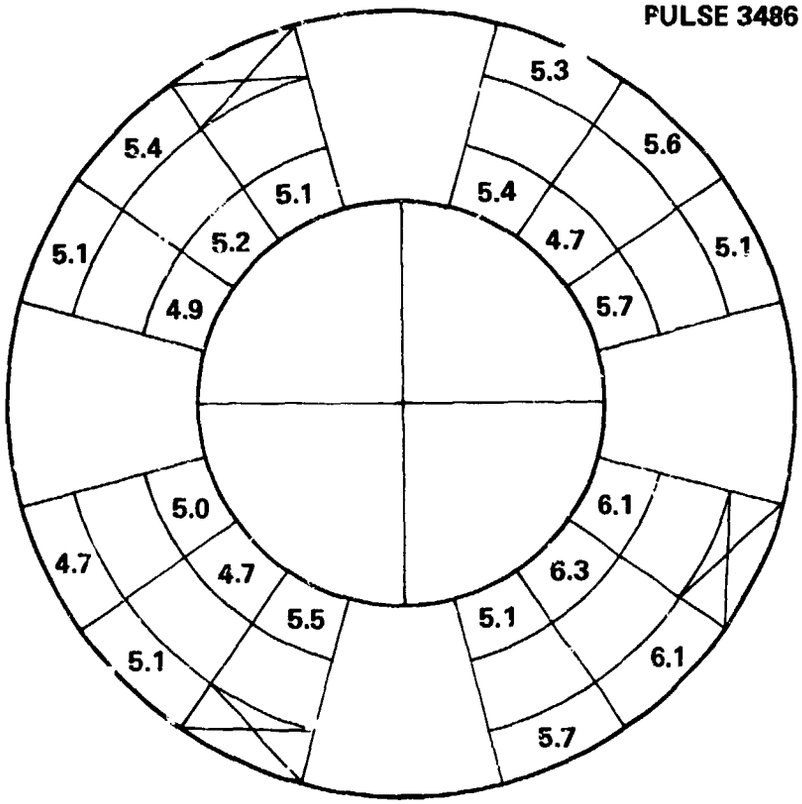
PULSE 3486
5.3
5.6
5.1
5.4
4.7
5.7
5.1
5.4
5.1
5.2
4.9
5.0
4.7
4.7
5.5
5.1
6.1
6.3
5.1
6.1
5.7

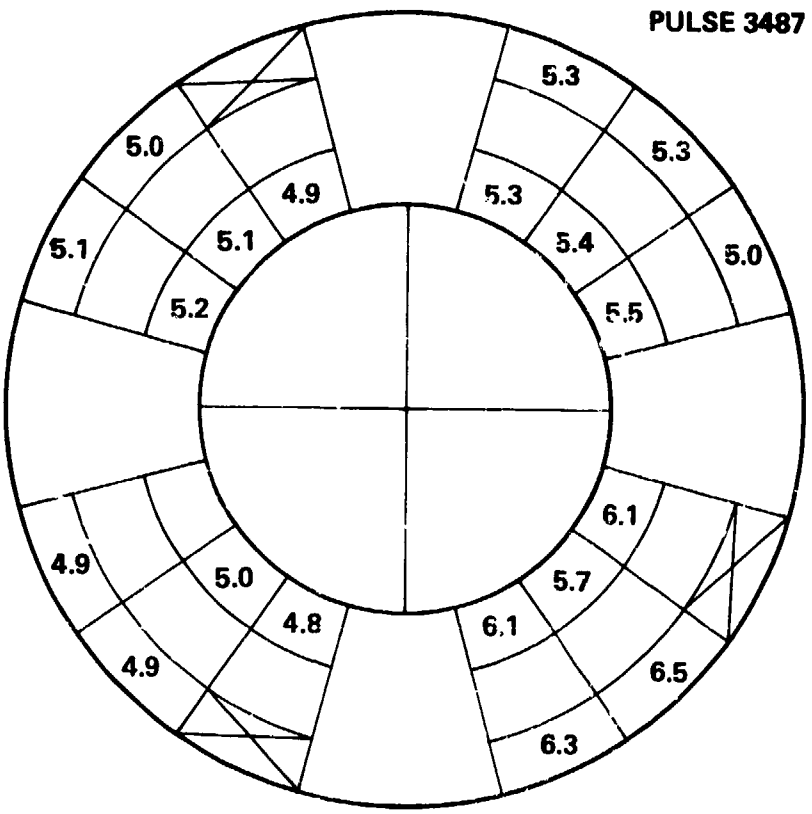
PULSE 3487
5.3
5.3
5.3
5.4
5.5
5.0
4.9
5.1
5.2
5.0
5.1
6.1
5.7
6.1
6.5
6.3
4.8
5.0
4.9
4.9

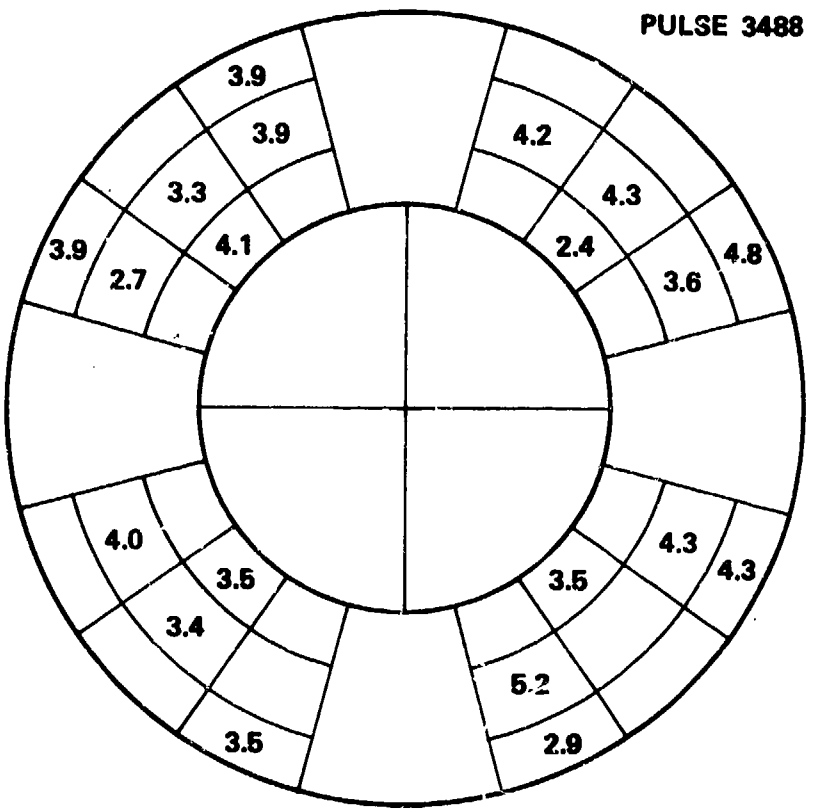
PULSE 3488
3.9
3.9
3.3
4.1
3.9
2.7
4.2
4.3
2.4
4.8
3.6
4.0
3.5
3.4
3.5
4.3
4.3
3.5
5.2
2.9

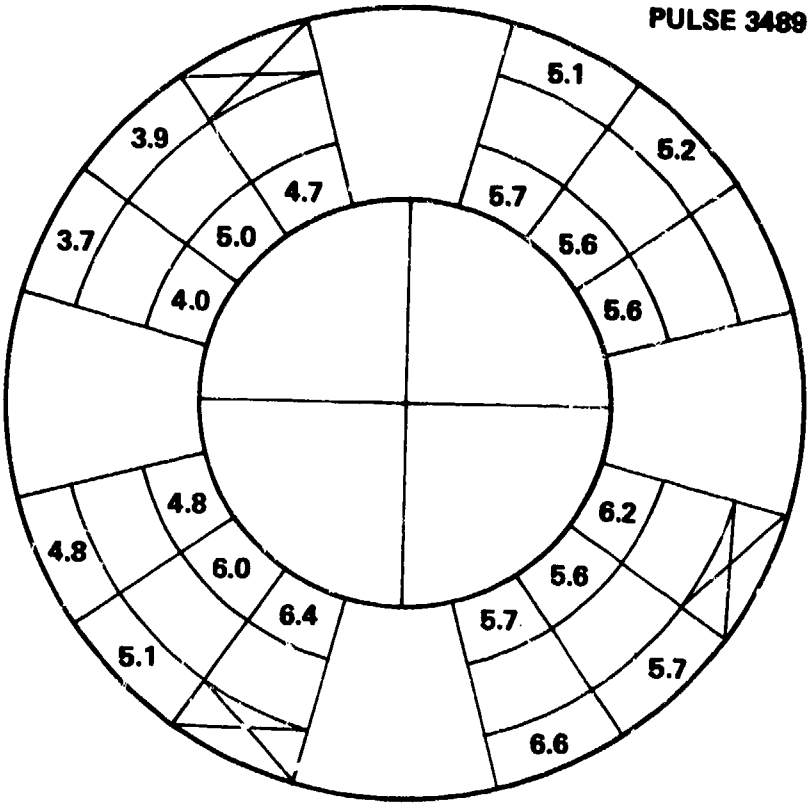
PULSE 3489
5.1
5.2
5.7
5.6
5.6
4.7
3.9
5.0
3.7
4.0
6.2
5.6
5.7
5.7
6.6
6.4
6.0
4.8
4.8
5.1

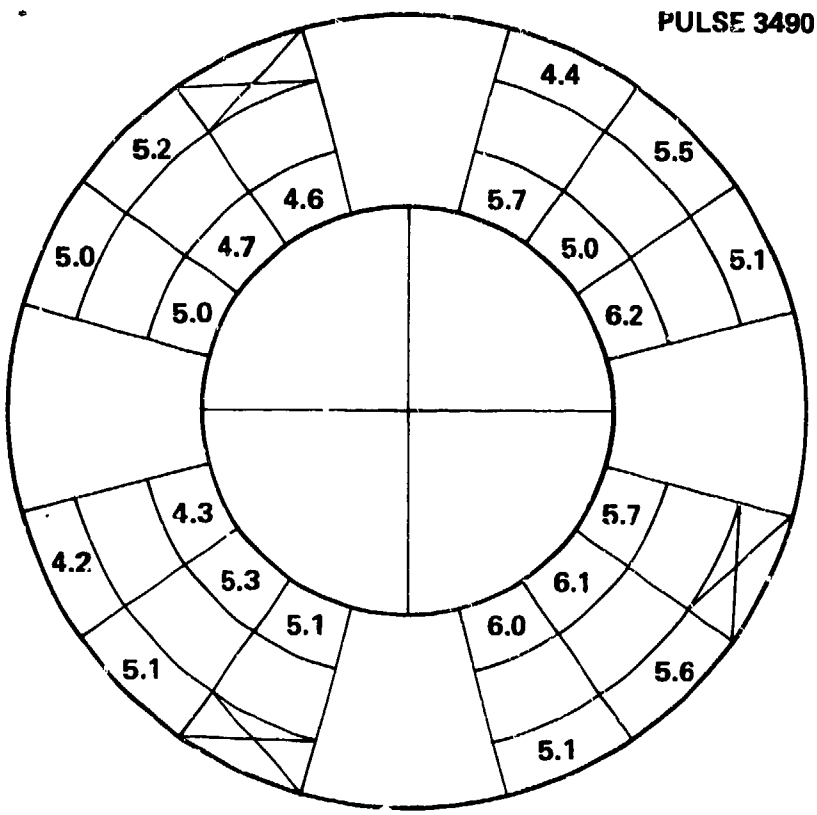
PULSE 3490
4.4
5.5
5.1
6.2
5.0
5.7
4.6
4.7
5.0
5.0
5.2
5.7
6.1
6.0
5.6
5.1
5.1
5.3
5.1
4.3
4.2

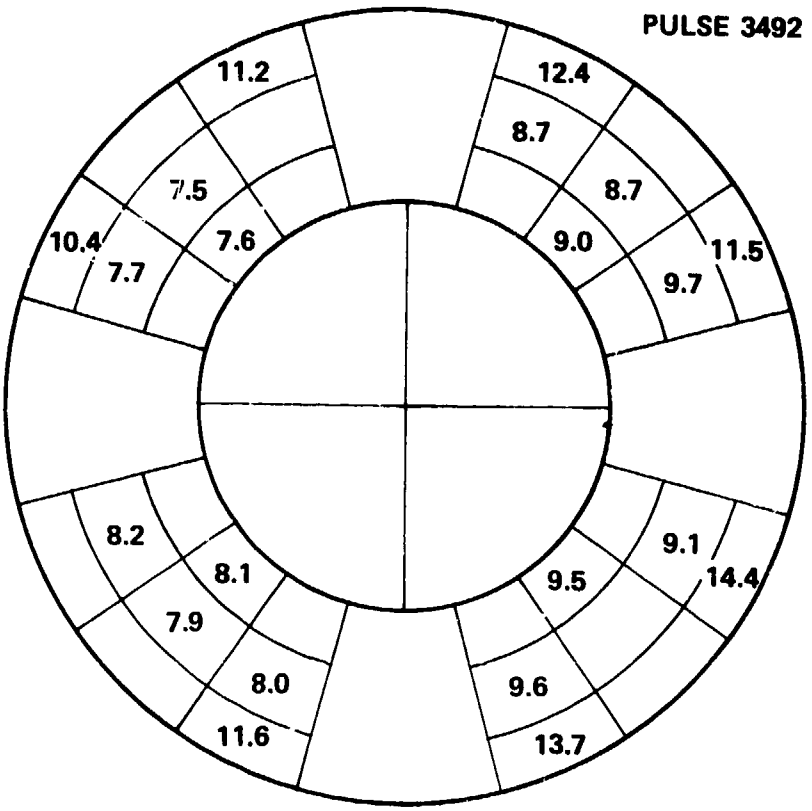
PULSE 3492
11.2
12.4
8.7
8.7
7.5
9.0
11.5
10.4
7.6
9.7
7.7
9.1
8.2
14.4
8.1
9.5
7.9
8.0
9.6
11.6
13.7

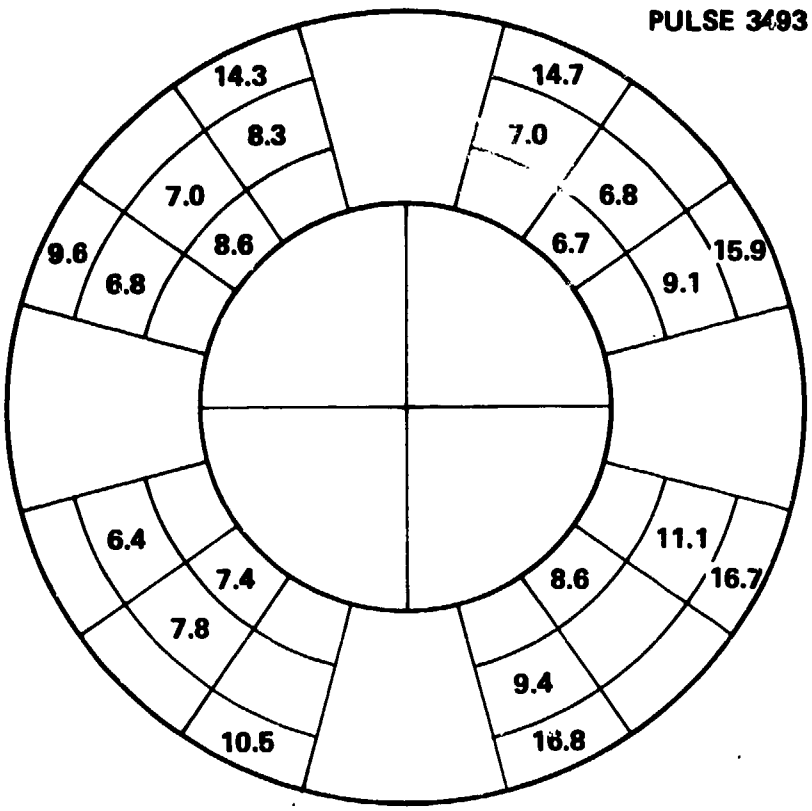
PULSE 3493
14.3
8.3
7.0
8.6
9.6
6.8
14.7
7.0
6.8
6.7
15.9
9.1
6.4
7.4
7.8
10.5
11.1
8.6
16.7
9.4
16.8

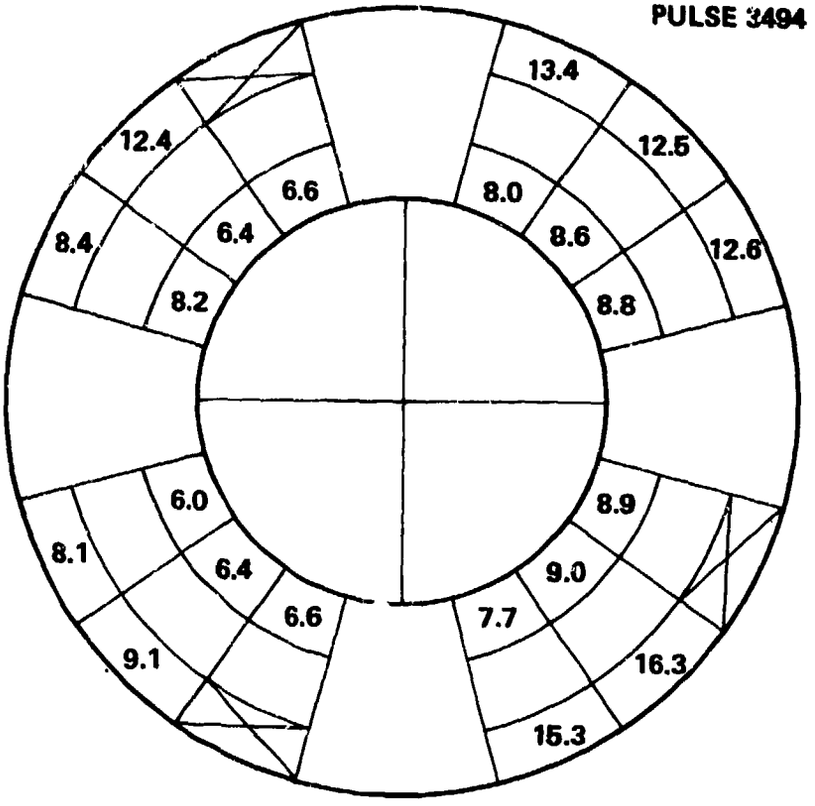
PULSE 3494
13.4
12.5
12.6
8.0
8.6
8.8
6.6
6.4
8.2
12.4
8.4
8.9
9.0
7.7
16.3
15.3
6.0
6.4
6.6
8.1
9.1

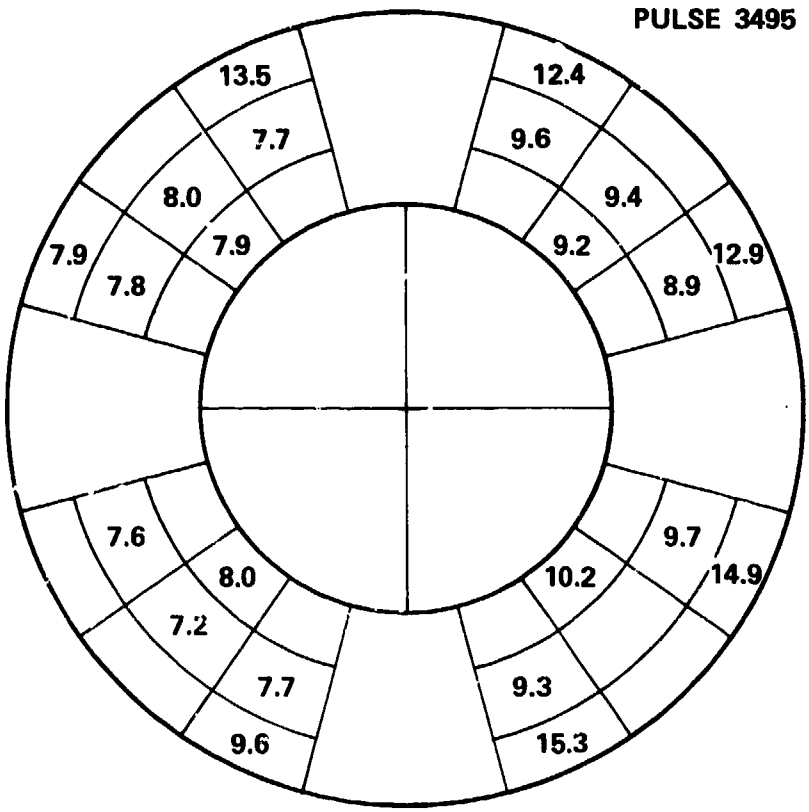
PULSE 3495
13.5
7.7
8.0
7.9
7.9
7.8
12.4
9.6
9.4
9.2
12.9
8.9
7.6
8.0
7.2
7.7
9.6
9.7
14.9
10.2
9.3
15.3

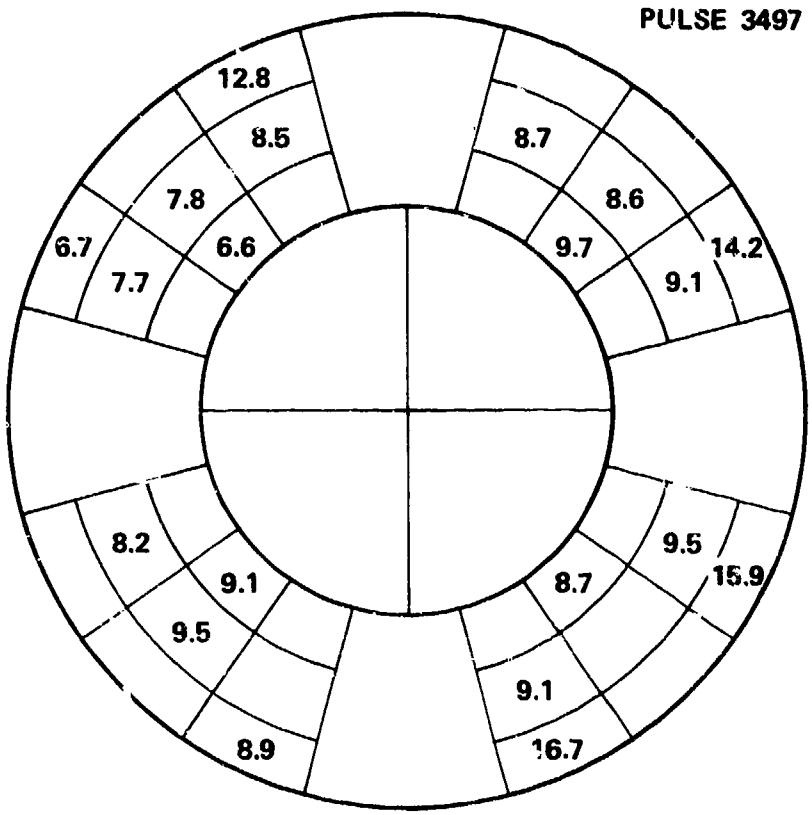
PULSE 3497
12.8
8.5
7.8
6.6
6.7
7.7
8.7
8.6
9.7
14.2
9.1
8.2
9.1
9.5
8.9
9.5
15.9
8.7
9.1
16.7

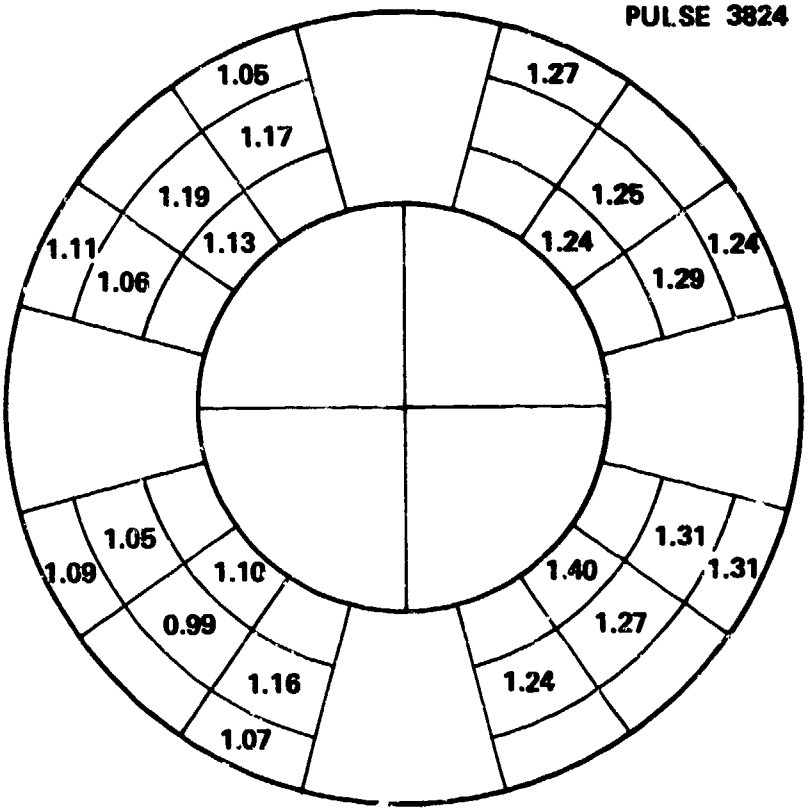
PULSE 3824
1.05
1.17
1.19
1.13
1.11
1.06
1.27
1.25
1.24
1.24
1.29
1.05
1.09
1.10
0.99
1.16
1.07
1.31
1.40
1.31
1.27
1.24

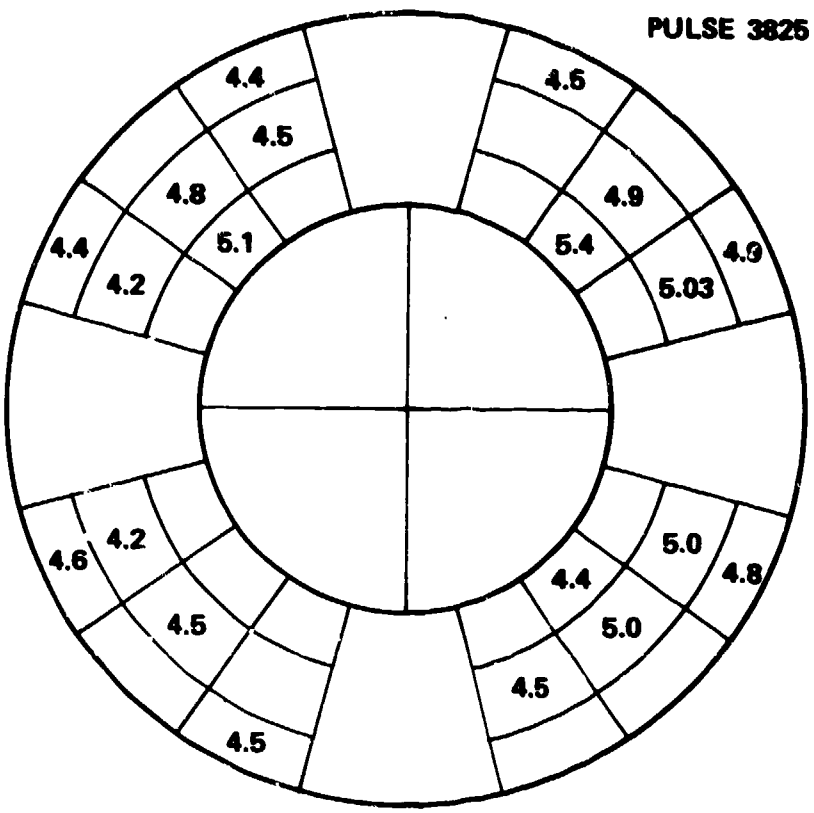
PULSE 3825
4.4
4.5
4.8
5.1
4.4
4.2
4.6
4.2
4.5
4.5
4.5
4.4
5.0
5.0
4.8
4.6
5.4
4.9
5.03
4.9

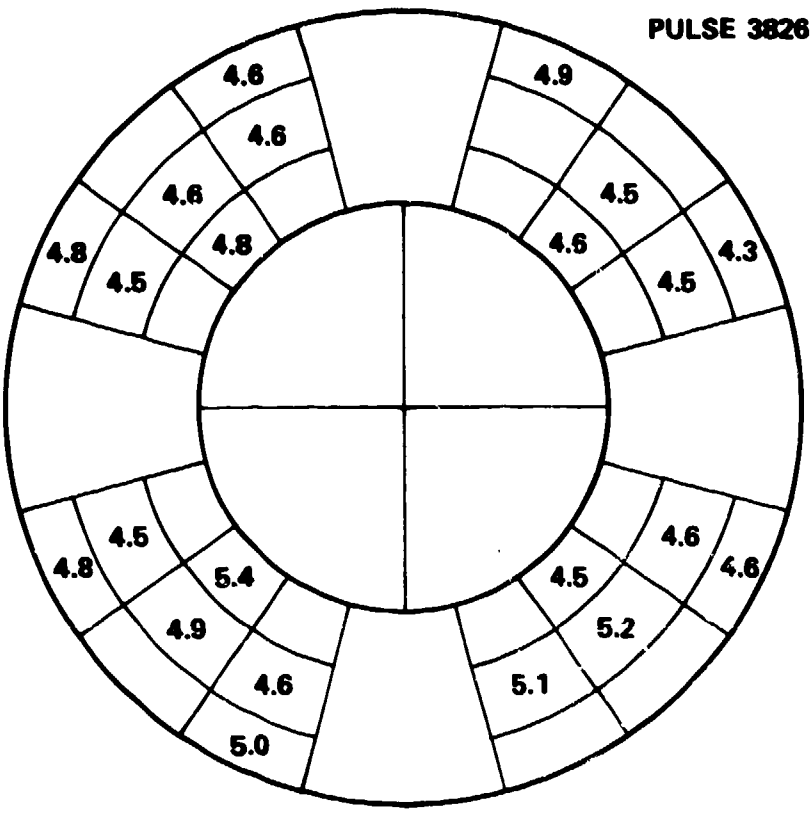
PULSE 3826
4.6
4.6
4.6
4.8
4.8
4.5
4.9
4.5
4.6
4.3
4.5
4.8
4.5
5.4
4.9
4.6
5.0
4.5
4.6
4.6
4.5
5.2
5.1

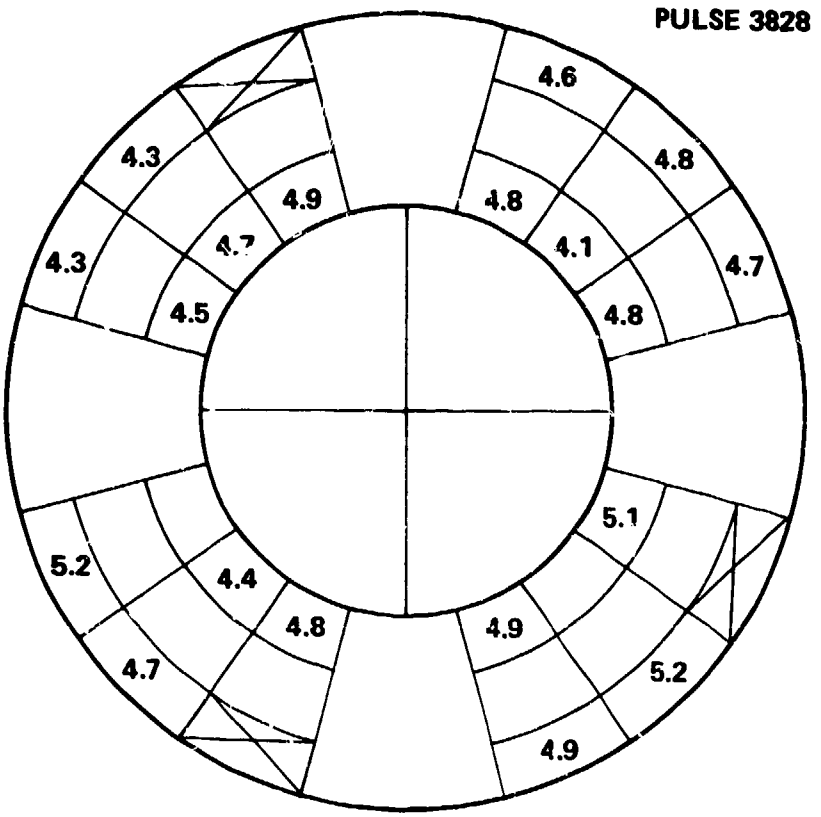
PULSE 3828
4.6
4.8
4.8
4.1
4.7
4.8
4.9
4.3
4.3
4.5
5.1
5.2
4.4
4.8
4.9
5.2
4.7
4.9

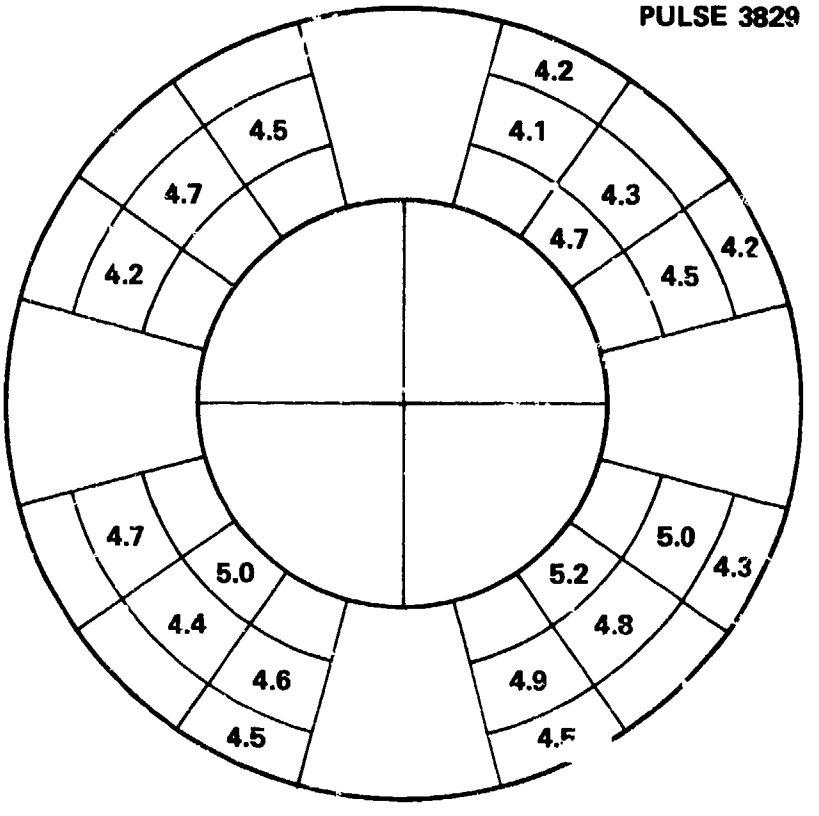
PULSE 3829
4.2
4.1
4.3
4.7
4.5
4.2
4.5
4.7
4.2
5.0
4.3
5.2
4.8
4.9
4.5
4.7
5.0
4.4
4.6
4.5

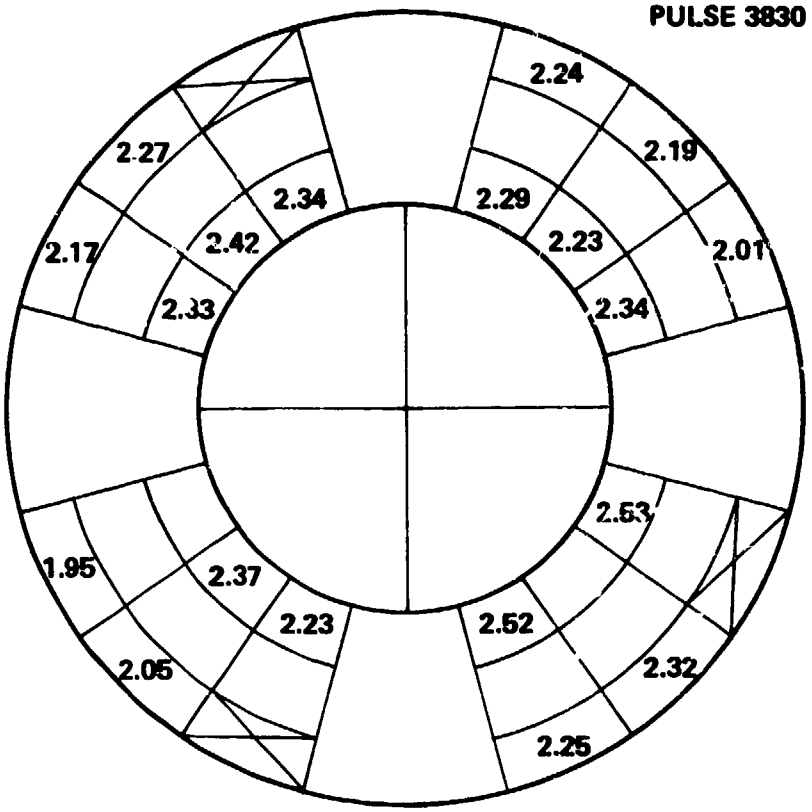
PULSE 3830
2.24
2.19
2.01
2.29
2.23
2.34
2.34
2.27
2.42
2.17
2.33
2.53
1.95
2.37
2.23
2.52
2.05
2.32
2.25

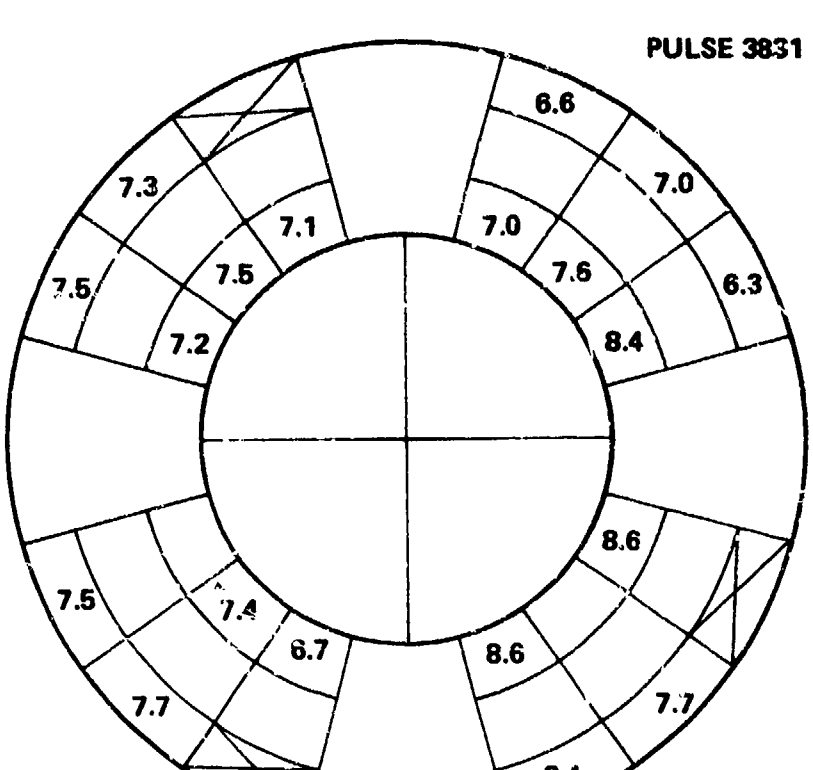

WITH RINC

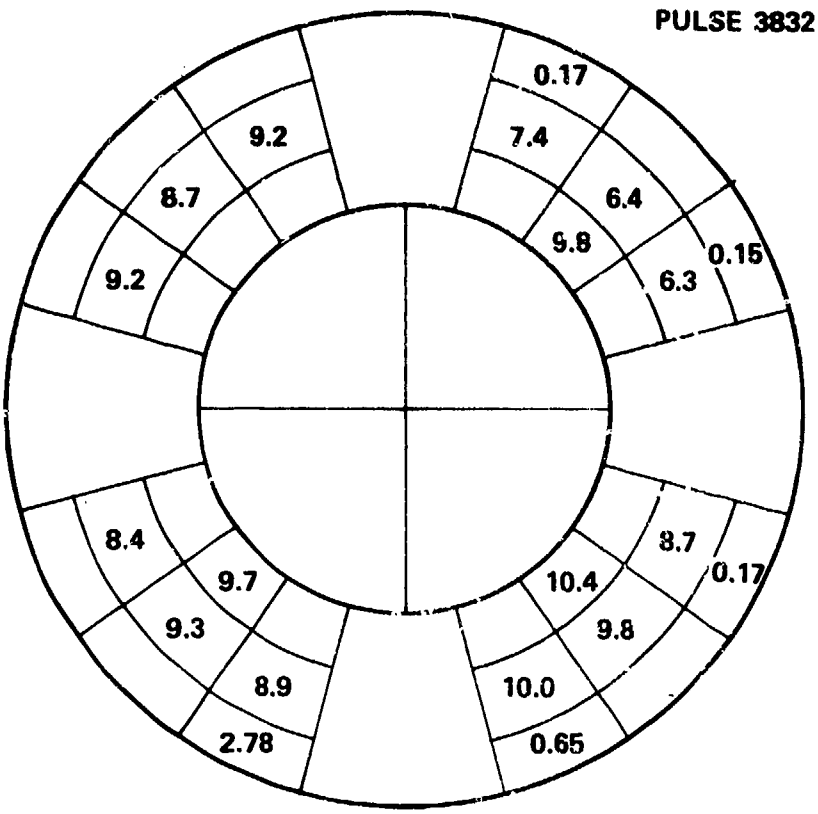
PULSE 3832
0.17
7.4
6.4
9.8
6.3
0.15
9.2
8.7
9.2
8.7
10.4
9.8
10.0
0.65
0.17
8.4
9.7
9.3
8.9
2.78

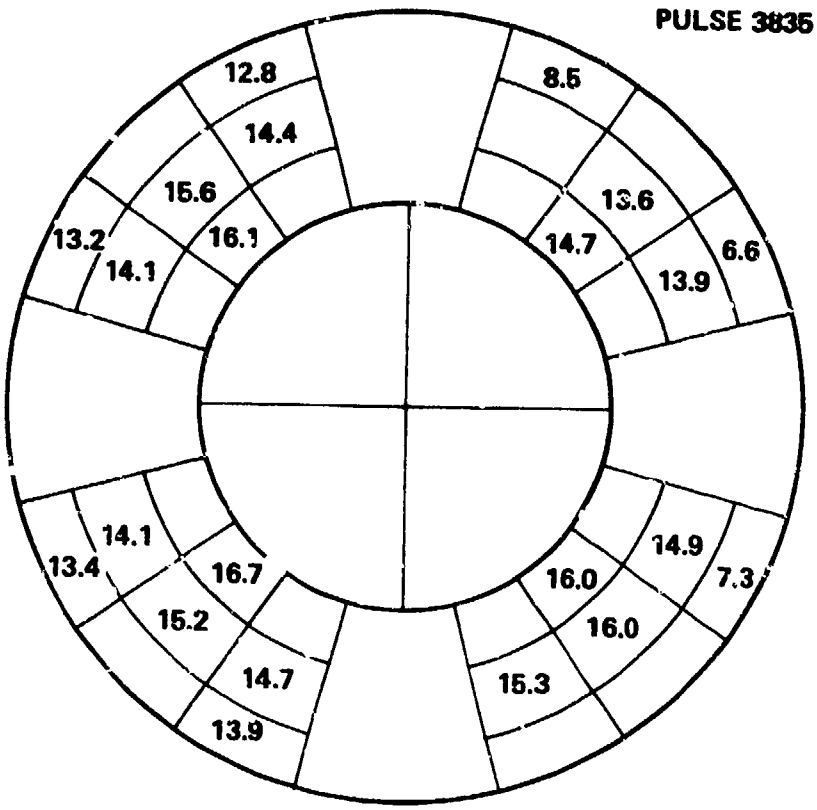
PULSE 3835
12.8
14.4
15.6
16.1
13.2
14.1
8.5
13.6
14.7
6.6
13.9
14.1
13.4
16.7
15.2
14.7
13.9
14.9
16.0
7.3
16.0
15.3

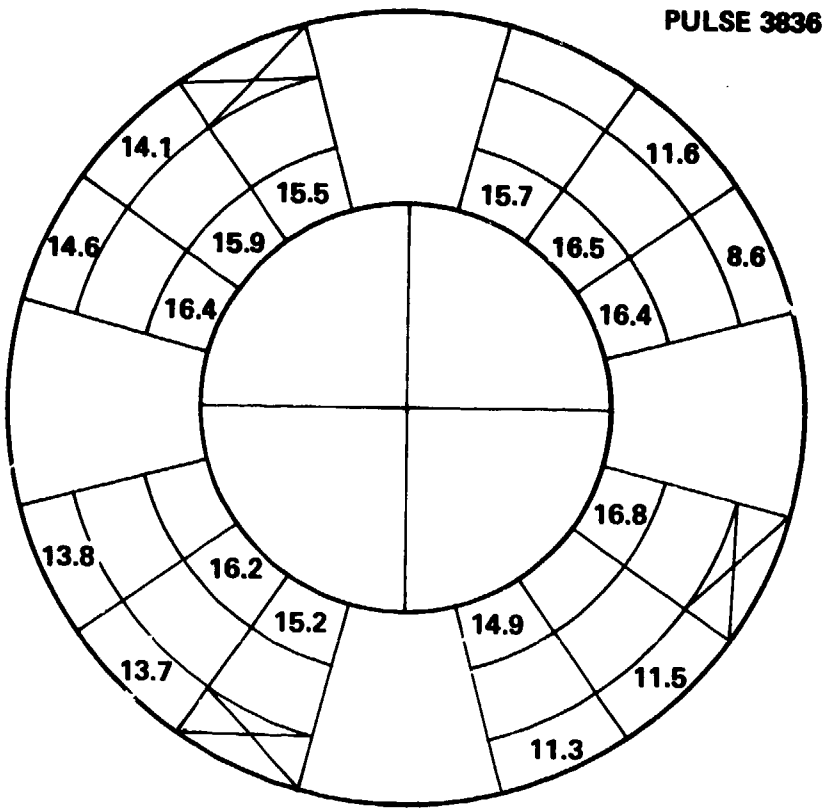
PULSE 3836
14.1
15.5
11.6
15.7
14.6
15.9
16.5
8.6
16.4
16.4
16.8
13.8
16.2
15.2
14.9
13.7
11.5
11.3

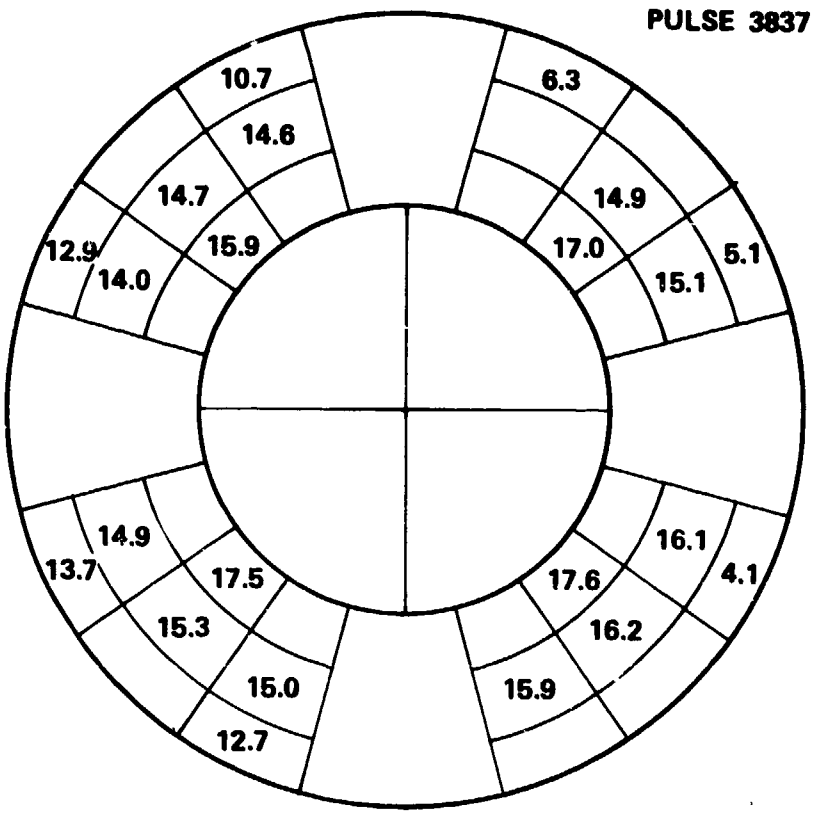
PULSE 3837
10.7
14.6
14.7
15.9
12.9
14.0
6.3
14.9
17.0
5.1
15.1
14.9
13.7
17.5
15.3
15.0
12.7
16.1
4.1
17.6
16.2
15.9

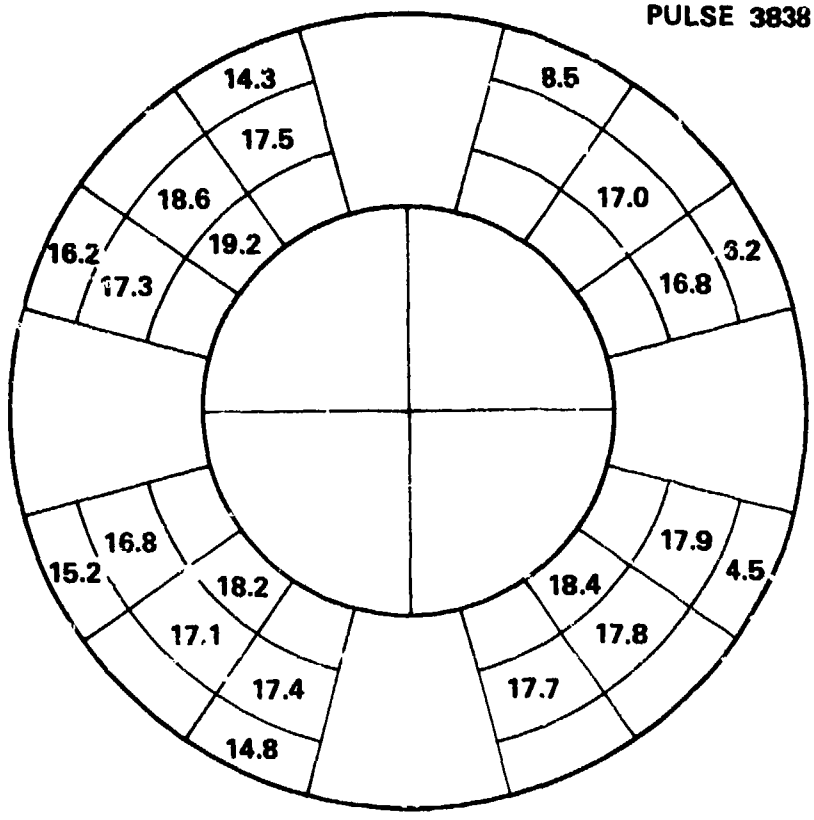
PULSE 3838
14.3
17.5
18.6
19.2
16.2
17.3
8.5
17.0
3.2
16.8
16.8
15.2
18.2
17.1
17.4
14.8
17.9
4.5
18.4
17.8
17.7

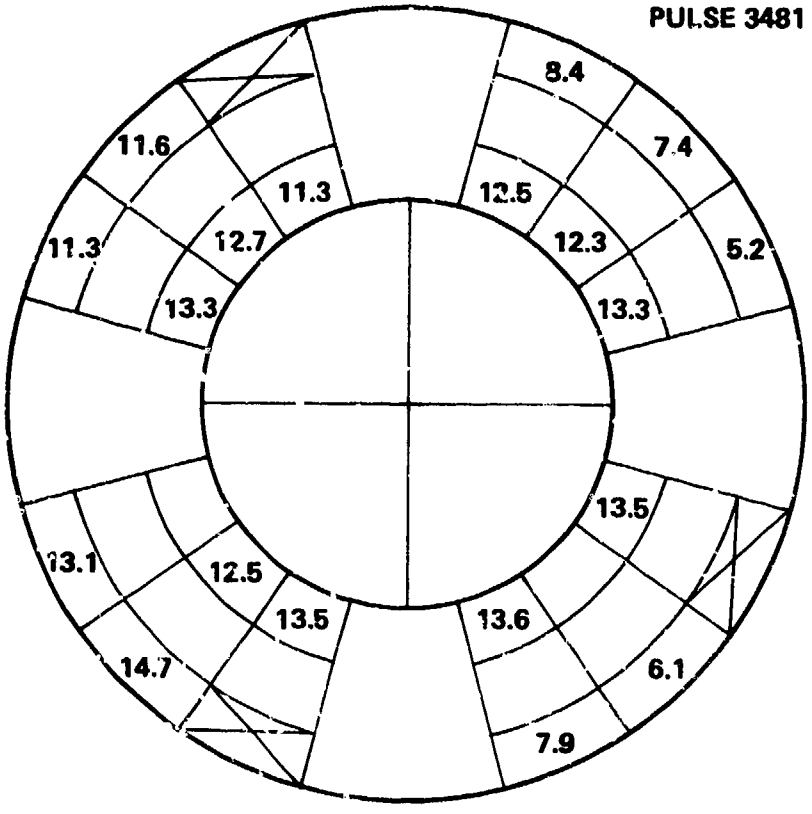
PULSE 3481
8.4
7.4
5.2
13.3
12.3
12.5
11.3
12.7
13.3
11.3
11.6
13.5
13.6
6.1
7.9
13.5
12.5
13.1
14.7

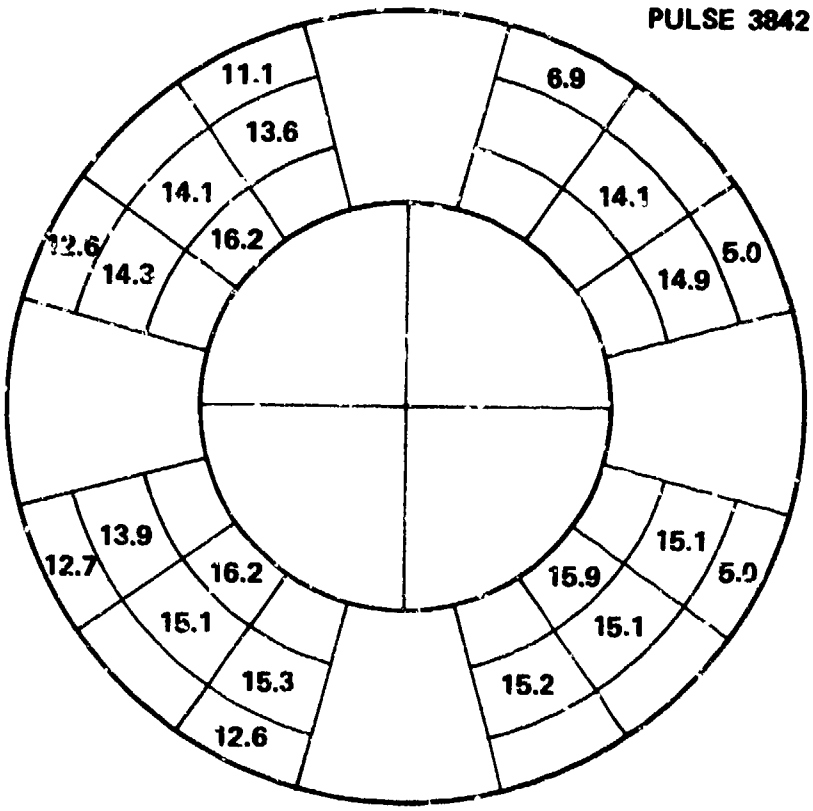
PULSE 3842
11.1
13.6
14.1
16.2
12.6
14.3
6.9
14.1
14.9
5.0
13.9
12.7
16.2
15.1
15.3
12.6
15.9
15.1
15.2
15.1
5.0

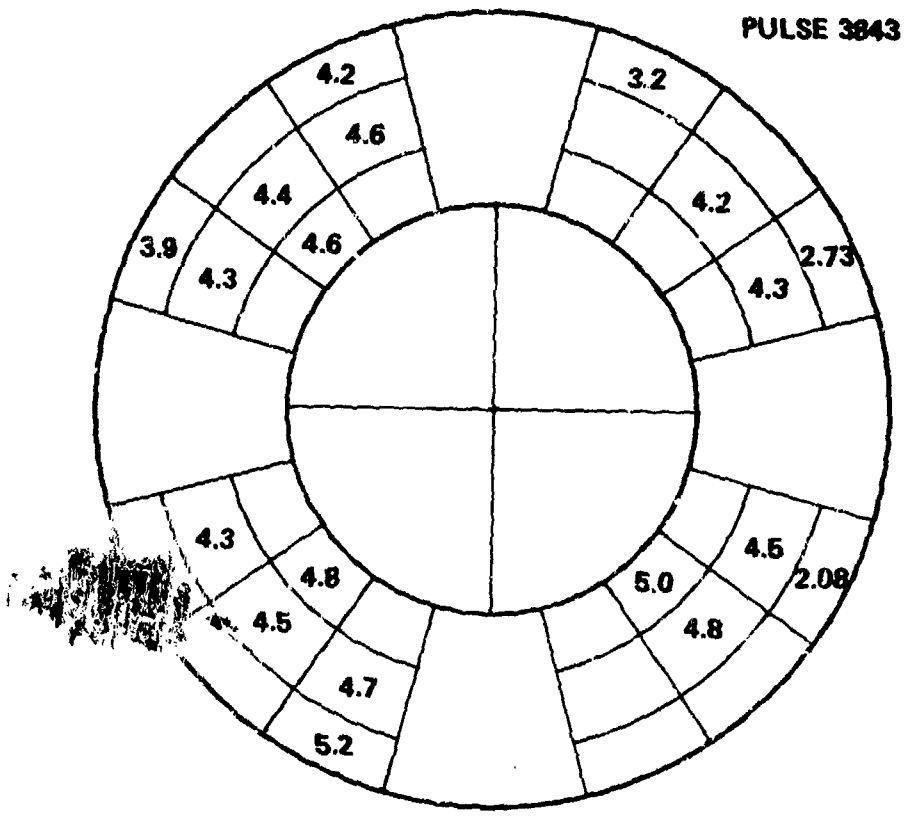
PULSE 3843
4.2
4.6
4.4
3.9
4.6
4.3
3.2
4.2
2.73
4.3
4.3
4.8
4.5
4.7
5.2
5.0
4.5
2.08
4.8

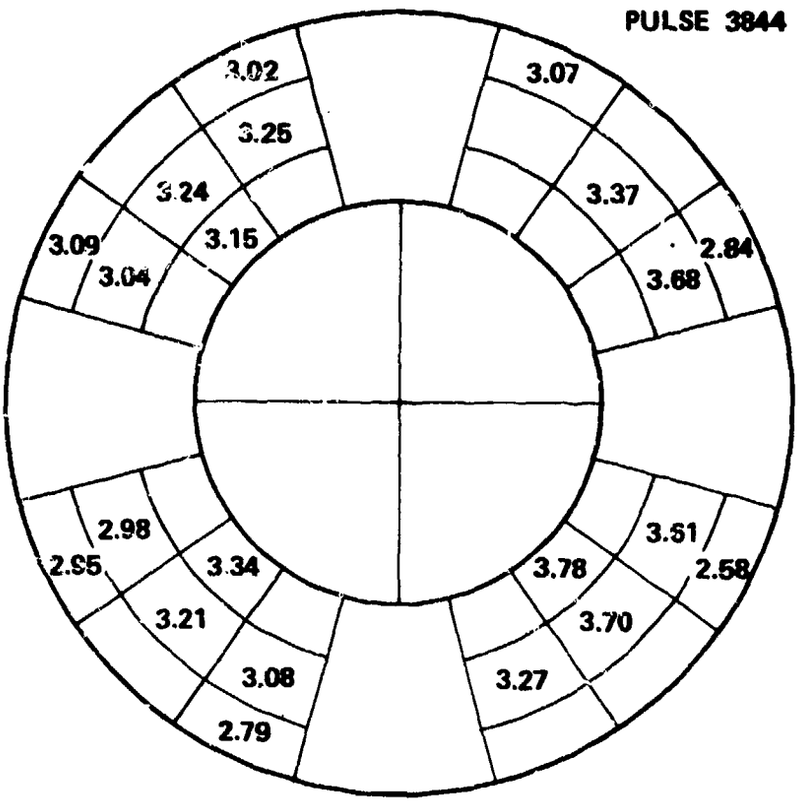
PULSE 3844
3.02
3.25
3.24
3.15
3.09
3.04
3.07
3.37
2.84
3.68
2.98
2.95
3.34
3.21
3.08
2.79
3.51
2.58
3.78
3.70
3.27

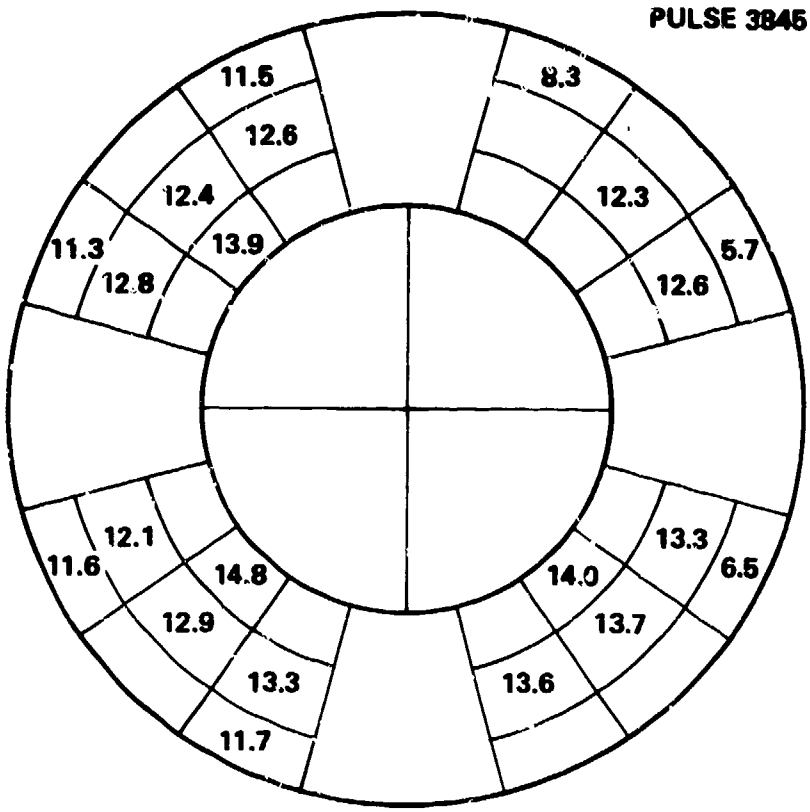
PULSE 3845
11.5
12.6
12.4
13.9
11.3
12.8
8.3
12.3
5.7
12.6
12.1
11.6
14.8
12.9
13.3
11.7
13.3
14.0
6.5
13.7
13.6

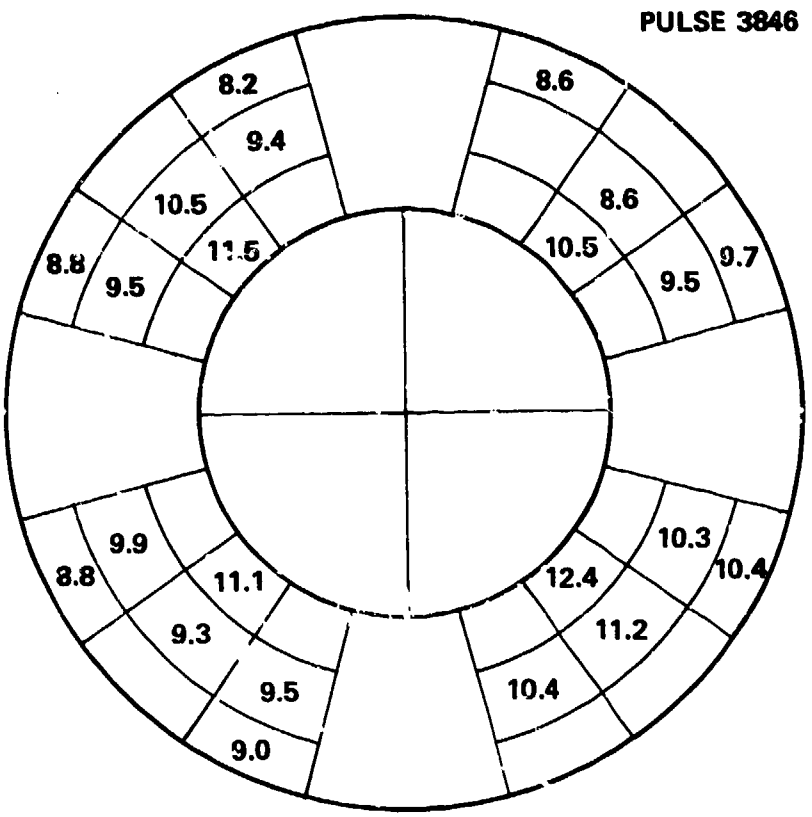
PULSE 3846
8.2
9.4
10.5
11.5
8.8
9.5
8.6
8.6
10.5
9.5
9.7
9.9
8.8
11.1
9.3
9.5
9.0
10.3
10.4
12.4
11.2
10.4

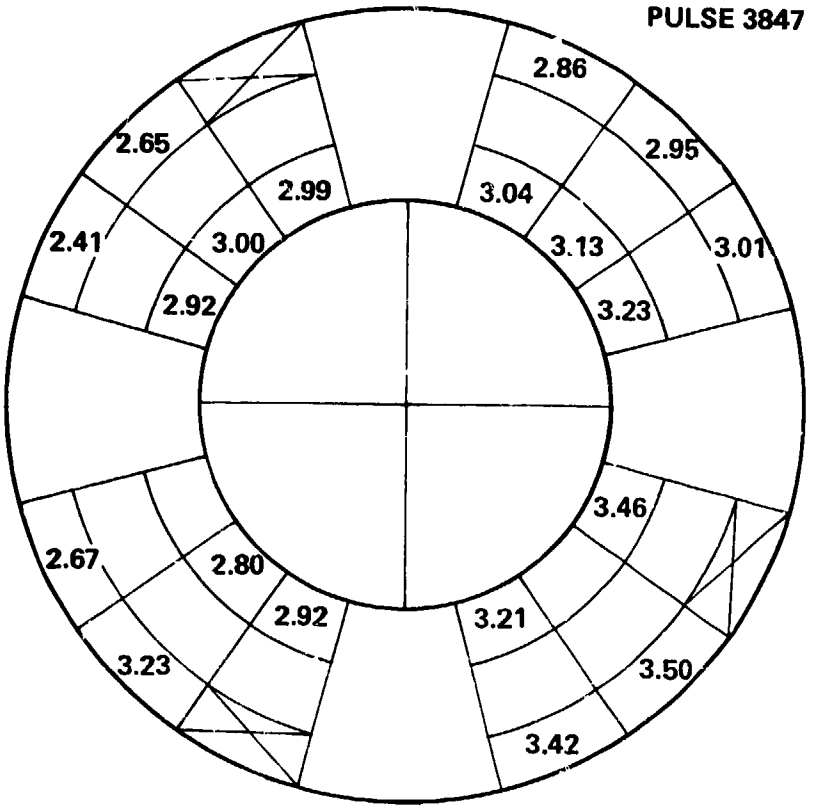
PULSE 3847
2.86
2.95
3.01
3.04
3.13
3.23
2.99
2.65
2.41
3.00
2.92
3.46
3.21
3.50
3.42
2.67
2.80
2.92
3.23

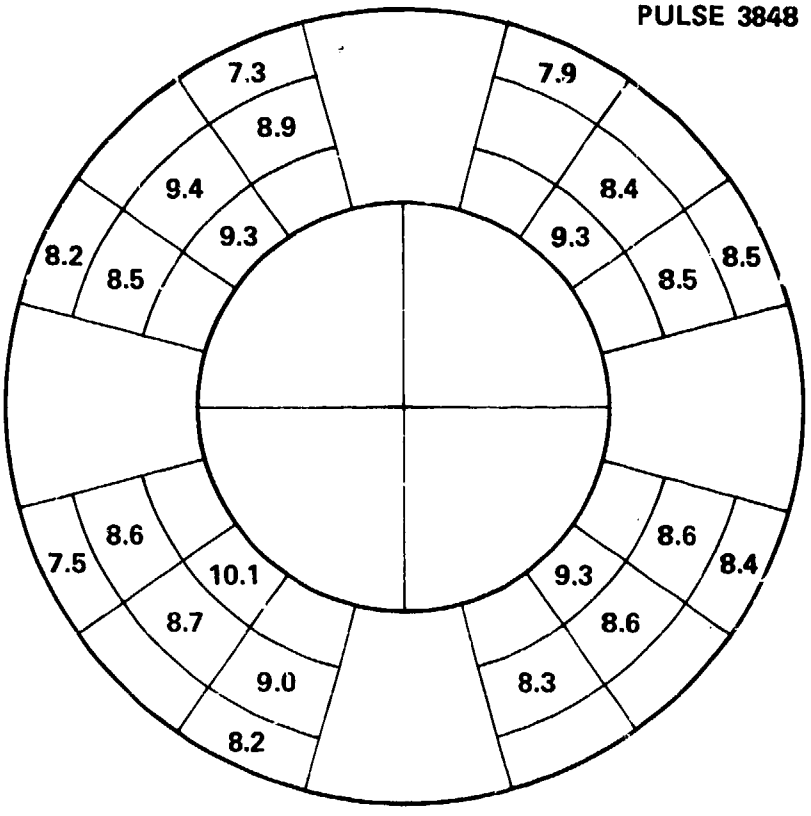
PULSE 3848
7.3
8.9
9.4
9.3
8.2
8.5
7.9
8.4
9.3
8.5
8.5
8.6
7.5
10.1
8.7
9.0
8.2
8.6
9.3
8.6
8.4
8.3

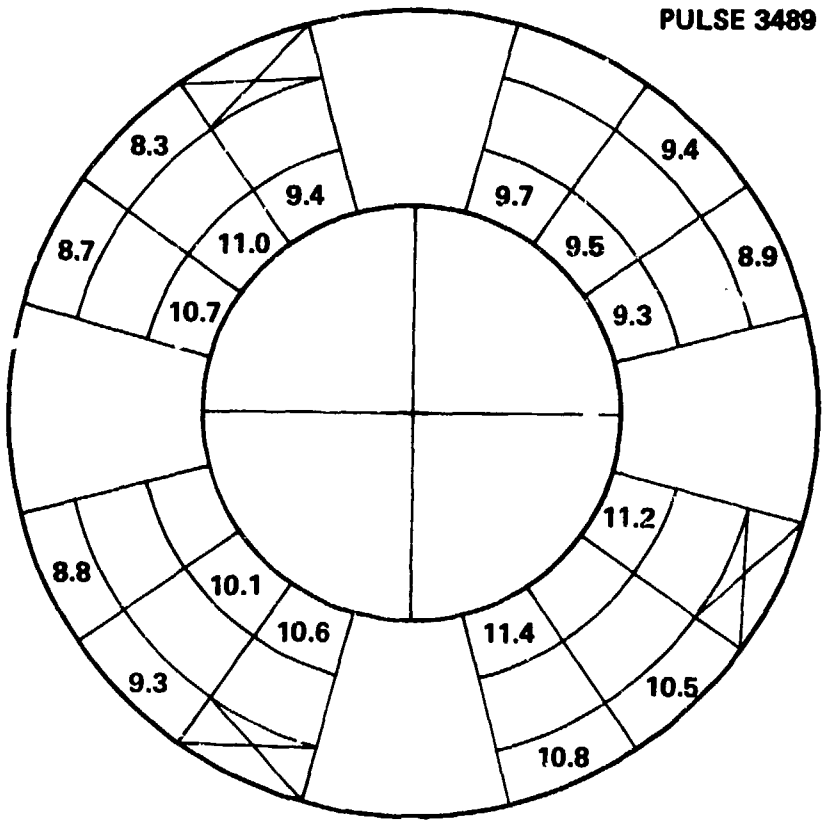
PULSE 3489
8.3
9.4
8.7
11.0
10.7
9.7
9.4
9.5
8.9
9.3
11.2
8.8
10.1
10.6
9.3
11.4
10.5
10.8

APPENDIX A-2

HIGH RESOLUTION FLUENCE MAPS

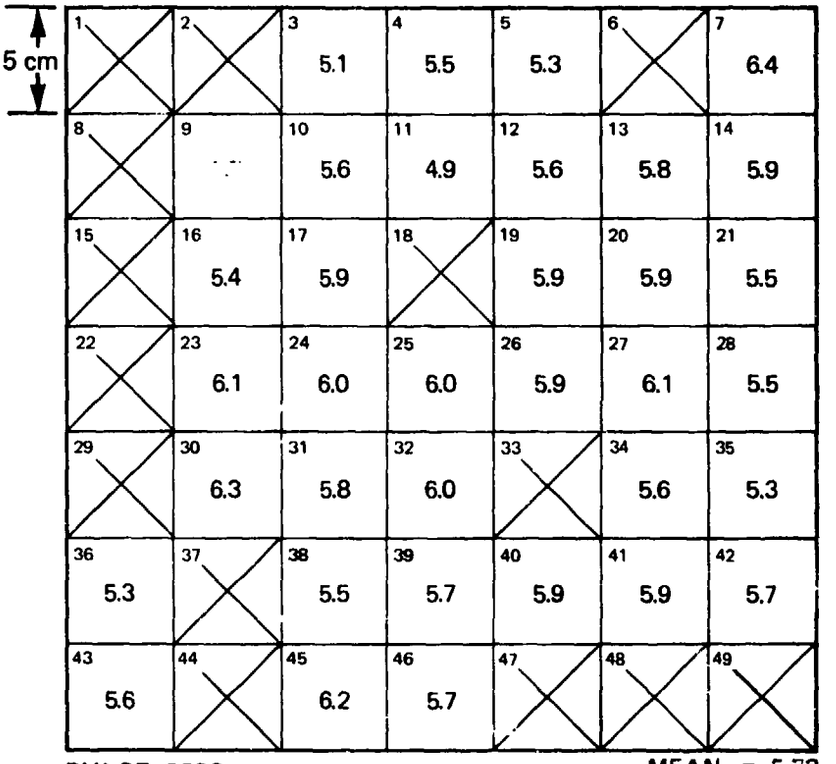

PULSE 3839

MEAN = 5.73
MSD = 0.33

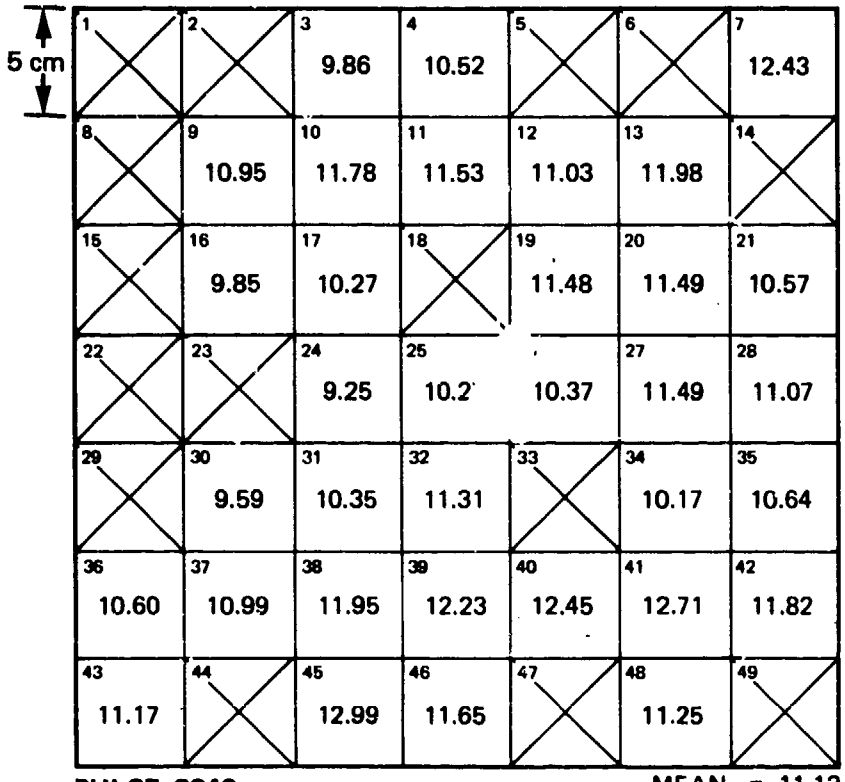

PULSE 3840

MEAN = 11.12
MSD = 0.92

APPENDIX B-1

DEPOSITION PROFILES MEASURED BY
OUTER FOIL STACK CALORIMETER AND CALCULATED FROM
DIODE VOLTAGE AND CURRENT WAVEFORMS.
GRAPHITE FOIL DENSITY WAS 1.75 GM/CM^3.
ALL CALCULATIONS ASSUMED ELECTRONS WERE NORMALLY INCIDENT.

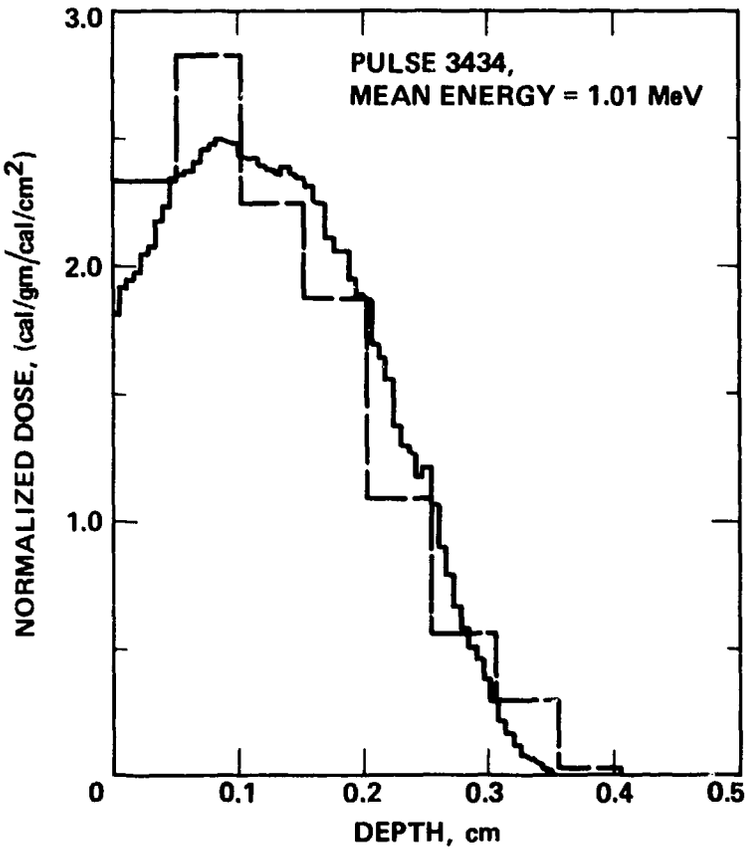
PULSE 3434,
MEAN ENERGY = 1.01 MeV
NORMALIZED DOSE, (cal/gm/cal/cm²)
3.0
2.0
1.0
0
0.1
0.2
0.3
0.4
0.5
DEPTH, cm

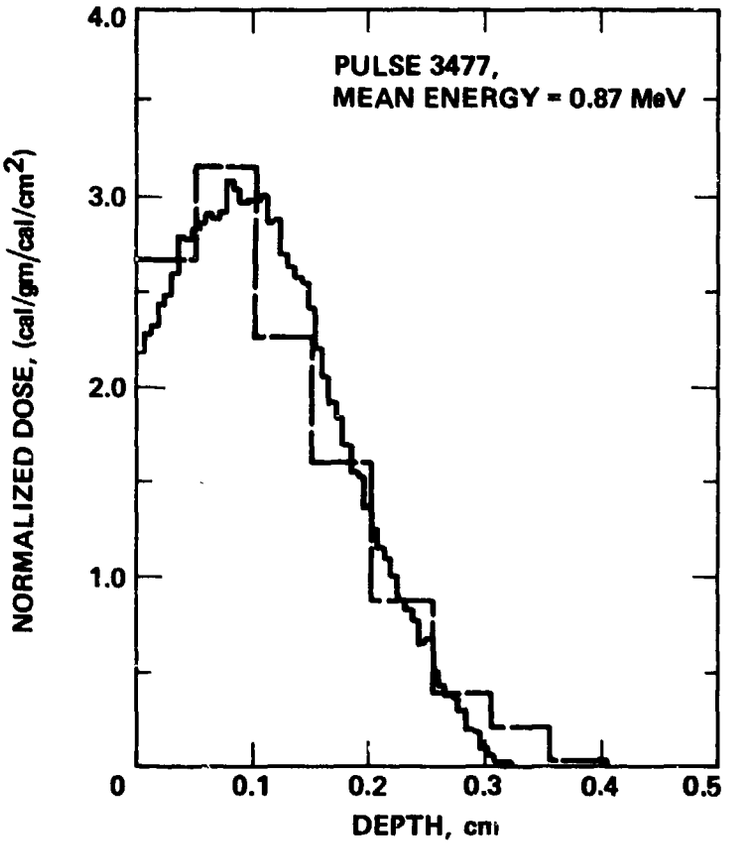
PULSE 3477,
MEAN ENERGY = 0.87 MeV
NORMALIZED DOSE, (cal/gm/cal/cm^2)
4.0
3.0
2.0
1.0
0
0.1
0.2
0.3
0.4
0.5
DEPTH, cm

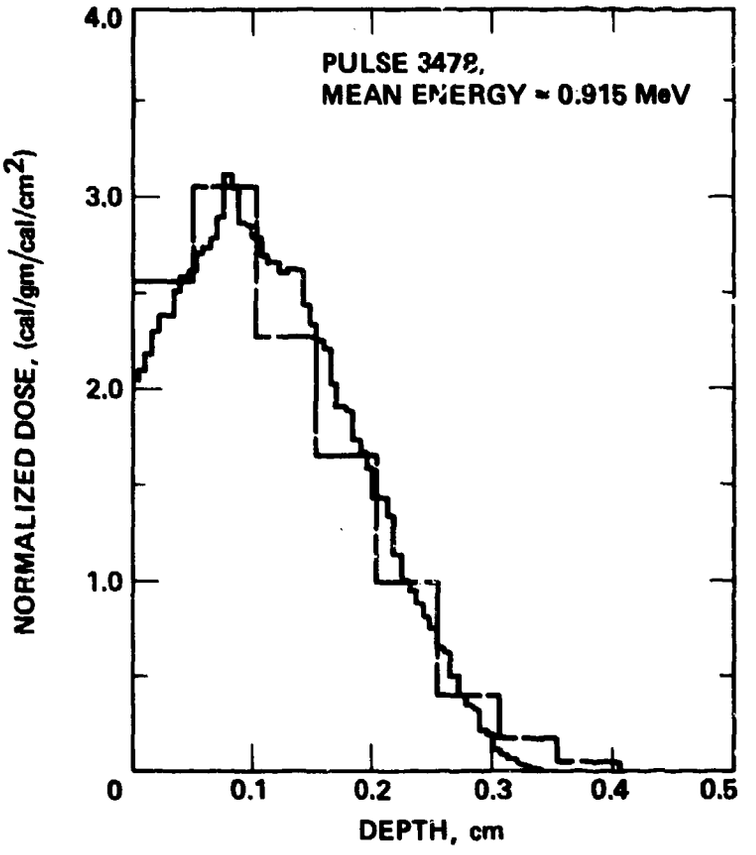
PULSE 3478,
MEAN ENERGY ≈ 0.915 MeV
NORMALIZED DOSE, (cal/gm/cal/cm^2)
4.0
3.0
2.0
1.0
0
0.1
0.2
0.3
0.4
0.5
DEPTH, cm

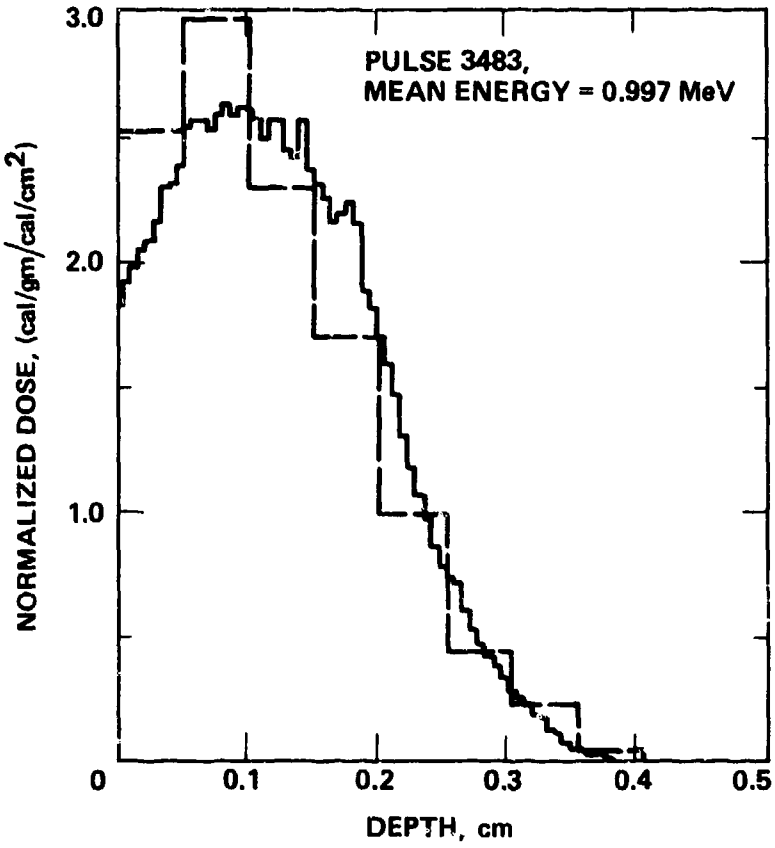
PULSE 3483,
MEAN ENERGY = 0.997 MeV
NORMALIZED DOSE, (cal/gm/cal/cm²)
3.0
2.0
1.0
0
0.1
0.2
0.3
0.4
0.5
DEPTH, cm

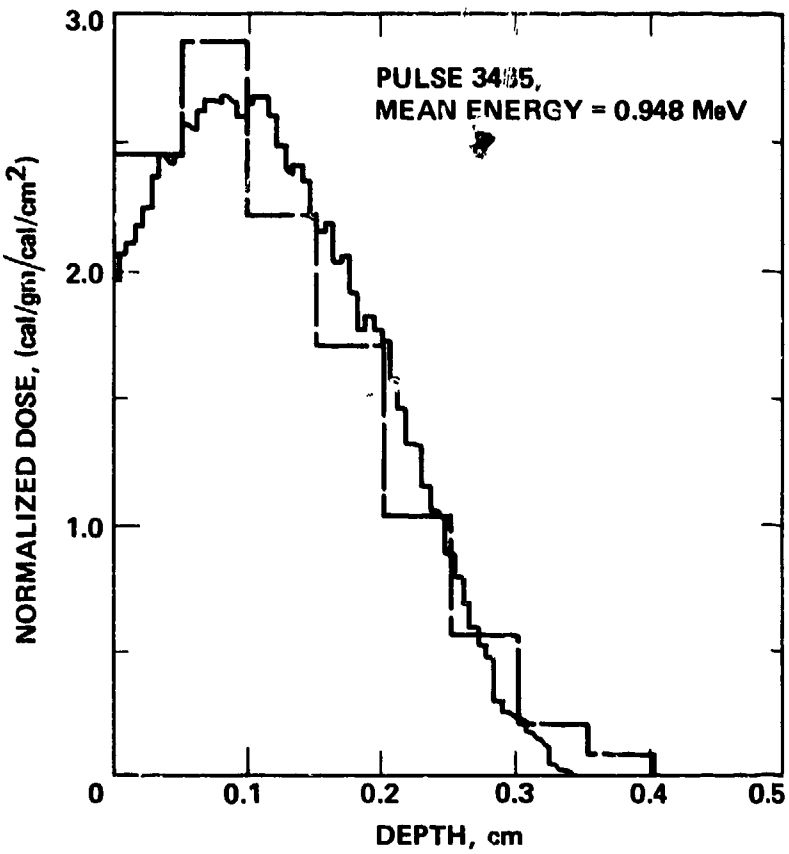
PULSE 3485,
MEAN ENERGY = 0.948 MeV
NORMALIZED DOSE, (cal/gm)/(cal/cm²)
3.0
2.0
1.0
0
0.1
0.2
0.3
0.4
0.5
DEPTH, cm

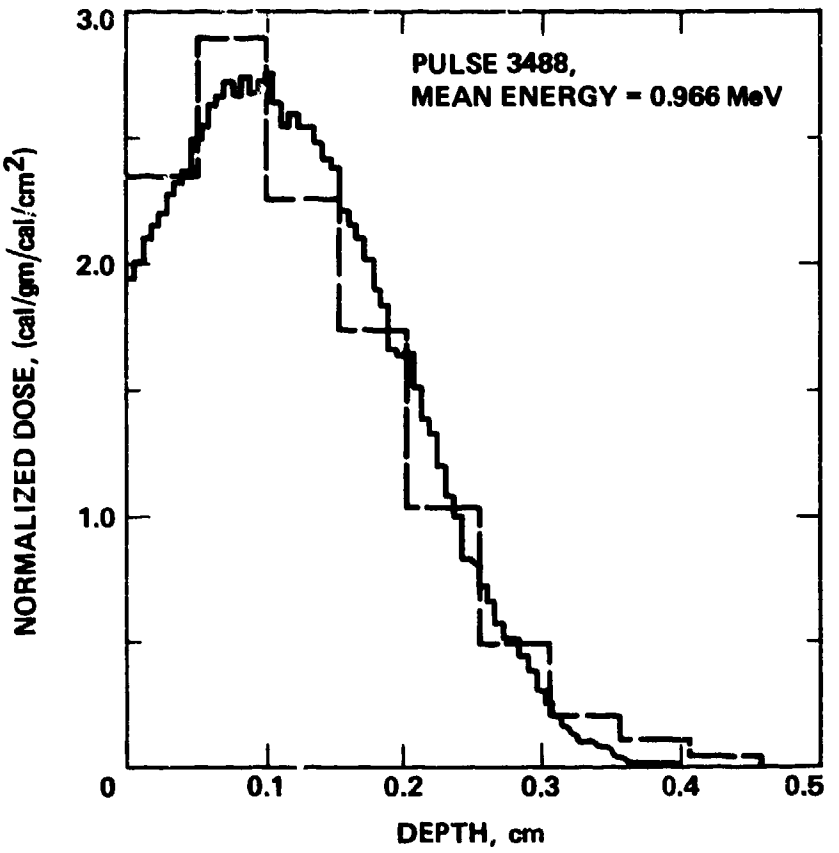
PULSE 3488,
MEAN ENERGY = 0.966 MeV
NORMALIZED DOSE, (cal/gm/cal/cm²)
3.0
2.0
1.0
0
0.1
0.2
0.3
0.4
0.5
DEPTH, cm

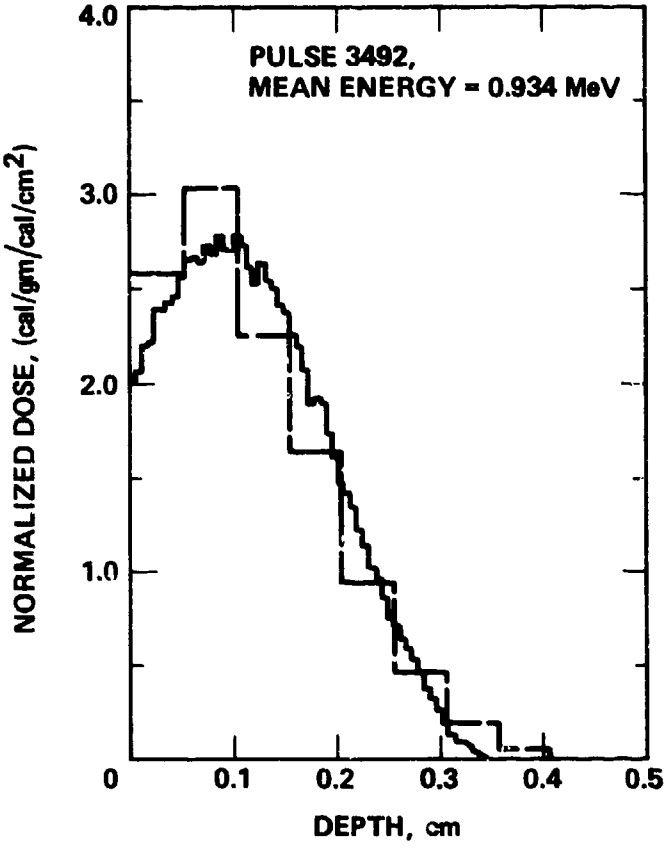
PULSE 3492,
MEAN ENERGY = 0.934 MeV
NORMALIZED DOSE, (cal/gm/cal/cm²)
4.0
3.0
2.0
1.0
0
0.1
0.2
0.3
0.4
0.5
DEPTH, cm

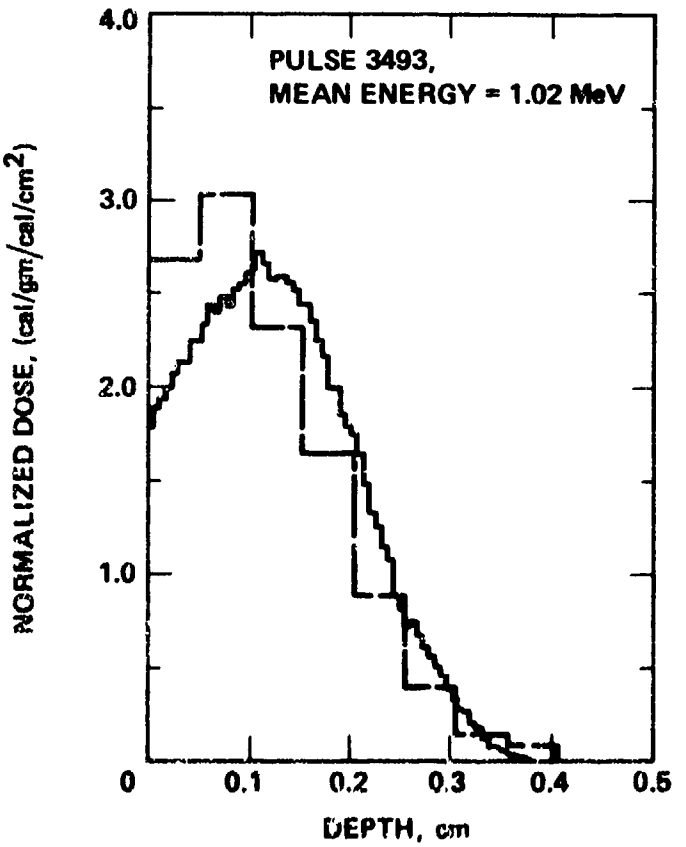
PULSE 3493,
MEAN ENERGY = 1.02 MeV
NORMALIZED DOSE, (cal/gm/cal/cm²)
4.0
3.0
2.0
1.0
0
0.1
0.2
0.3
0.4
0.5
DEPTH, cm

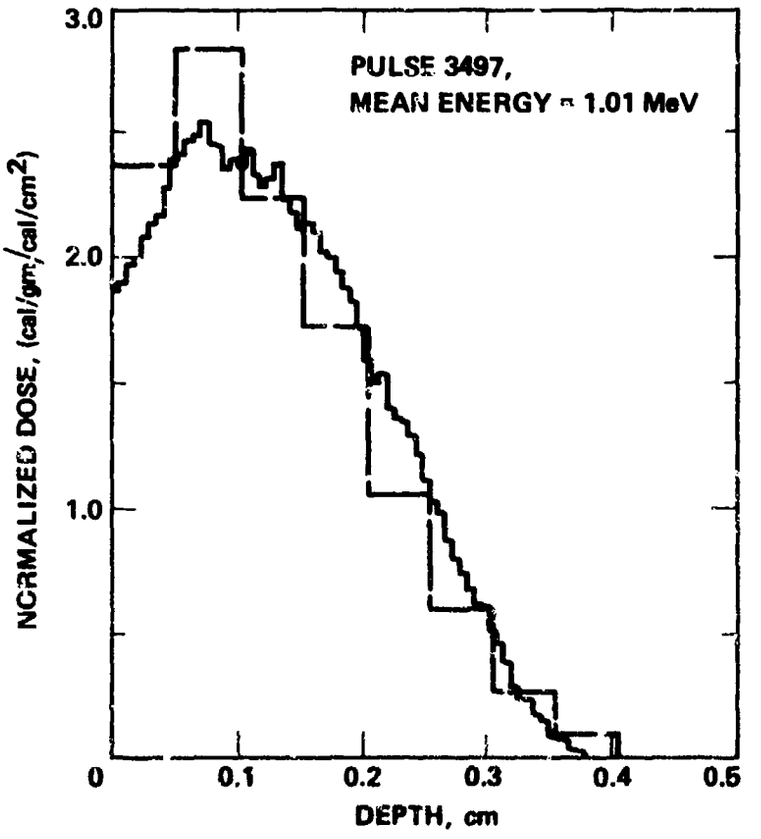
PULSE 3497,
MEAN ENERGY = 1.01 MeV
NORMALIZED DOSE, (cal/gm)/(cal/cm²)
3.0
2.0
1.0
0
0.1
0.2
0.3
0.4
0.5
DEPTH, cm

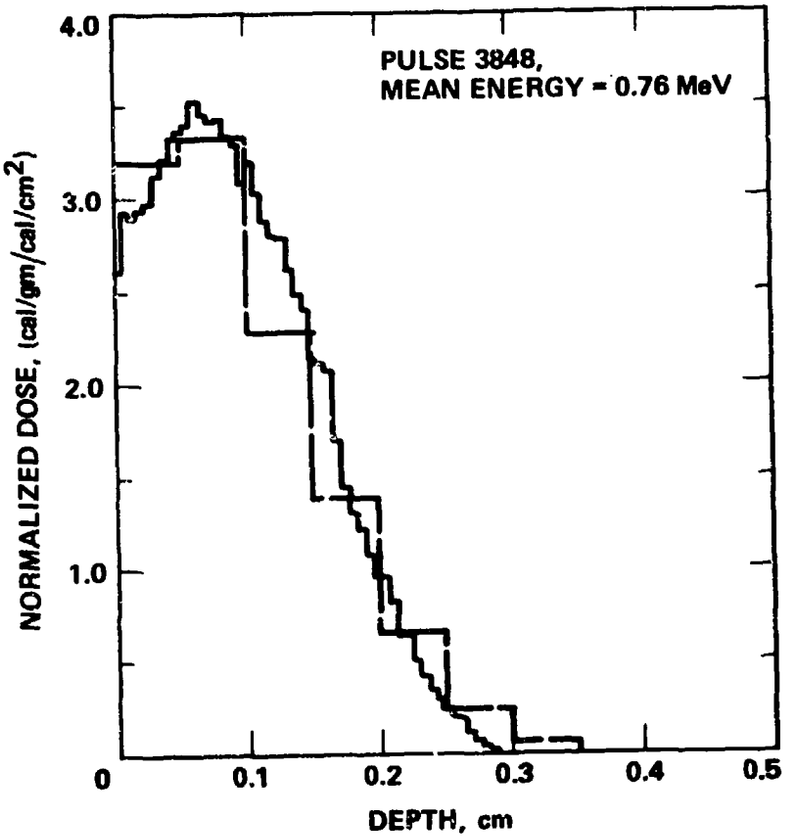
PULSE 3848,
MEAN ENERGY = 0.76 MeV
NORMALIZED DOSE, (cal/gm/cal/cm²)
4.0
3.0
2.0
1.0
0
0.1
0.2
0.3
0.4
0.5
DEPTH, cm

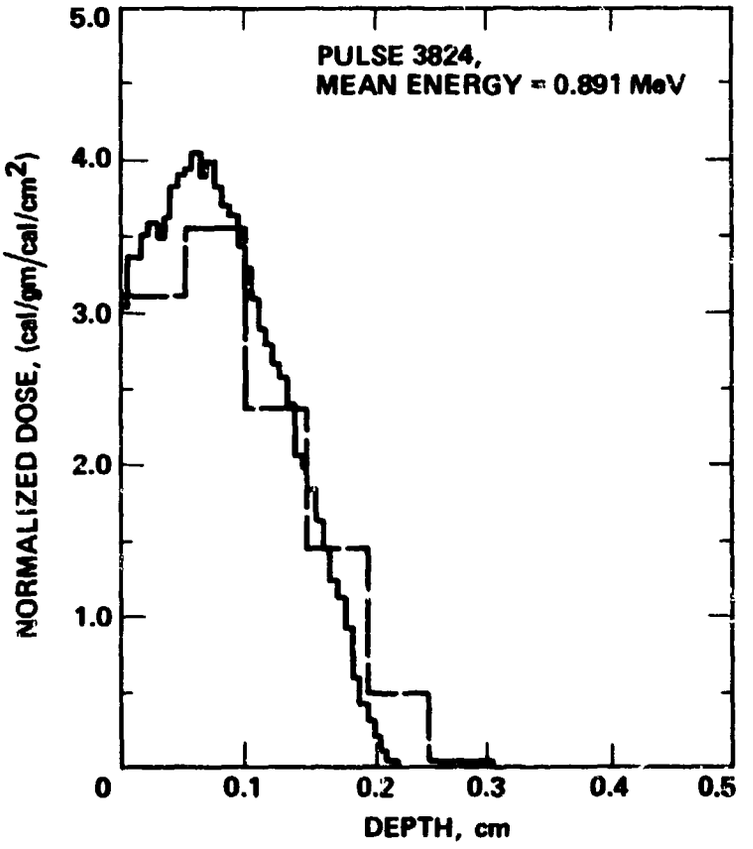
PULSE 3824,
MEAN ENERGY = 0.891 MeV
NORMALIZED DOSE, (cal/gm/cal/cm²)
5.0
4.0
3.0
2.0
1.0
0
0.1
0.2
0.3
0.4
0.5
DEPTH, cm

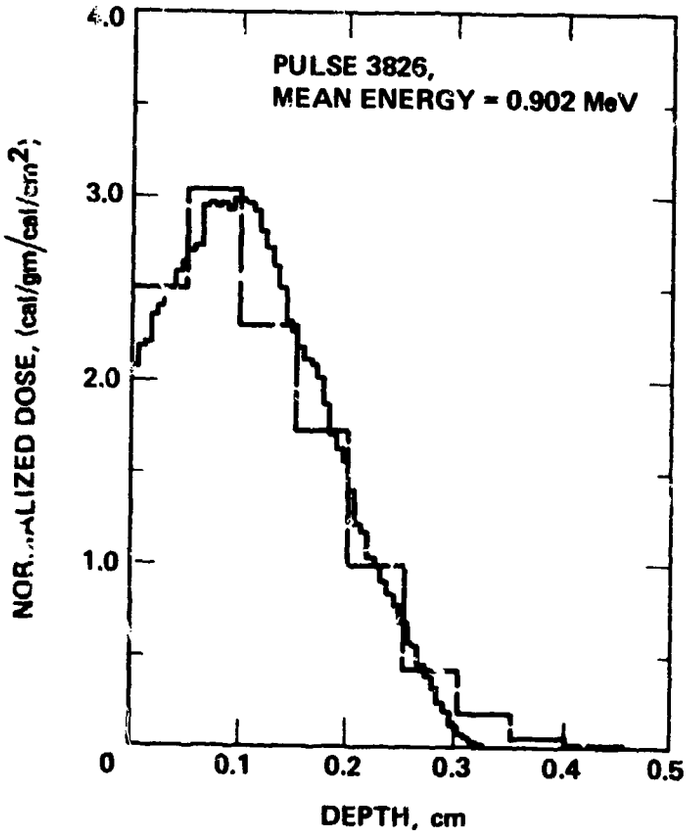
PULSE 3826,
MEAN ENERGY = 0.902 MeV
NOR...ALIZED DOSE, (cal/gm/cal/cm²)
4.0
3.0
2.0
1.0
0
0.1
0.2
0.3
0.4
0.5
DEPTH, cm

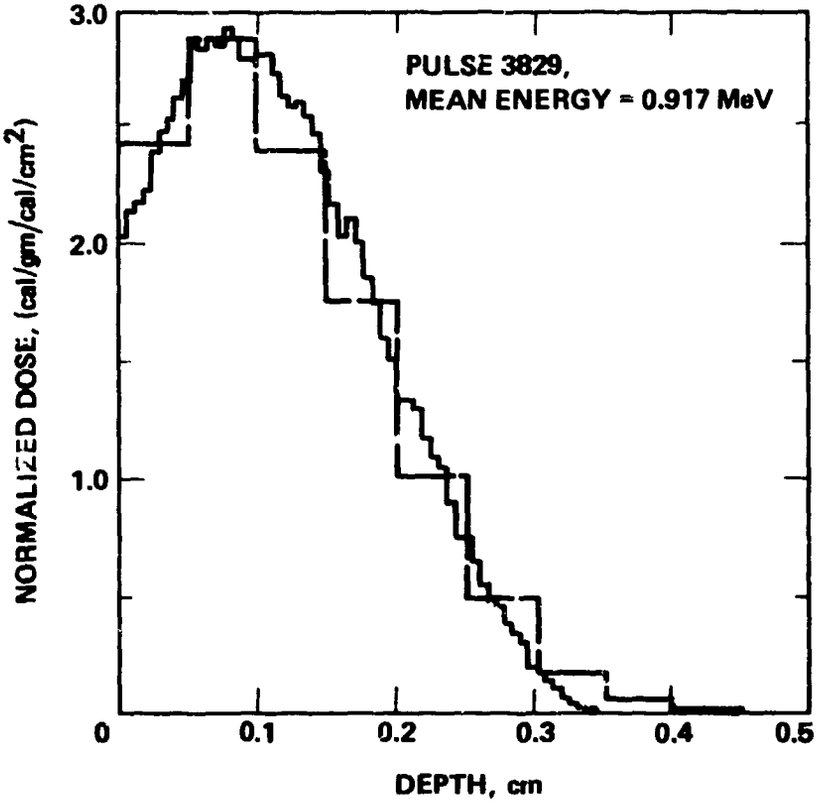
PULSE 3829,
MEAN ENERGY = 0.917 MeV
NORMALIZED DOSE, (cal/gm/cal/cm^2)
3.0
2.0
1.0
0
0.1
0.2
0.3
0.4
0.5
DEPTH, cm

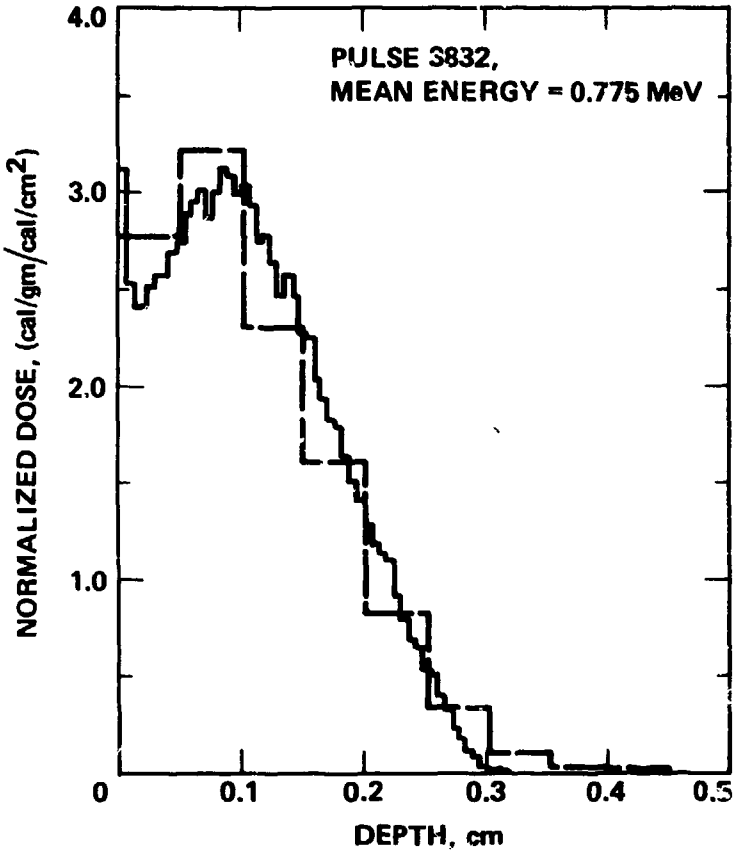
PULSE 3832,
MEAN ENERGY = 0.775 MeV
NORMALIZED DOSE, (cal/gm/cal/cm^2)
4.0
3.0
2.0
1.0
0
0.1
0.2
0.3
0.4
0.5
DEPTH, cm

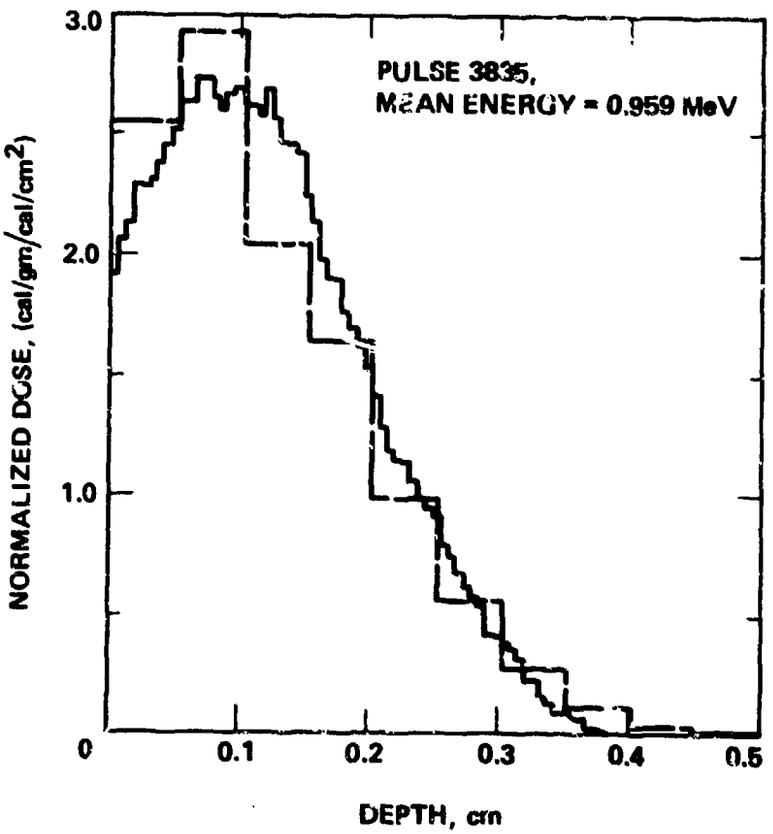
PULSE 3835,
MEAN ENERGY = 0.959 MeV
NORMALIZED DOSE, (cal/gm/cal/cm²)
3.0
2.0
1.0
0
0.1
0.2
0.3
0.4
0.5
DEPTH, cm

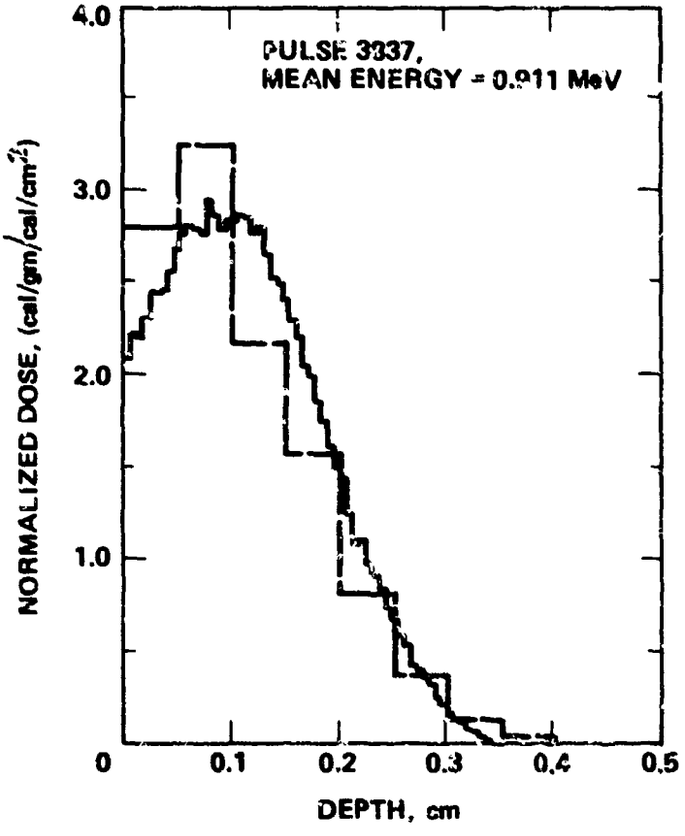
PULSE 3337,
MEAN ENERGY = 0.911 MeV
NORMALIZED DOSE, (cal/gm/cal/cm²)
4.0
3.0
2.0
1.0
0
0.1
0.2
0.3
0.4
0.5
DEPTH, cm

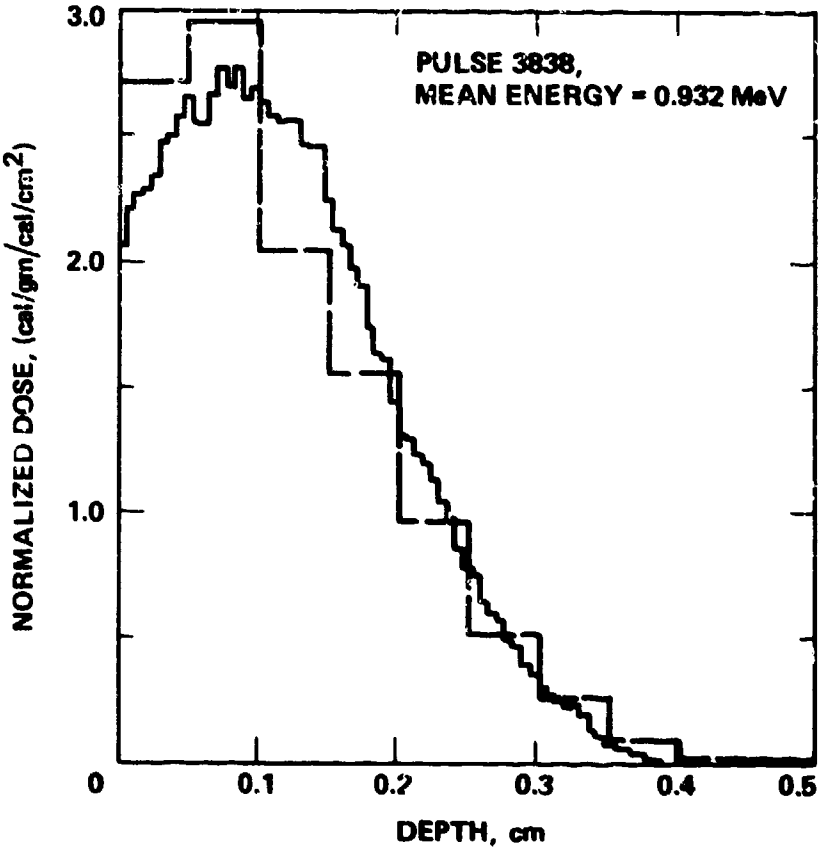
PULSE 3838,
MEAN ENERGY = 0.932 MeV
NORMALIZED DOSE, (cal/gm/cal/cm²)
3.0
2.0
1.0
0
0.1
0.2
0.3
0.4
0.5
DEPTH, cm

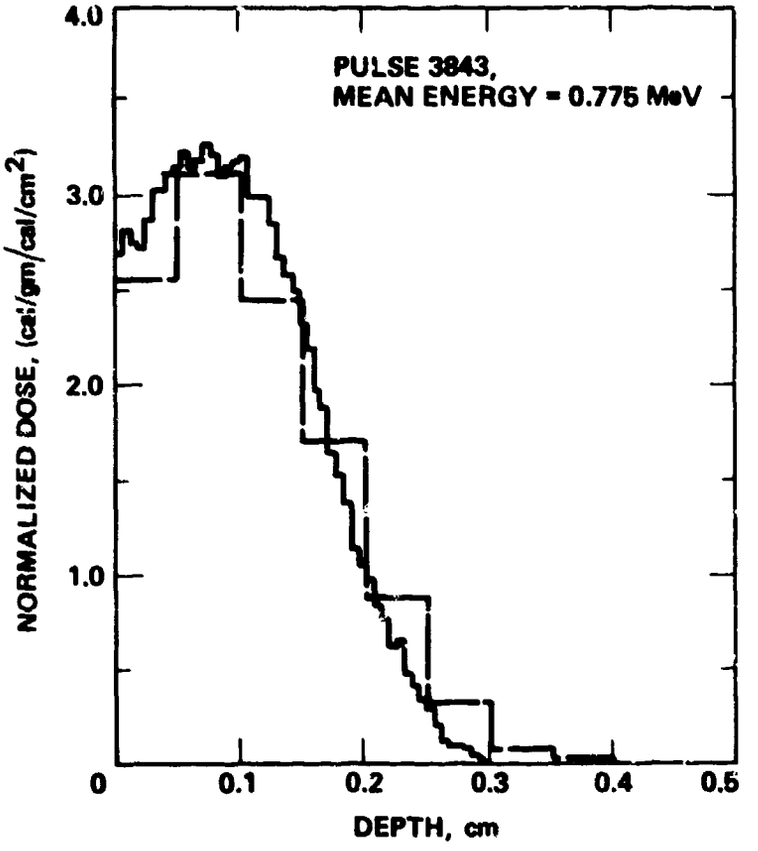
PULSE 3843,
MEAN ENERGY = 0.775 MeV
NORMALIZED DOSE, (cal/gm/cal/cm²)
4.0
3.0
2.0
1.0
0
0.1
0.2
0.3
0.4
0.5
DEPTH, cm

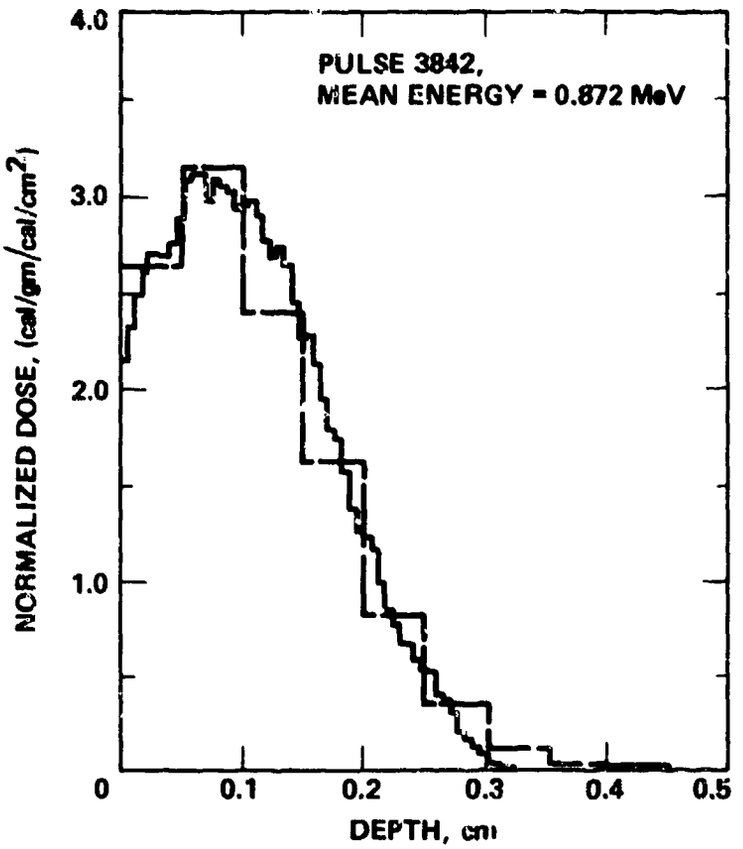
PULSE 3842,
MEAN ENERGY = 0.872 MeV
NORMALIZED DOSE, (cal/gm/cal/cm²)
DEPTH, cm
4.0
3.0
2.0
1.0
0
0.1
0.2
0.3
0.4
0.5

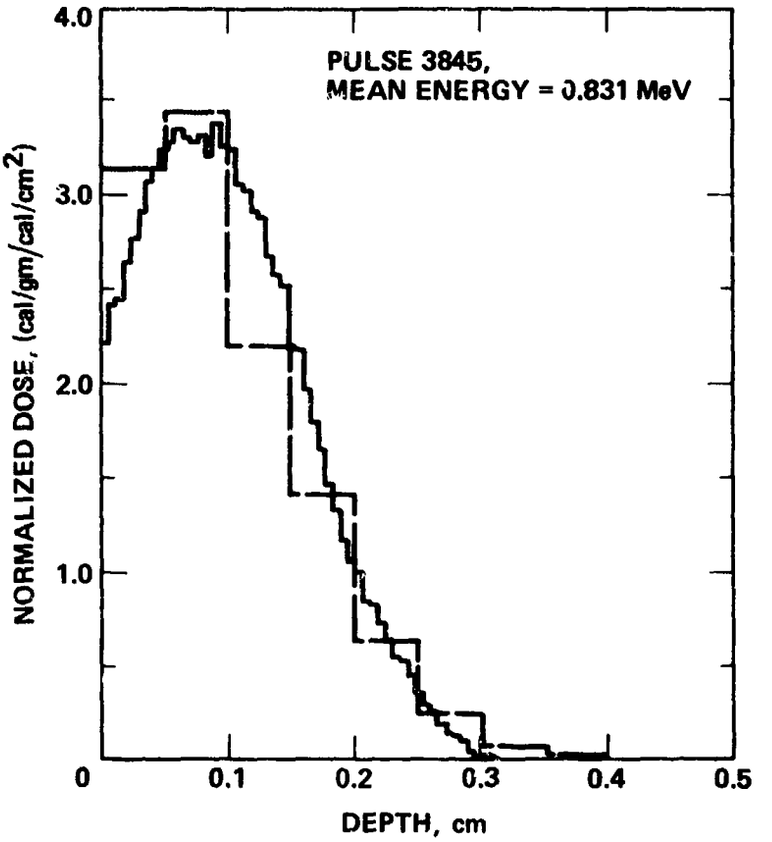
PULSE 3845,
MEAN ENERGY = 0.831 MeV
NORMALIZED DOSE, (cal/gm/cal/cm²)
4.0
3.0
2.0
1.0
0
0.1
0.2
0.3
0.4
0.5
DEPTH, cm

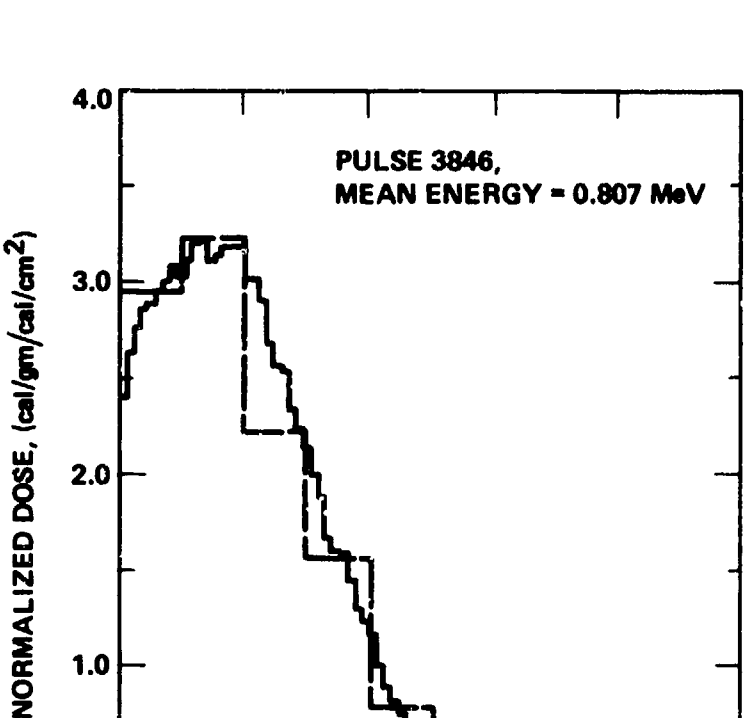
PULSE 3846,
MEAN ENERGY = 0.807 MeV
NORMALIZED DOSE, (cal/gm/cal/cm²)
DEPTH, cm
4.0
3.0
2.0
1.0
0
0.1
0.2
0.3
0.4
0.5

APPENDIX B-2

DEPOSITION PROFILES MEASURED BY INNER FOIL STACK CALORIMETER

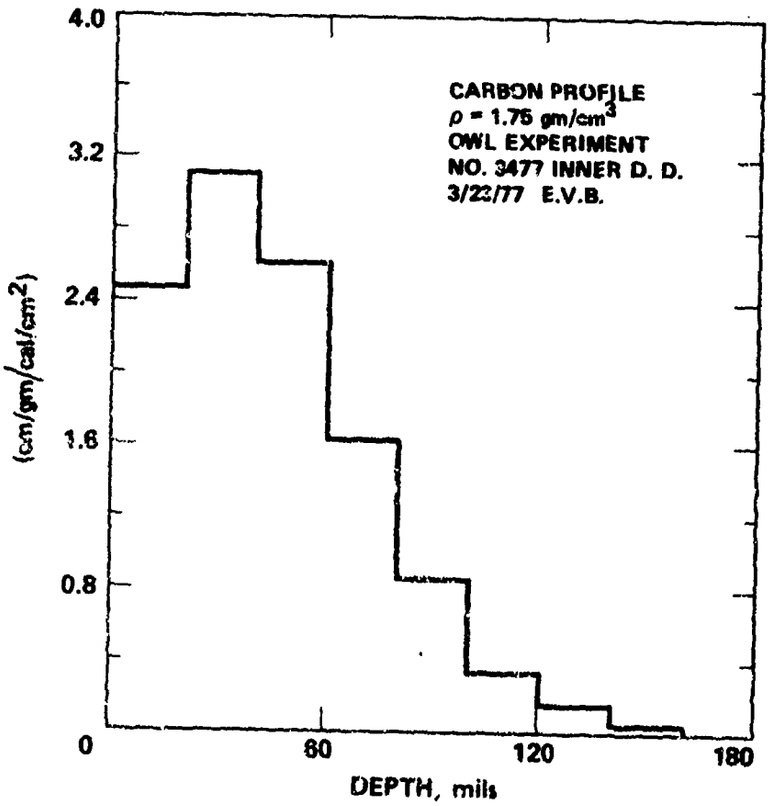
CARBON PROFILE
ρ = 1.75 gm/cm³
OWL EXPERIMENT
NO. 3477 INNER D. D.
3/22/77 E.V.B.
4.0
3.2
2.4
1.6
0.8
0
60
120
180
(cm/gm/cal/cm²)
DEPTH, mils

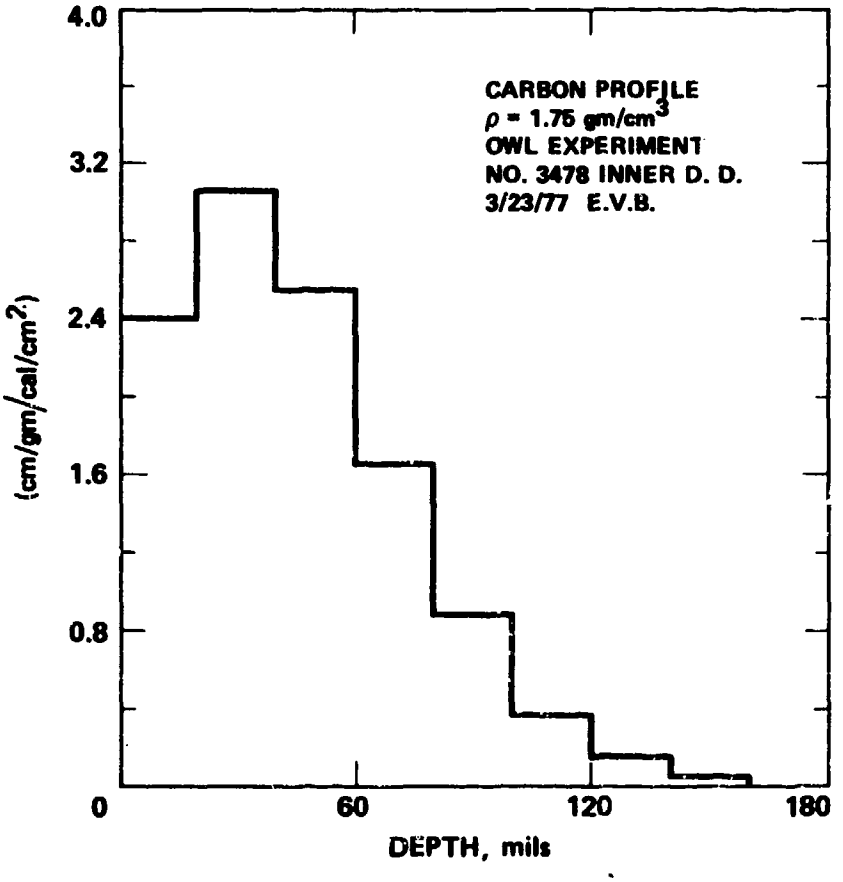
CARBON PROFILE
ρ = 1.75 gm/cm3
OWL EXPERIMENT
NO. 3478 INNER D. D.
3/23/77 E.V.B.
4.0
3.2
2.4
1.6
0.8
0
60
120
180
(cm/gm/cal/cm2)
DEPTH, mils

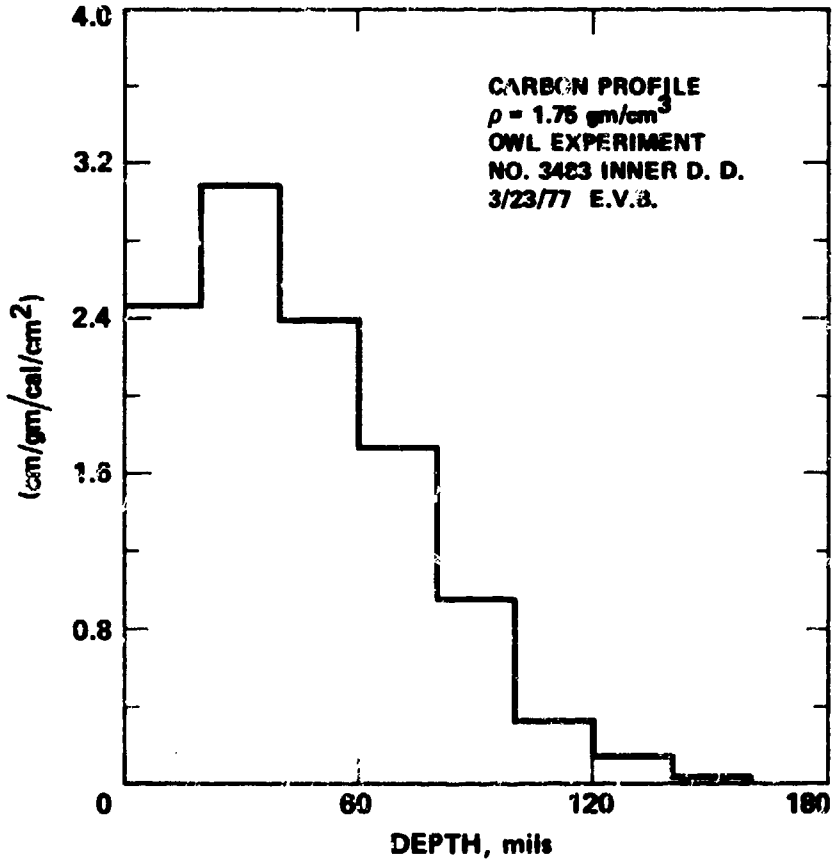
CARBON PROFILE
ρ = 1.75 gm/cm³
OWL EXPERIMENT
NO. 3483 INNER D. D.
3/23/77 E.V.S.
4.0
3.2
2.4
1.6
0.8
0
60
120
180
(cm/gm/cal/cm²)
DEPTH, mils

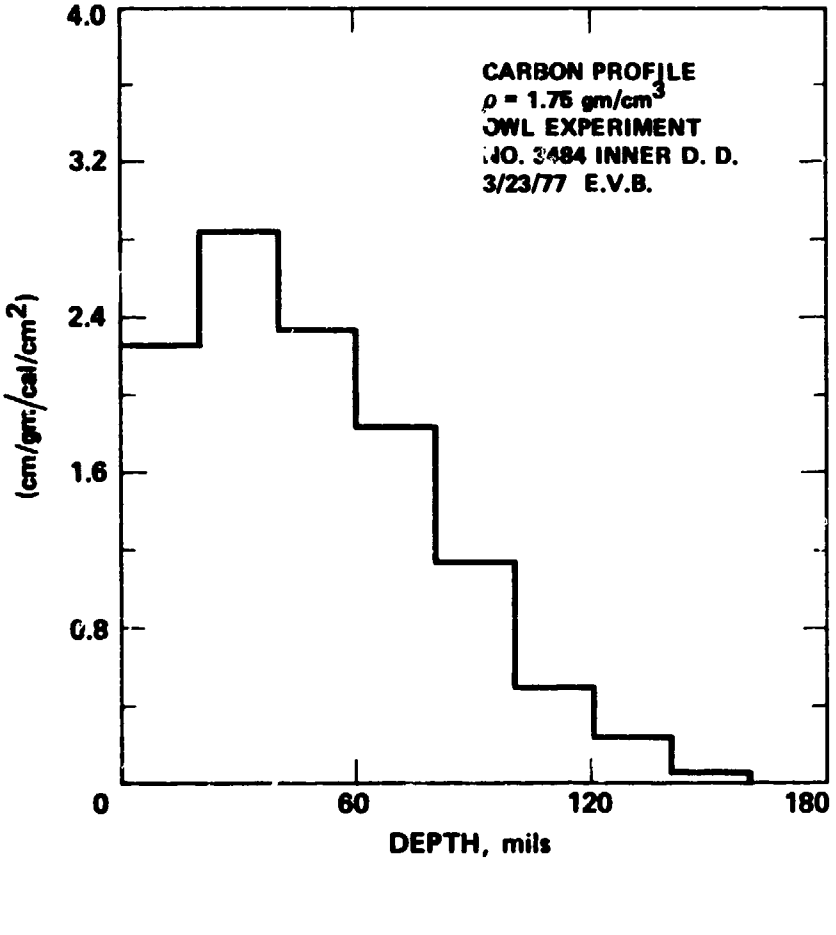
CARBON PROFILE
ρ = 1.75 gm/cm3
OWL EXPERIMENT
NO. 3484 INNER D. D.
3/23/77 E.V.B.
4.0
3.2
2.4
1.6
0.8
0
60
120
180
(cm/gm)/cal/cm2)
DEPTH, mils

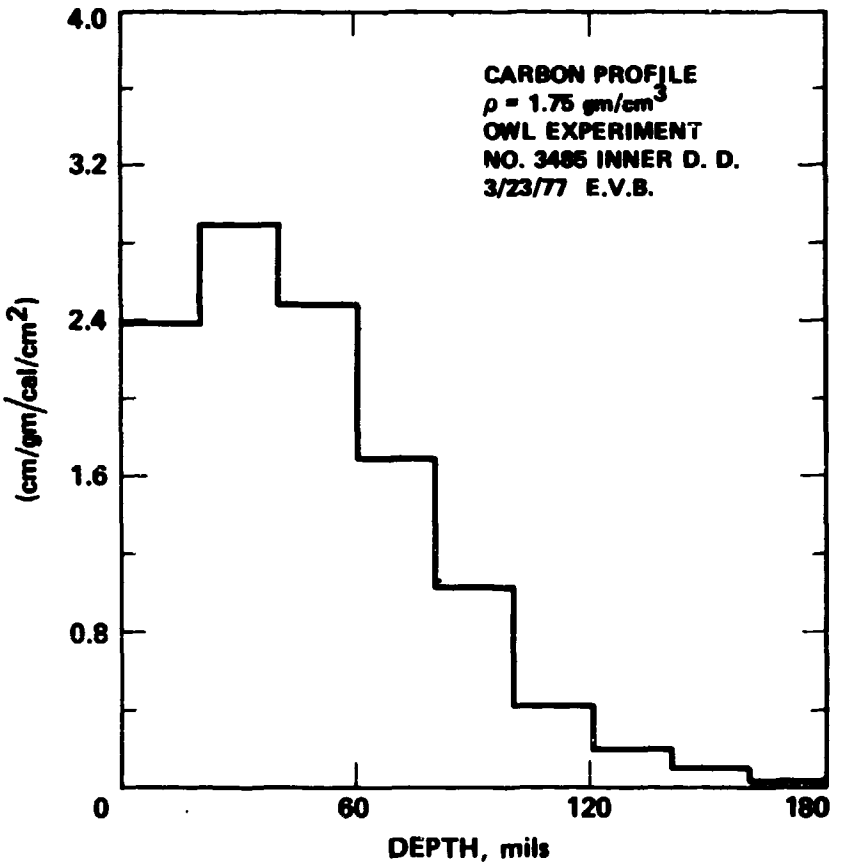
CARBON PROFILE
ρ = 1.75 gm/cm3
OWL EXPERIMENT
NO. 3486 INNER D. D.
3/23/77 E.V.B.
4.0
3.2
2.4
1.6
0.8
0
60
120
180
(cm/gm/cal/cm2)
DEPTH, mils

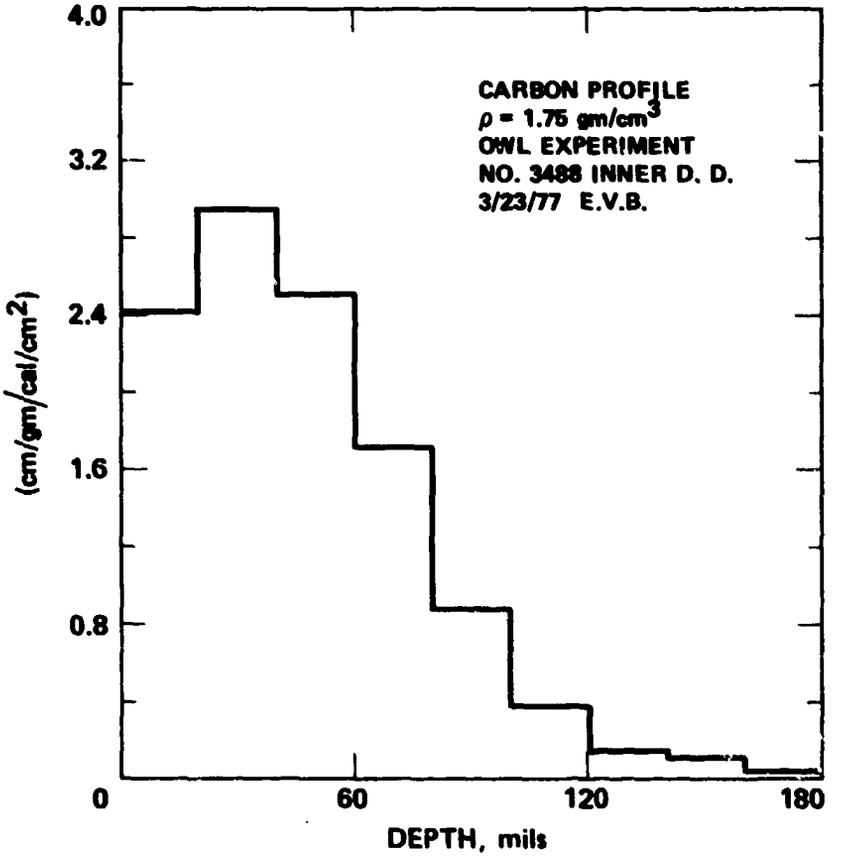
CARBON PROFILE
ρ = 1.75 gm/cm3
OWL EXPERIMENT
NO. 3488 INNER D. D.
3/23/77 E.V.B.
4.0
3.2
2.4
1.6
0.8
0
60
120
180
(cm/gm/cal/cm2)
DEPTH, mils

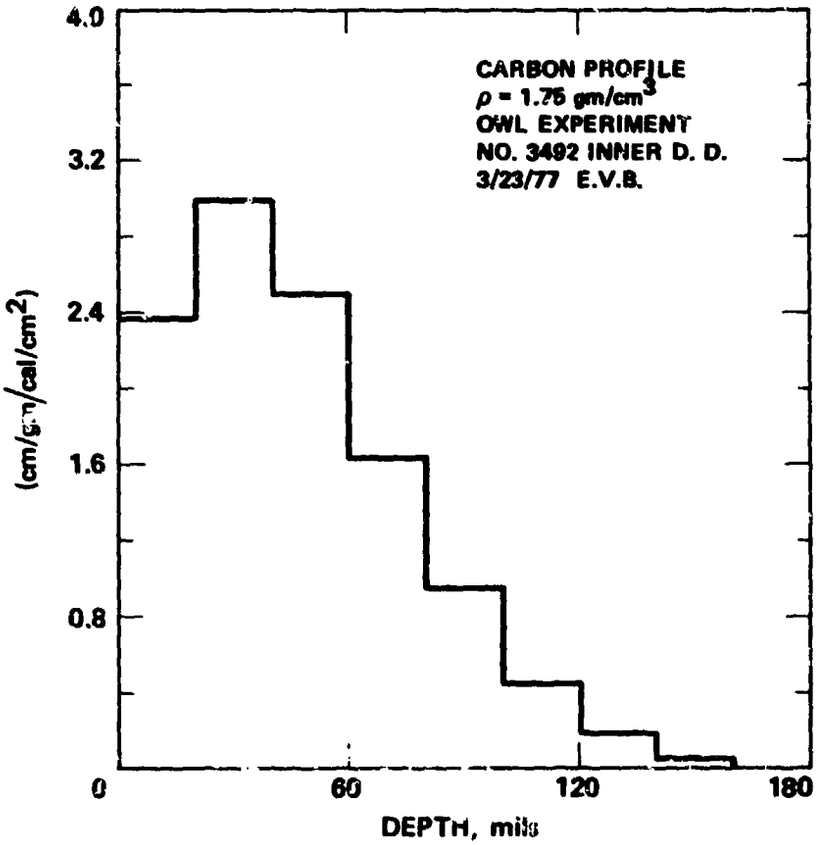
CARBON PROFILE
ρ = 1.75 gm/cm3
OWL EXPERIMENT
NO. 3492 INNER D. D.
3/23/77 E.V.B.
4.0
3.2
2.4
1.6
0.8
0
60
120
180
DEPTH, mils

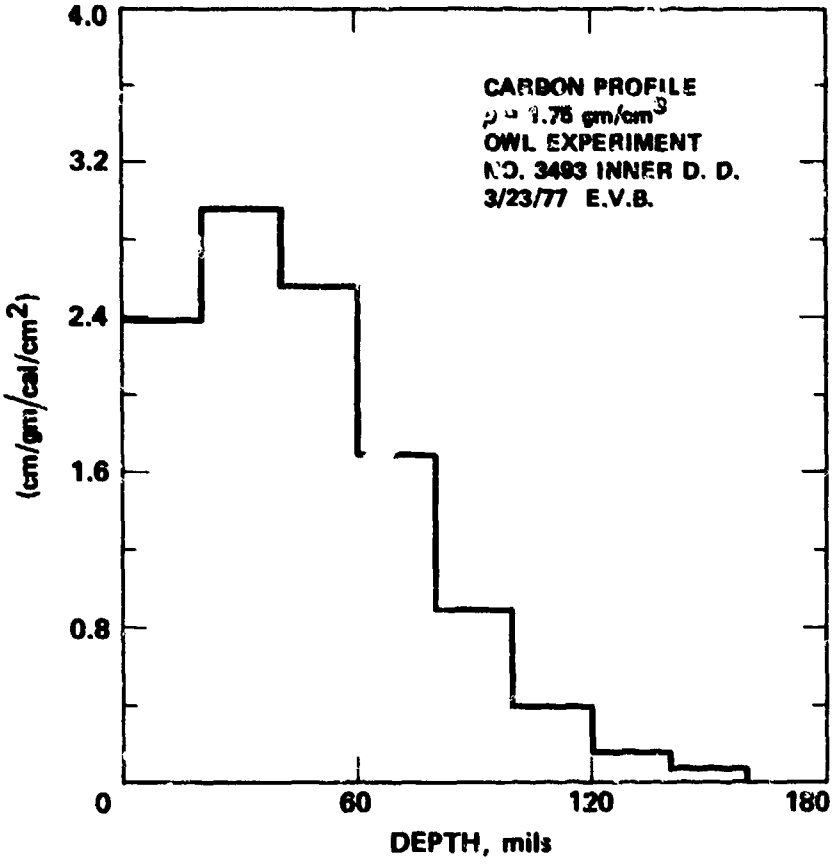
CARBON PROFILE
ρ = 1.75 gm/cm³
OWL EXPERIMENT
NO. 3493 INNER D. D.
3/23/77 E.V.B.
4.0
3.2
2.4
1.6
0.8
0
60
120
180
(cm/gm/cal/cm²)
DEPTH, mils

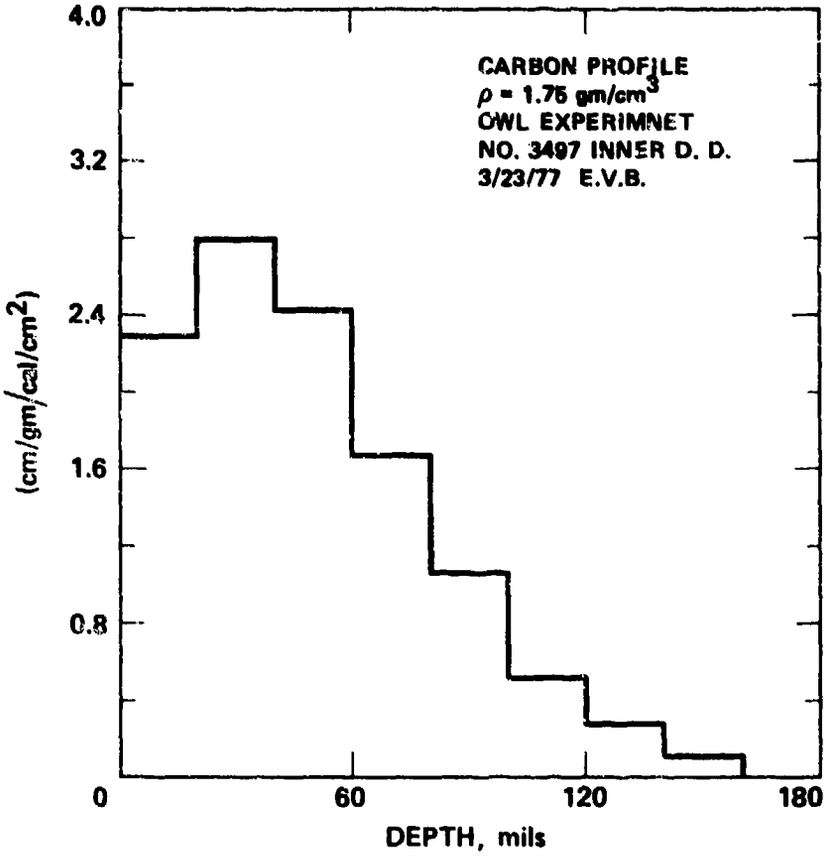
CARBON PROFILE
ρ = 1.75 gm/cm3
OWL EXPERIMNET
NO. 3497 INNER D. D.
3/23/77 E.V.B.
4.0
3.2
2.4
1.6
0.8
0
60
120
180
(cm/gm/cal/cm2)
DEPTH, mils

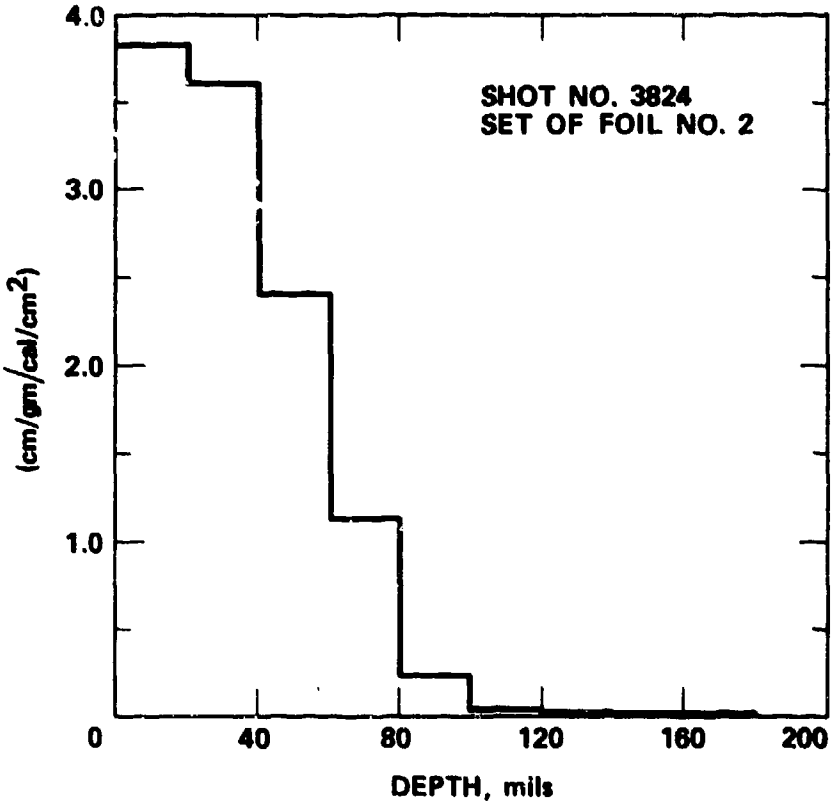
SHOT NO. 3824
SET OF FOIL NO. 2
4.0
3.0
2.0
1.0
0
40
80
120
160
200
(cm/gm/cal/cm²)
DEPTH, mils

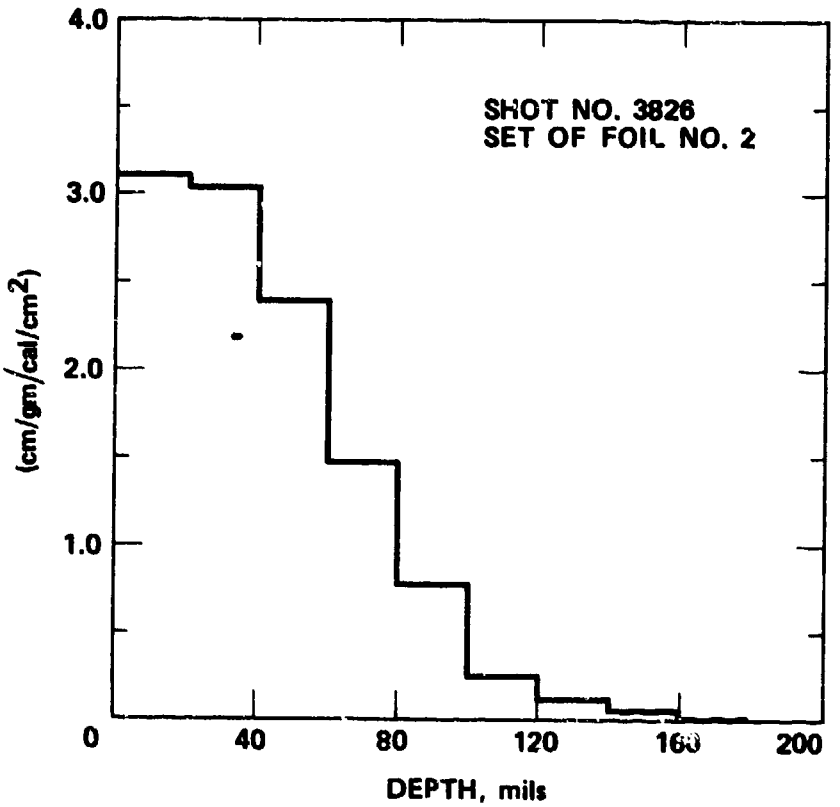
SHOT NO. 3826
SET OF FOIL NO. 2
4.0
3.0
2.0
1.0
0
40
80
120
160
200
(cm/gm/cal/cm²)
DEPTH, mils

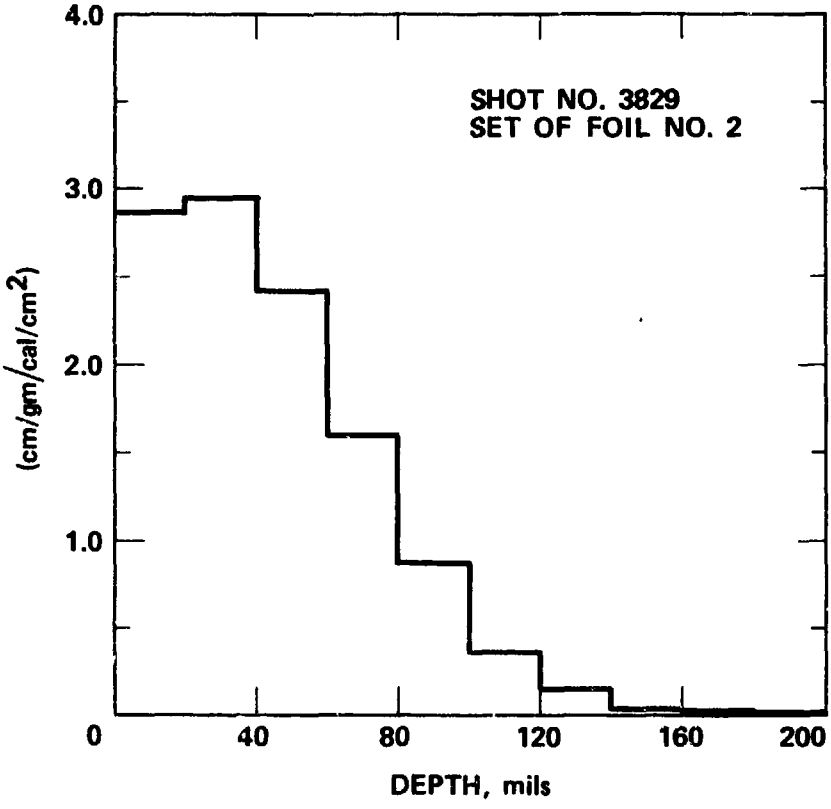
SHOT NO. 3829
SET OF FOIL NO. 2
4.0
3.0
2.0
1.0
0
40
80
120
160
200
(cm/gm/cal/cm²)
DEPTH, mils

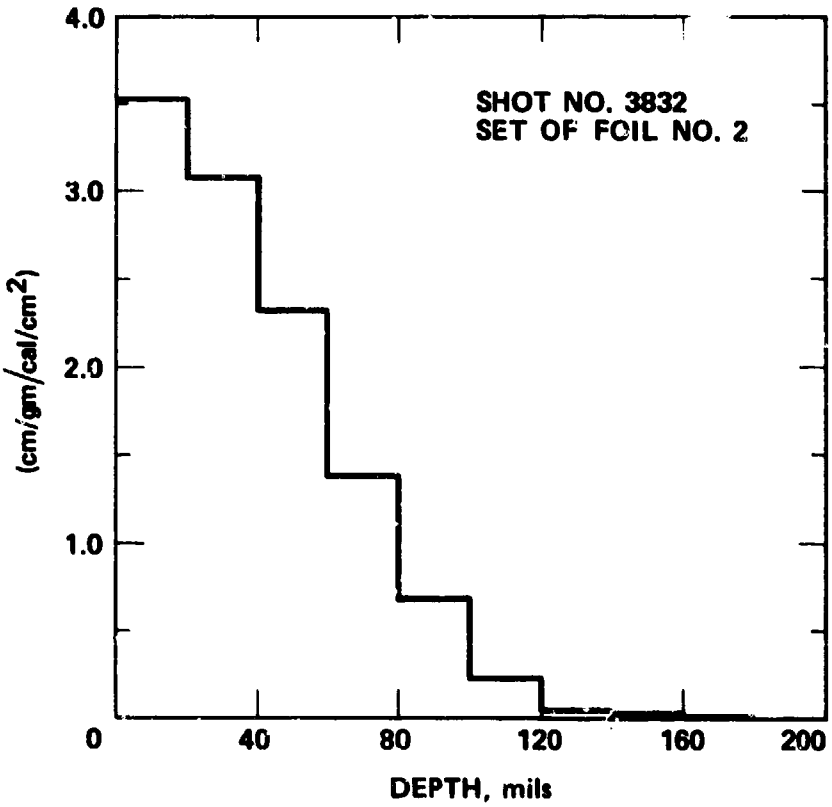
SHOT NO. 3832
SET OF FOIL NO. 2
4.0
3.0
2.0
1.0
0
40
80
120
160
200
(cm/gm/cal/cm²)
DEPTH, mils

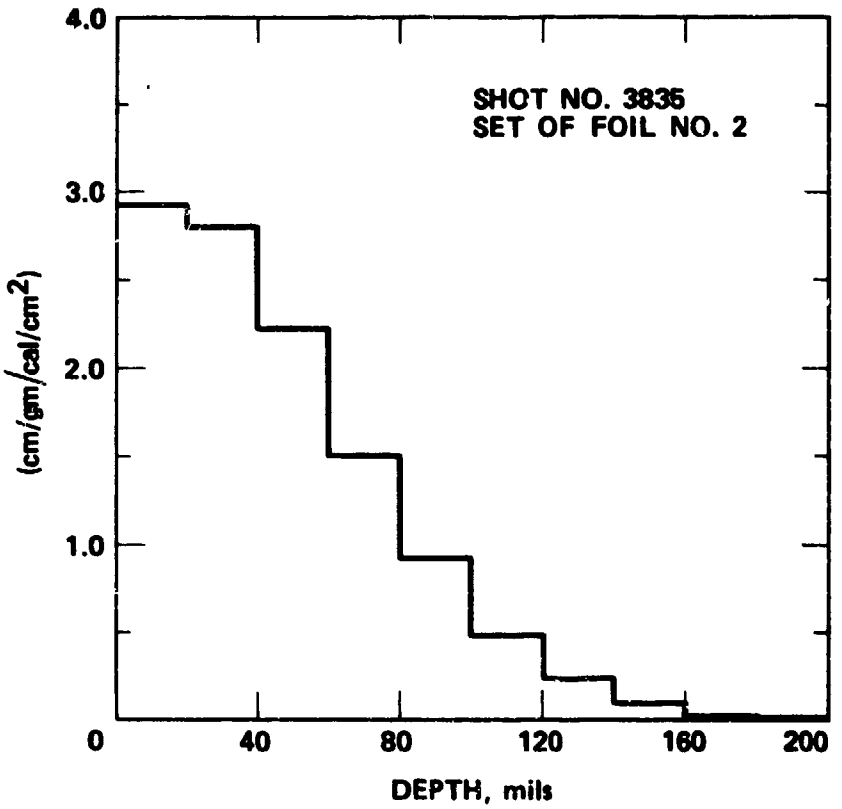
SHOT NO. 3835
SET OF FOIL NO. 2
4.0
3.0
2.0
1.0
0
40
80
120
160
200
(cm/gm/cal/cm²)
DEPTH, mils

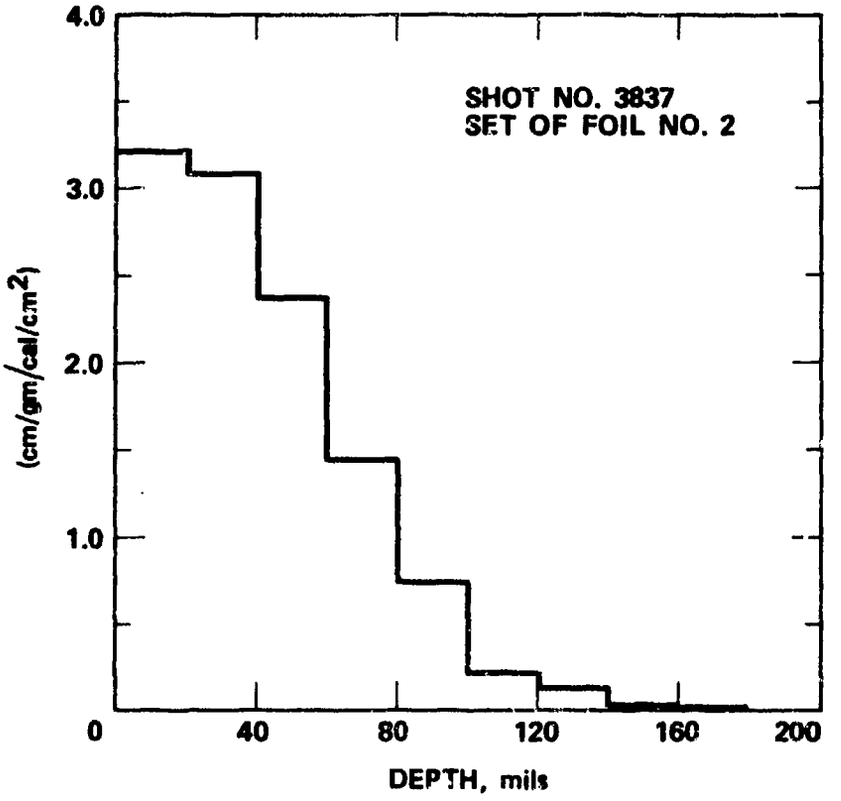
SHOT NO. 3837
SET OF FOIL NO. 2
4.0
3.0
2.0
1.0
0
40
80
120
160
200
(cm/gm/cal/cm²)
DEPTH, mils

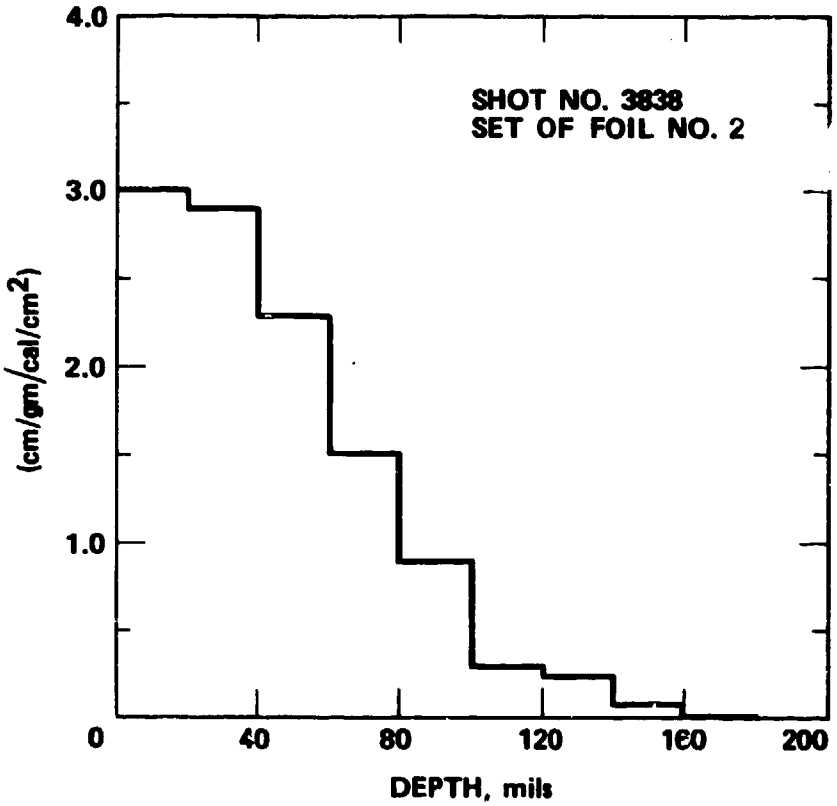
SHOT NO. 3838
SET OF FOIL NO. 2
4.0
3.0
2.0
1.0
0
40
80
120
160
200
(cm/gm/cal/cm²)
DEPTH, mils

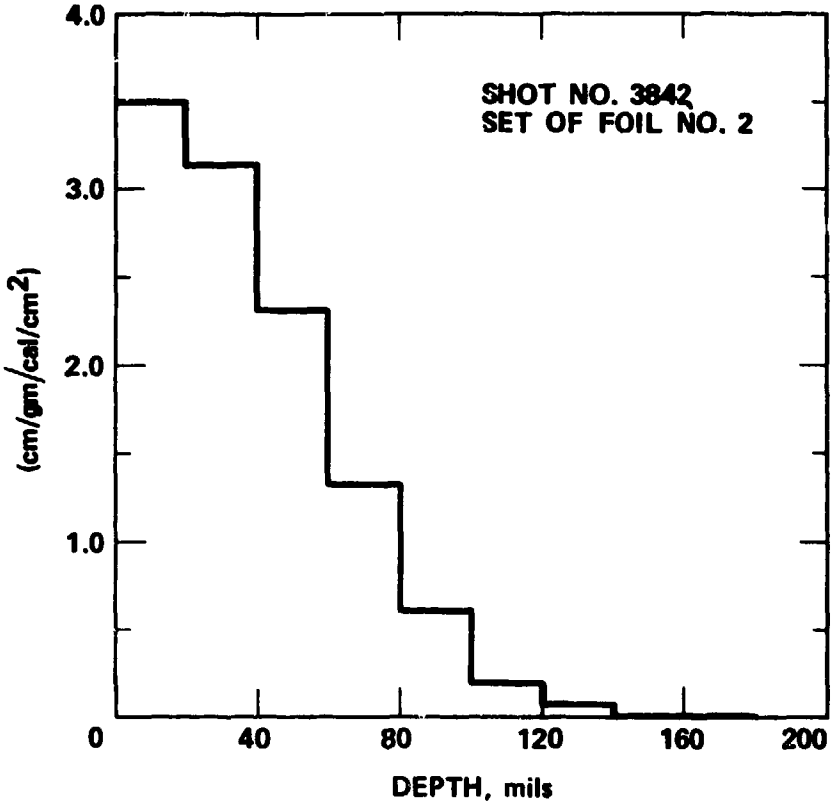
SHOT NO. 3842
SET OF FOIL NO. 2
4.0
3.0
2.0
1.0
0
40
80
120
160
200
(cm/gm/cal/cm²)
DEPTH, mils

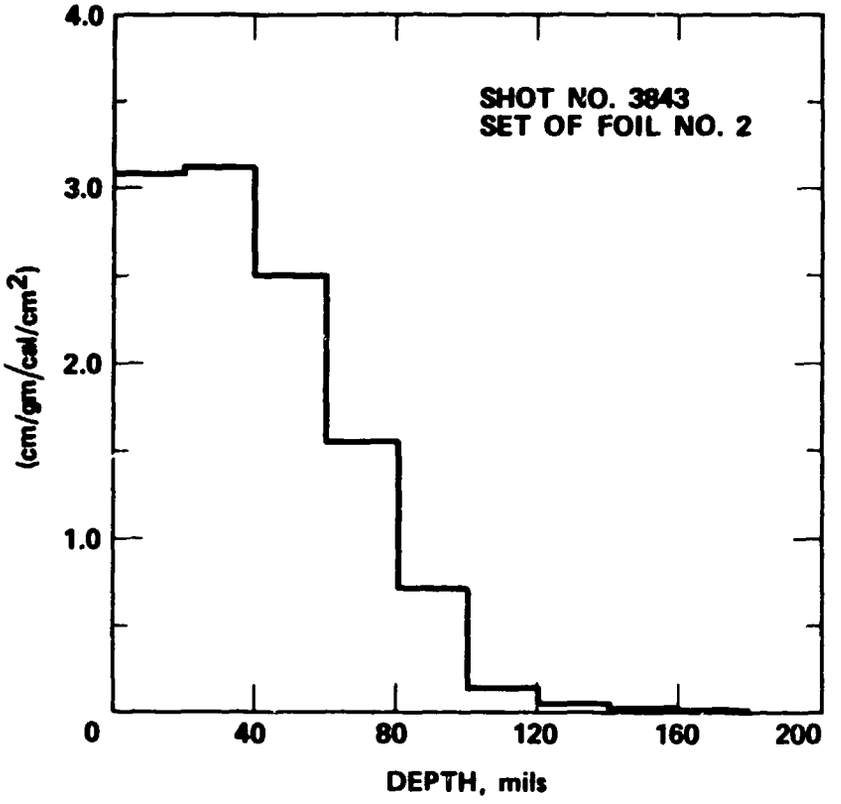
SHOT NO. 3843
SET OF FOIL NO. 2
4.0
3.0
2.0
1.0
0
40
80
120
160
200
(cm/gm/cal/cm²)
DEPTH, mils

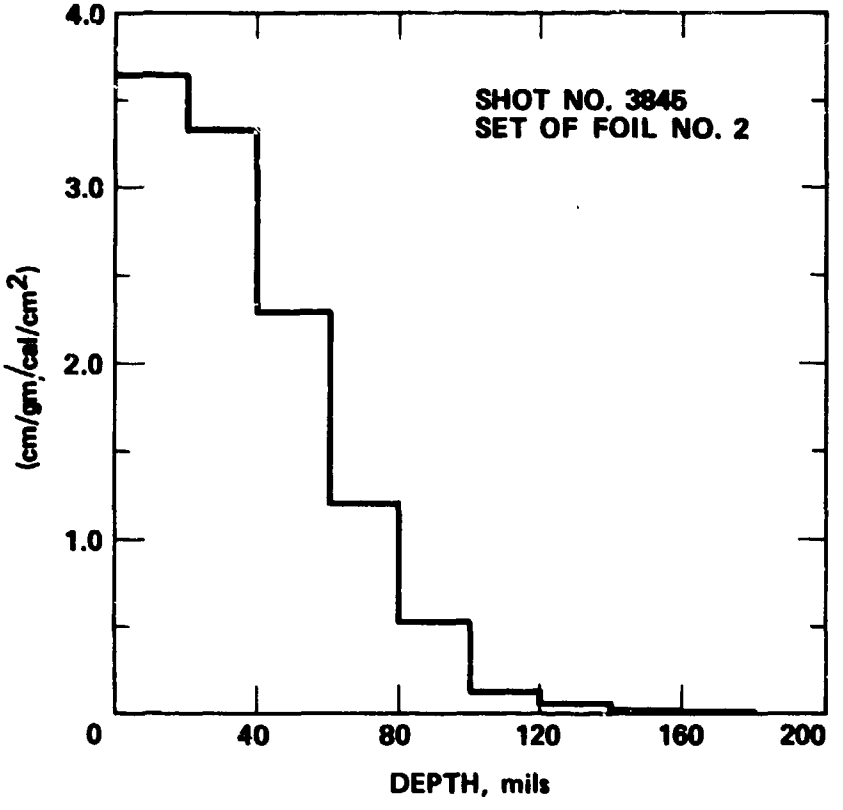
SHOT NO. 3845
SET OF FOIL NO. 2
4.0
3.0
2.0
1.0
0
40
80
120
160
200
(cm/gm/cal/cm²)
DEPTH, mils

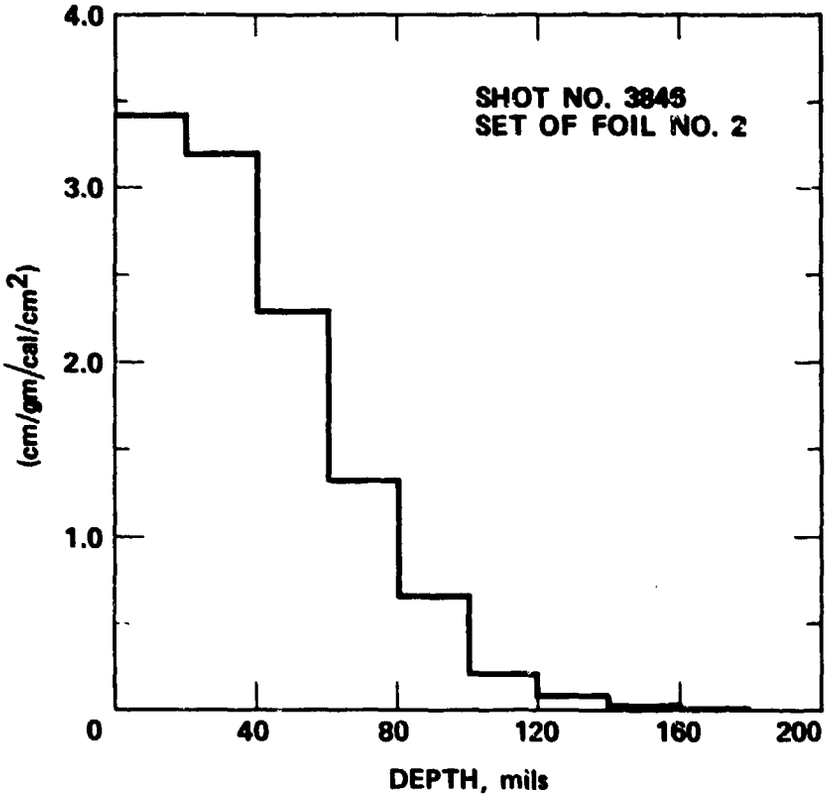
SHOT NO. 3845
SET OF FOIL NO. 2
4.0
3.0
2.0
1.0
0
40
80
120
160
200
(cm/gm/cal/cm²)
DEPTH, mils

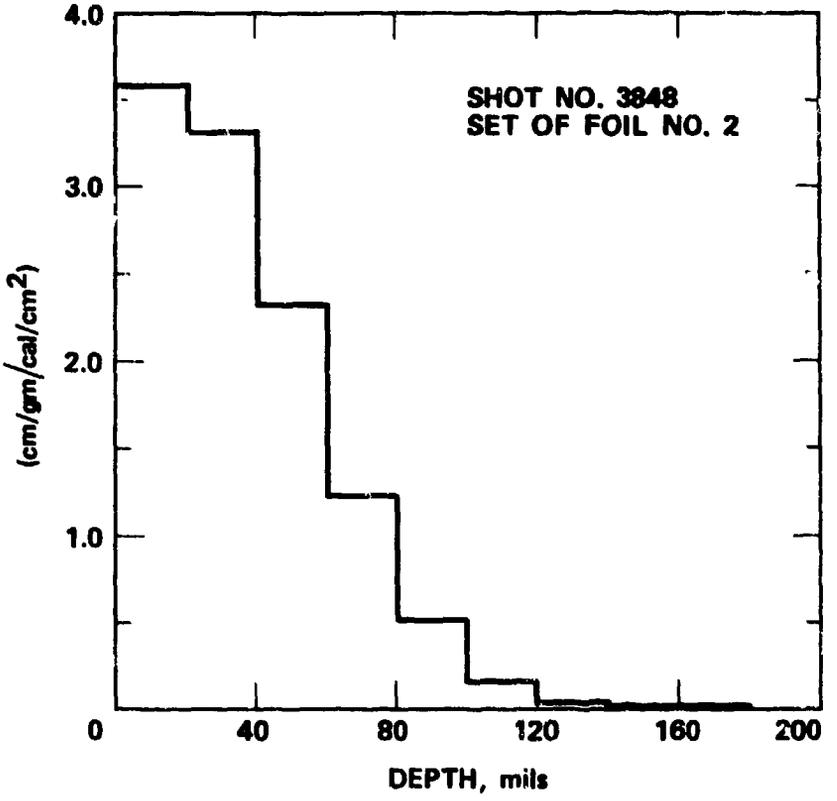
SHOT NO. 3848
SET OF FOIL NO. 2
4.0
3.0
2.0
1.0
0
40
80
120
160
200
(cm/gm/cal/cm²)
DEPTH, mils

APPENDIX C

DEPOSITION PROFILES IN ALUMINUM CALCULATED FROM VOLTAGE AND CURRENT WAVEFORMS

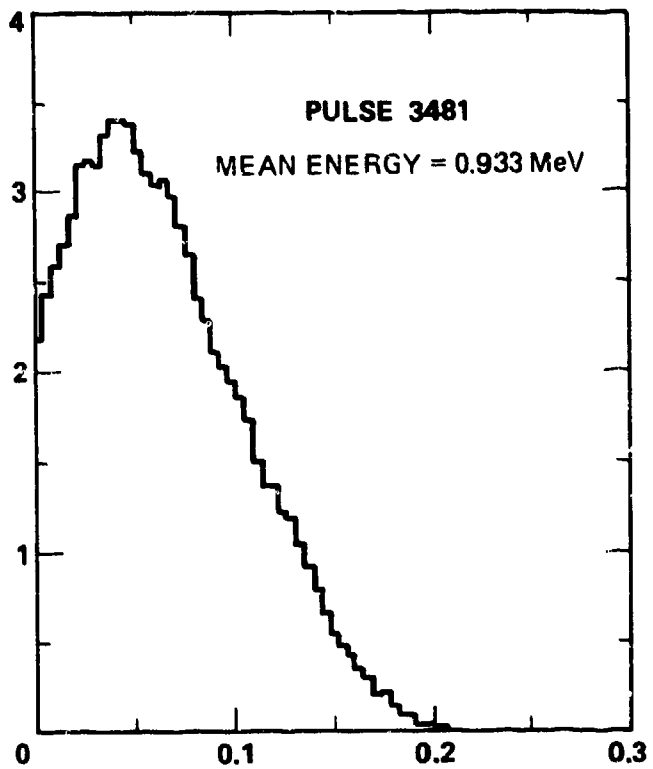
PULSE 3481
MEAN ENERGY = 0.933 MeV
4
3
2
1
0
0.1
0.2
0.3

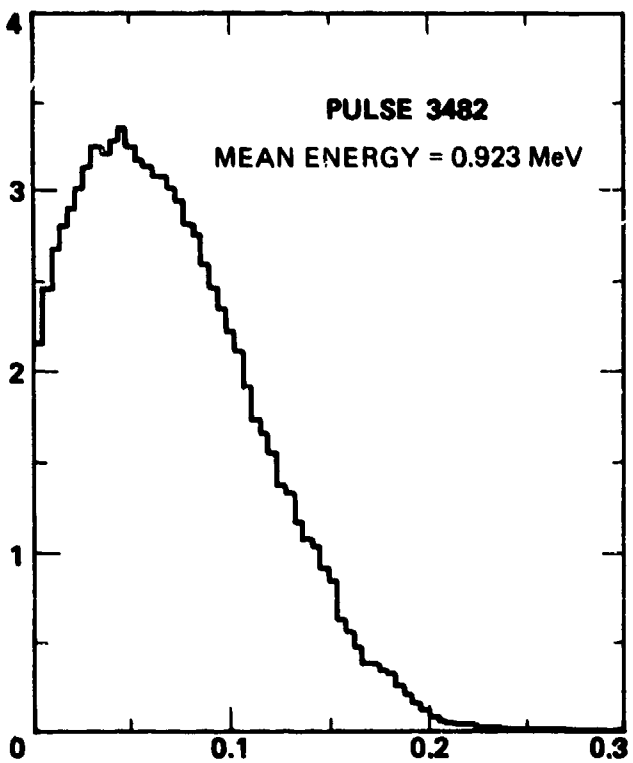
PULSE 3482
MEAN ENERGY = 0.923 MeV
4
3
2
1
0
0.1
0.2
0.3

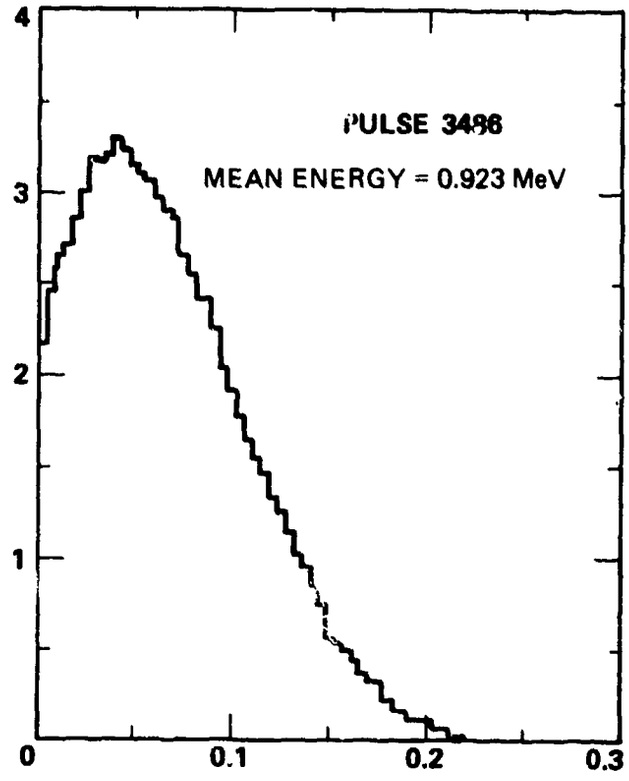
PULSE 3496
MEAN ENERGY = 0.923 MeV
4
3
2
1
0
0.1
0.2
0.3

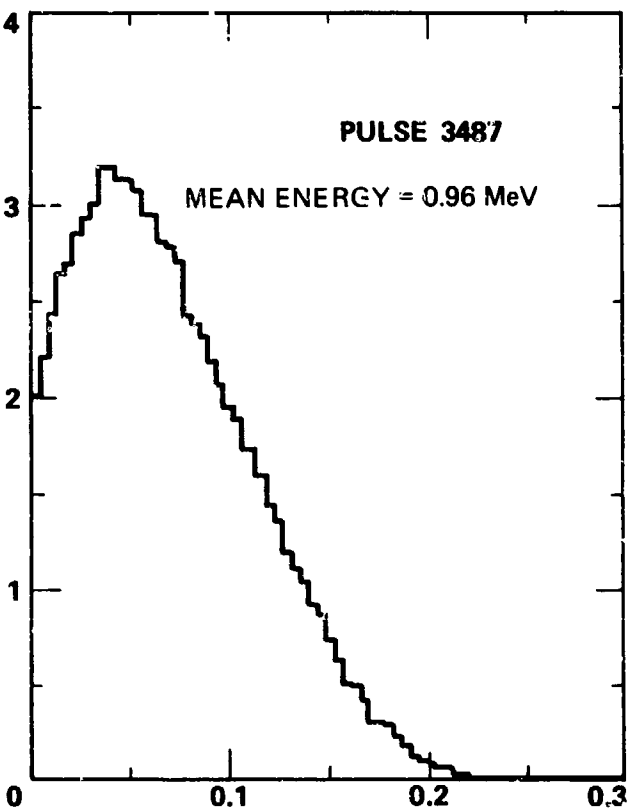
PULSE 3487
MEAN ENERGY = 0.96 MeV
4
3
2
1
0
0.1
0.2
0.3

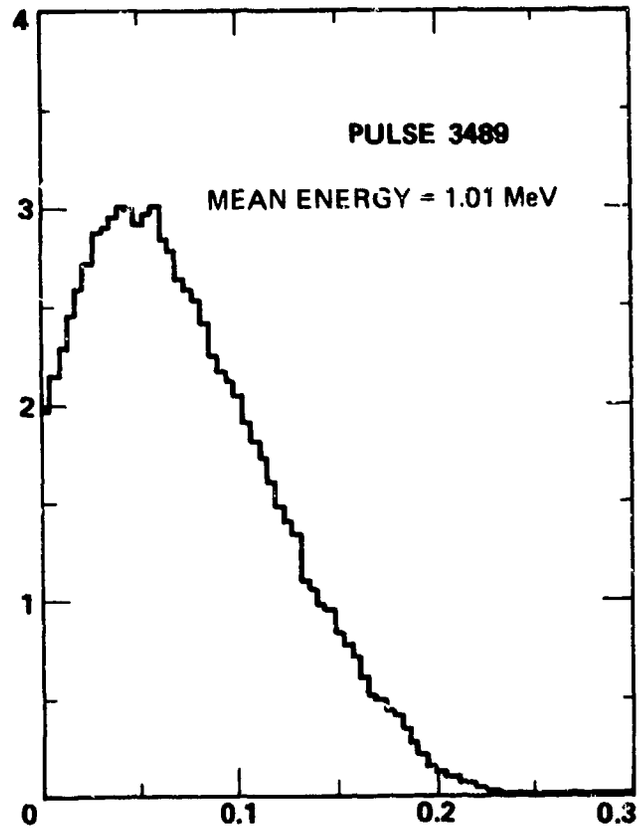
PULSE 3489
MEAN ENERGY = 1.01 MeV
4
3
2
1
0
0.1
0.2
0.3

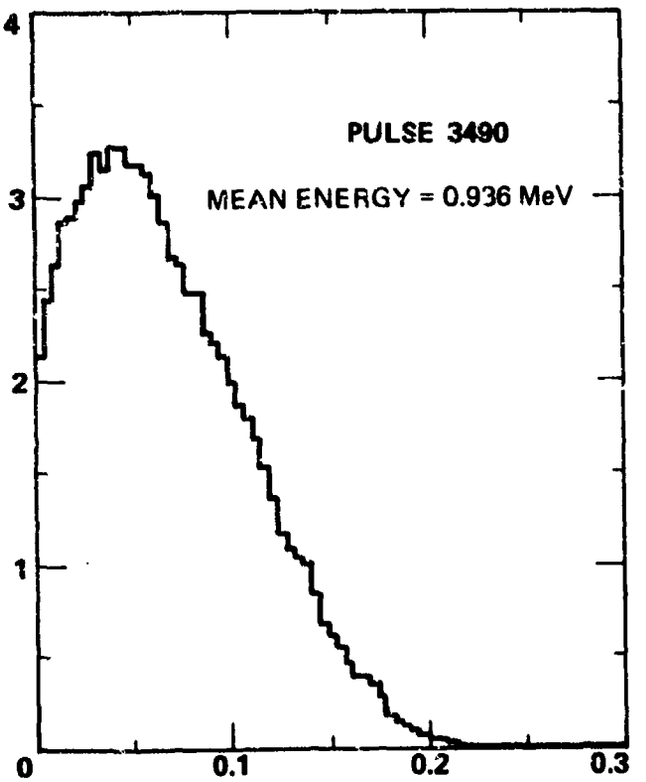
PULSE 3490
MEAN ENERGY = 0.936 MeV
4
3
2
1
0
0.1
0.2
0.3

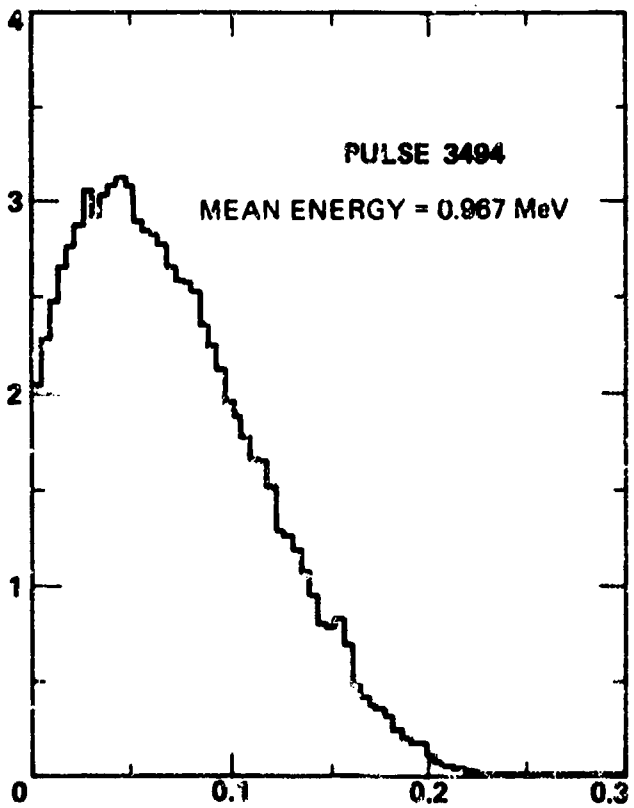
PULSE 3494
MEAN ENERGY = 0.967 MeV
4
3
2
1
0
0.1
0.2
0.3

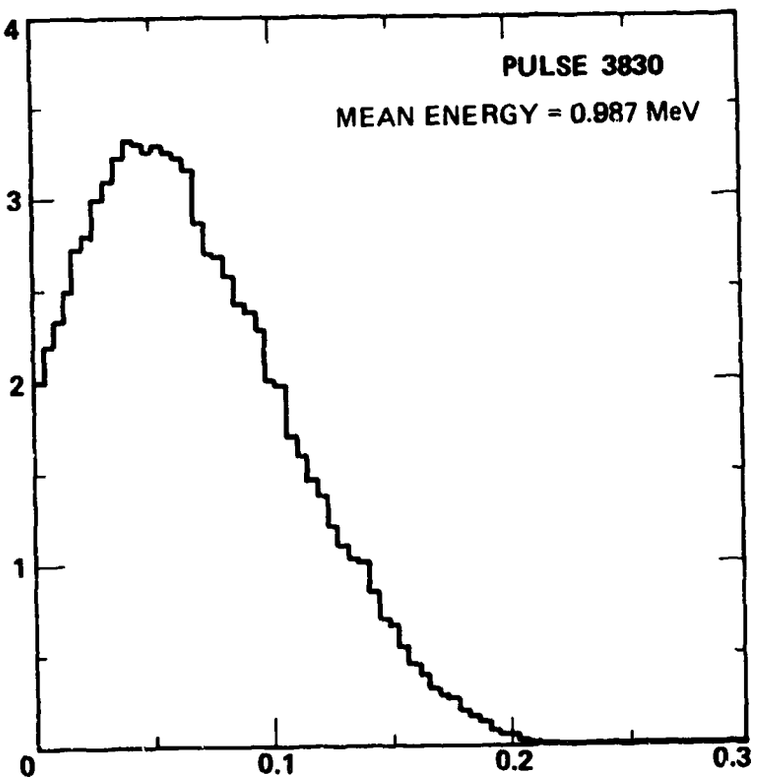
PULSE 3830
MEAN ENERGY = 0.987 MeV
4
3
2
1
0
0.1
0.2
0.3

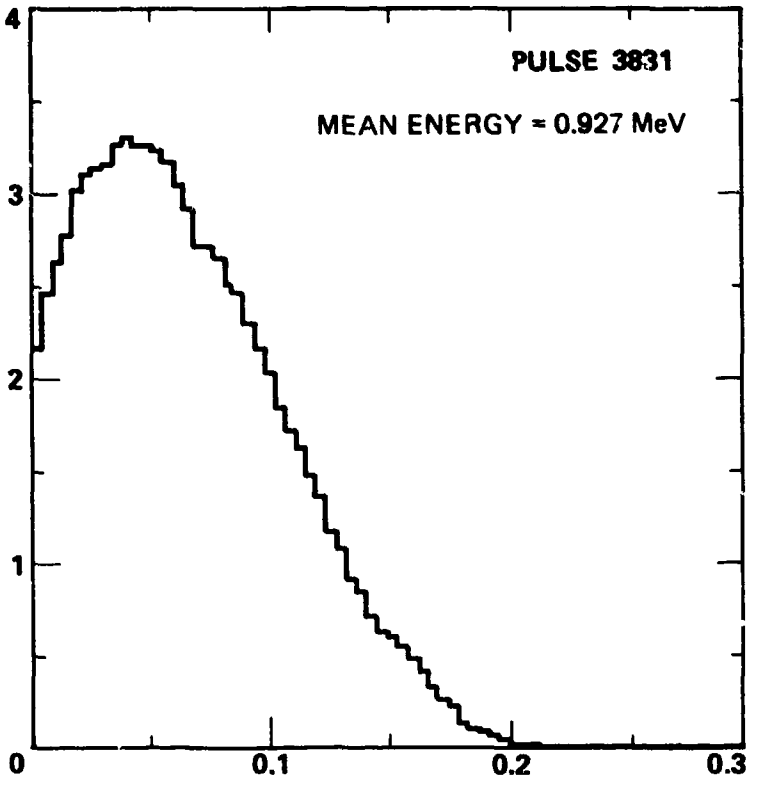
PULSE 3831
MEAN ENERGY = 0.927 MeV
4
3
2
1
0
0.1
0.2
0.3

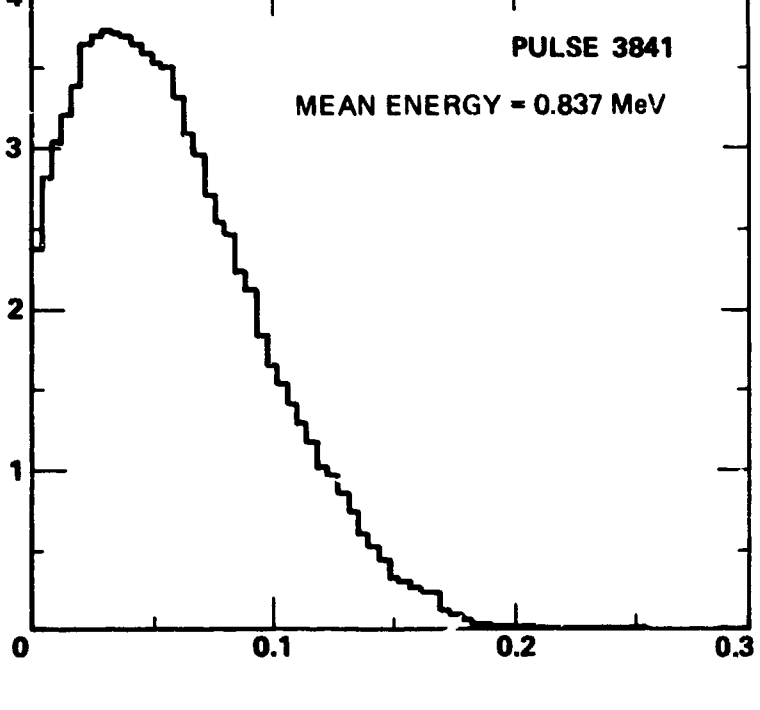
PULSE 3841
MEAN ENERGY = 0.837 MeV
4
3
2
1
0
0.1
0.2
0.3

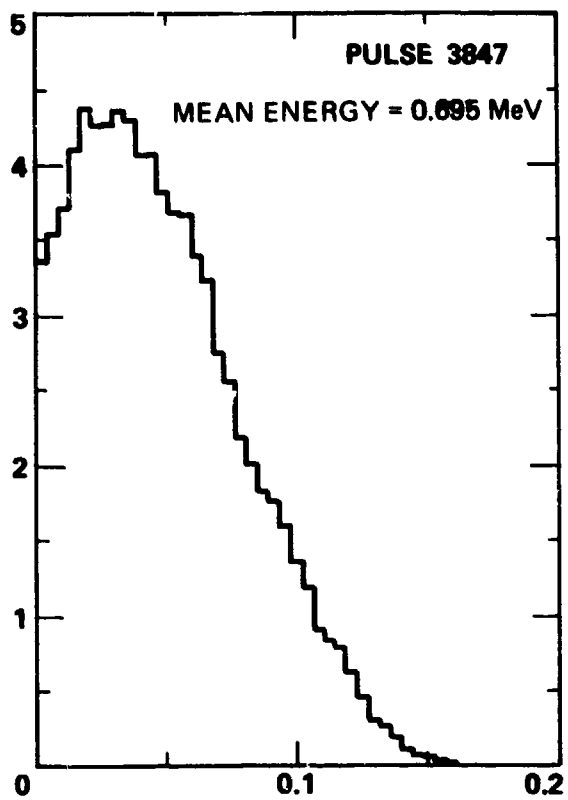
PULSE 3847
MEAN ENERGY = 0.695 MeV
5
4
3
2
1
0
0.1
0.2

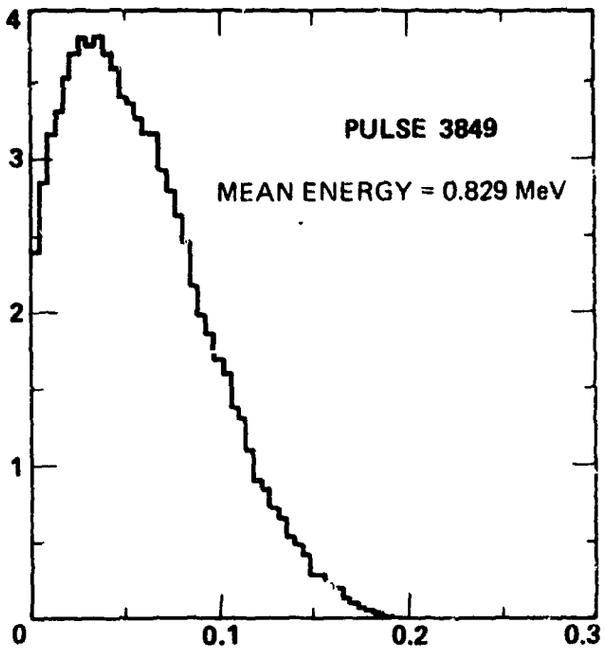
PULSE 3849
MEAN ENERGY = 0.829 MeV
4
3
2
1
0
0.1
0.2
0.3

APPENDIX D

STRAIN GAUGE RECORDS

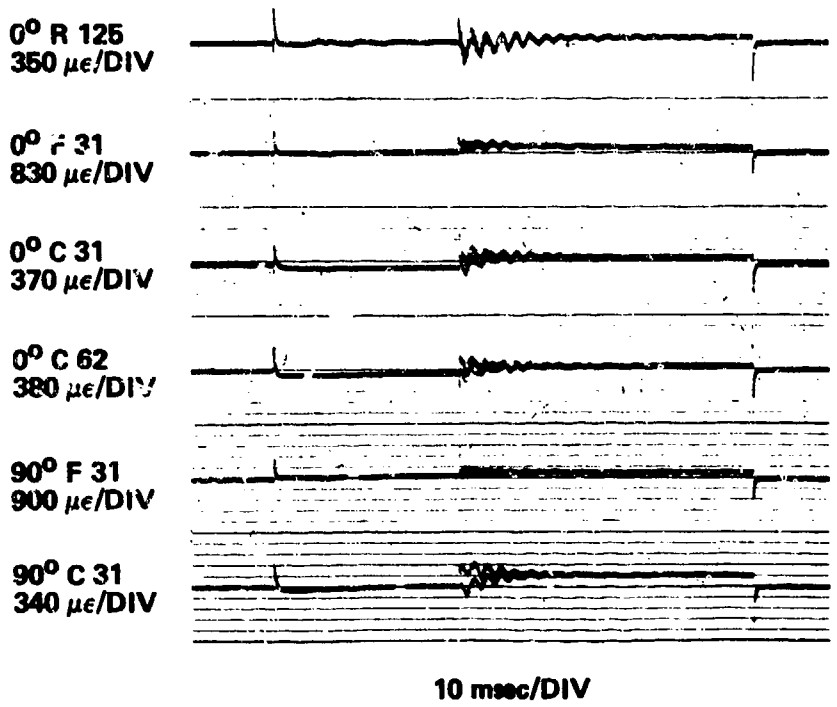

Figure D-1 Strain gauge records for pulse 3481. Gauges in Configuration I.

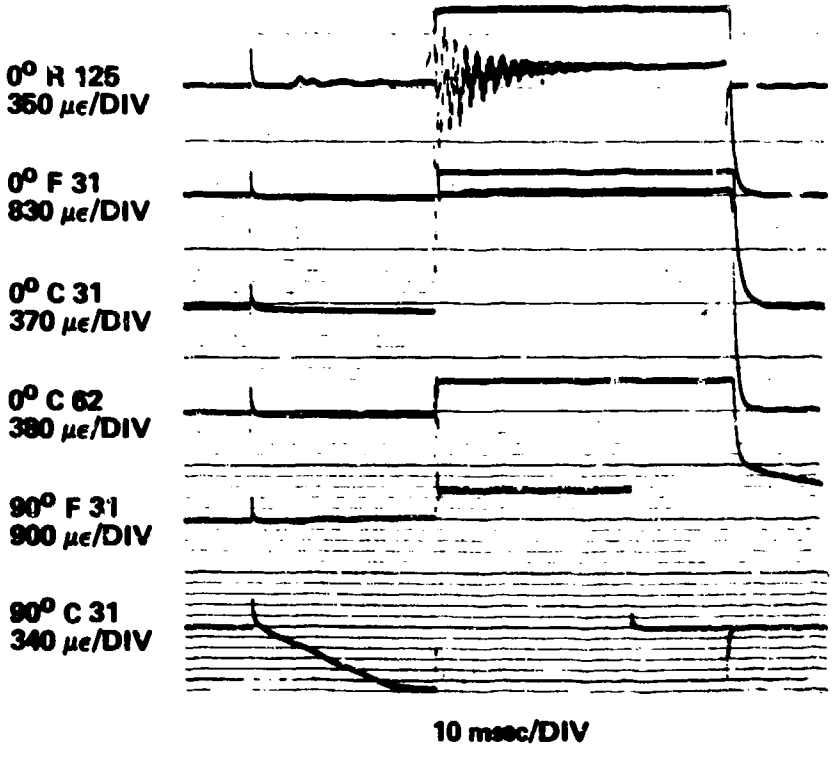

Figure D-2 Strain gauge records for pulse 3842. Gauges in Configuration I.

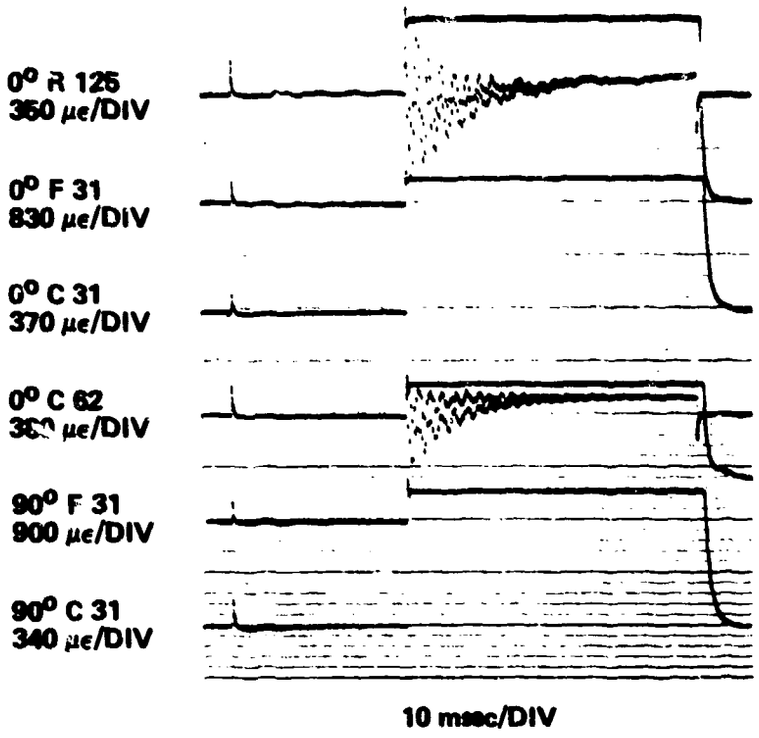

Figure D-3 Strain gauge records for pulse 3486. Gauges in Configuration I.

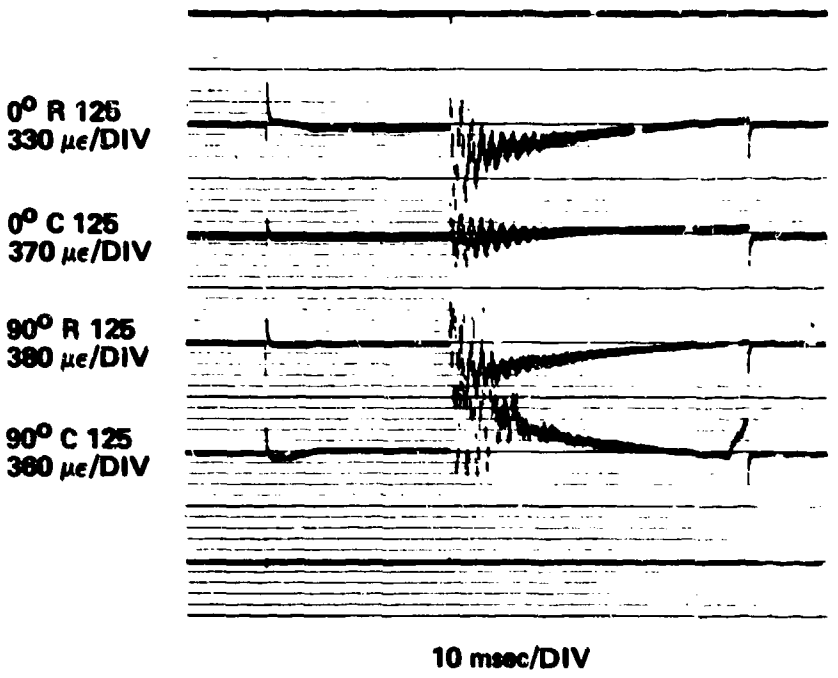

Figure D-4 Strain gauge records for pulse 3487. Gauges in Configuration II.

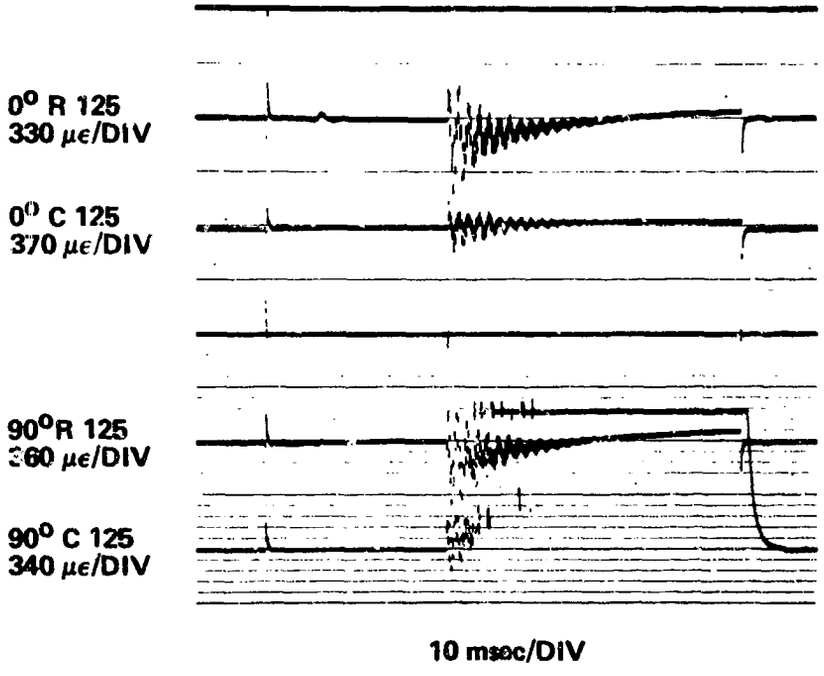

Figure D-5 Strain gauge records for pulse 3489. Gauges in Configuration II.

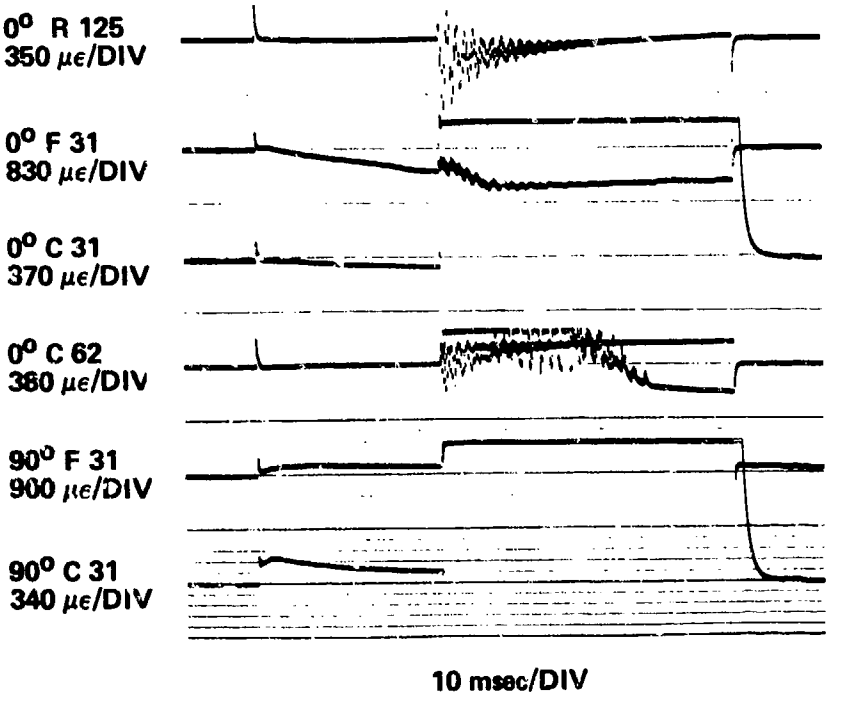

Figure D-6 Strain gauge records for pulse 3490. Gauges in Configuration I.

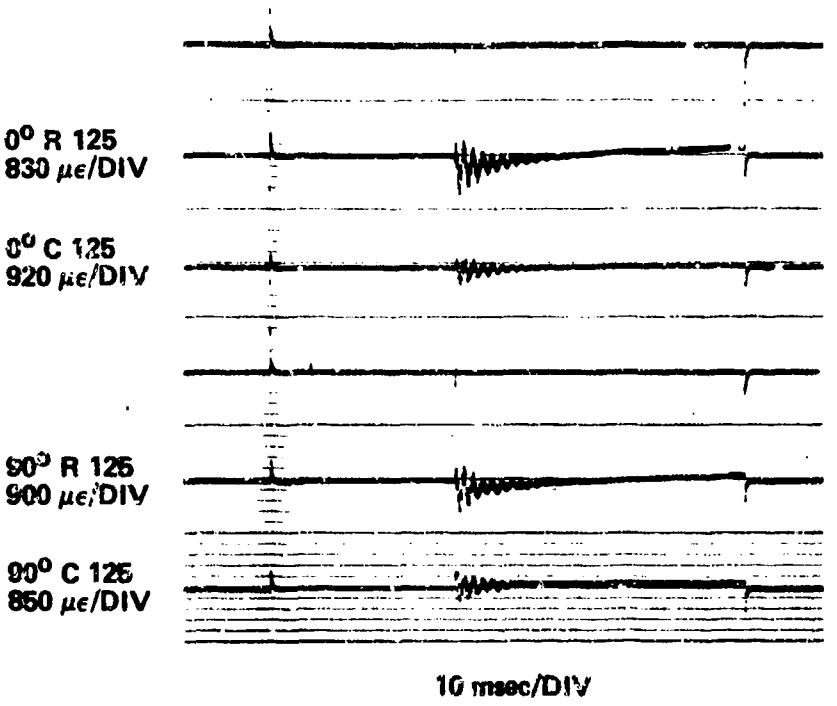

Figure D-7 Strain gauge records for pulse 3494. Gauges in Configuration II.

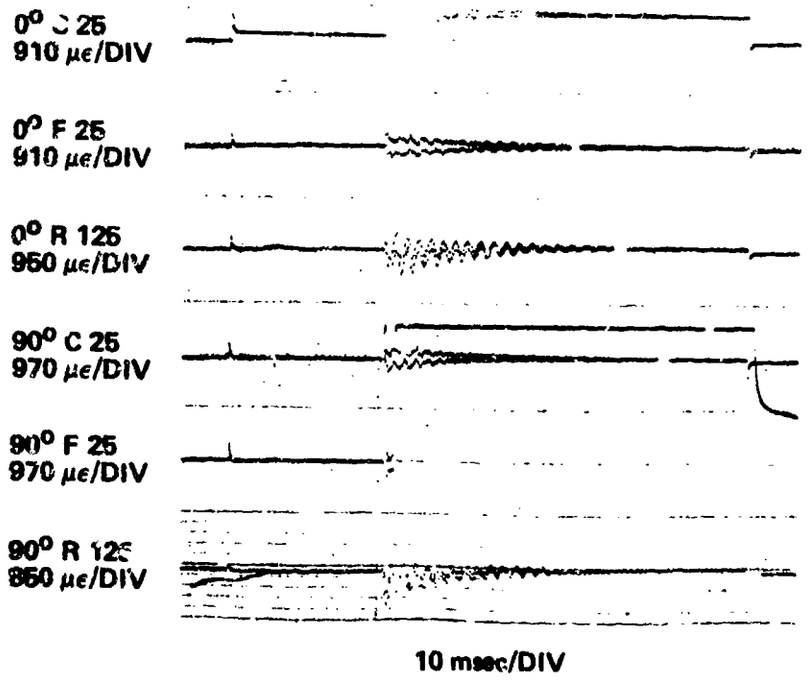

Figure D-8 Strain gauge records for pulse 3828. Gauges in Configuration III.

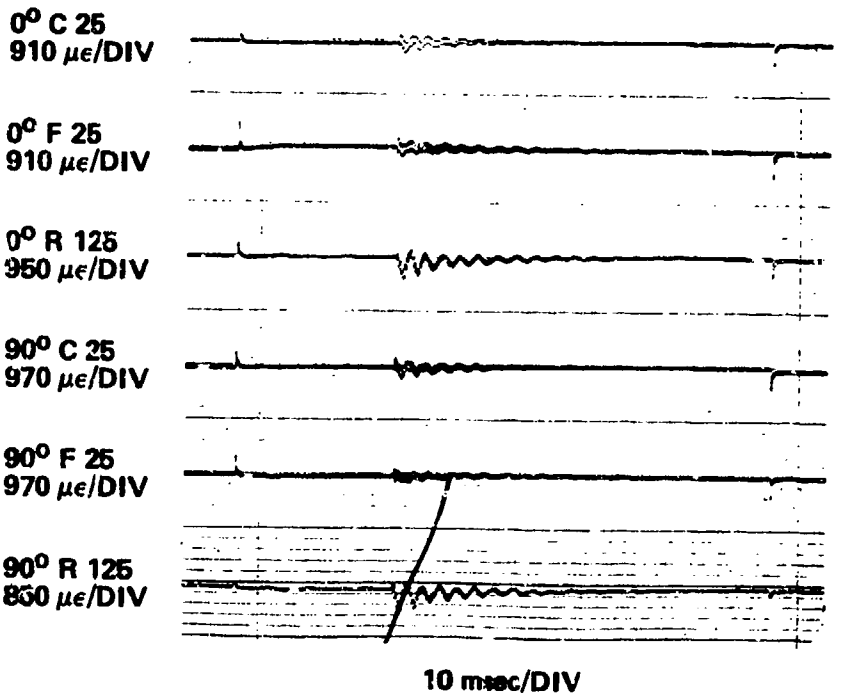

Figure D-9 Strain gauge records for pulse 3830. Gauges in Configuration III.

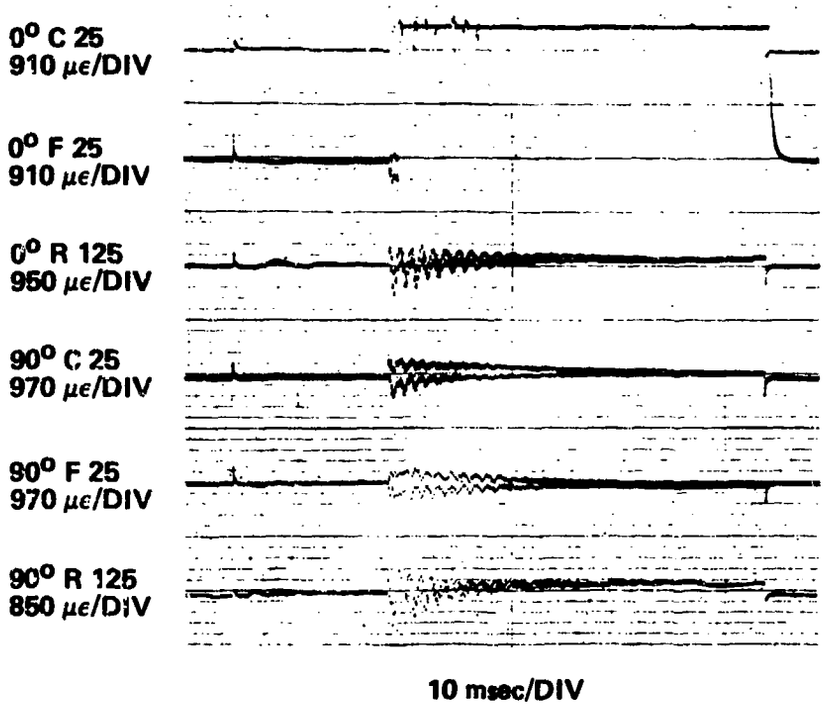

Figure D-10 Strain gauge records for pulse 3831. Gauges in Configuration III.

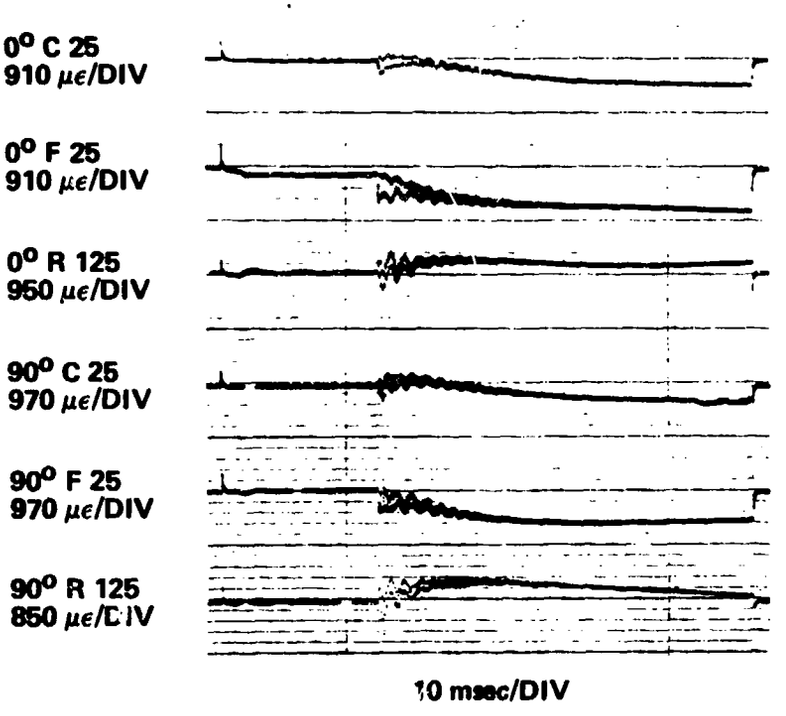

Figure D-11 Strain gauge records for pulse 3836. Gauges in Configuration III.

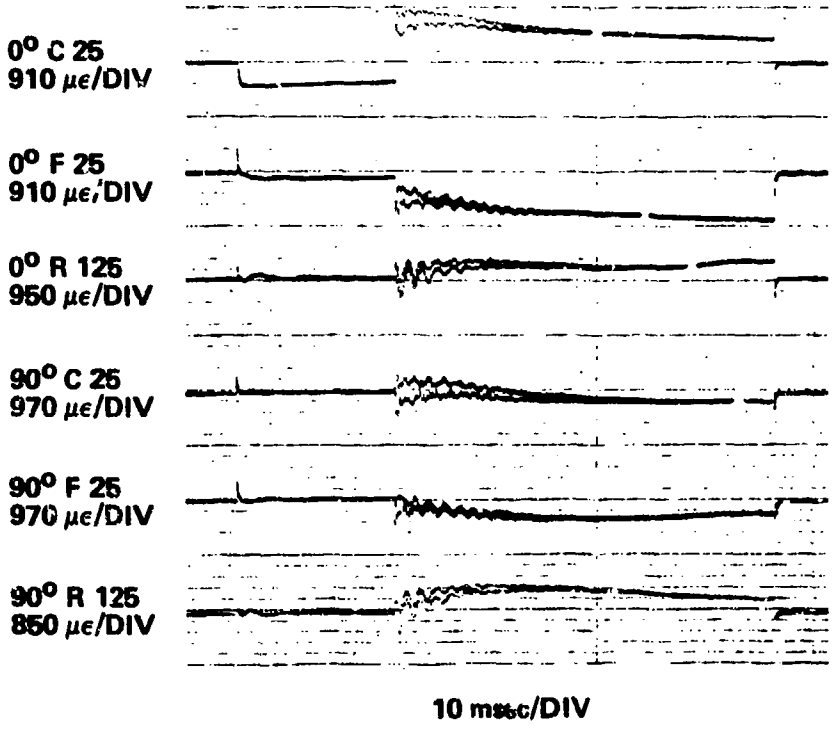

Figure D-12 Strain gauge records for pulse 3841. Gauges in Configuration III.

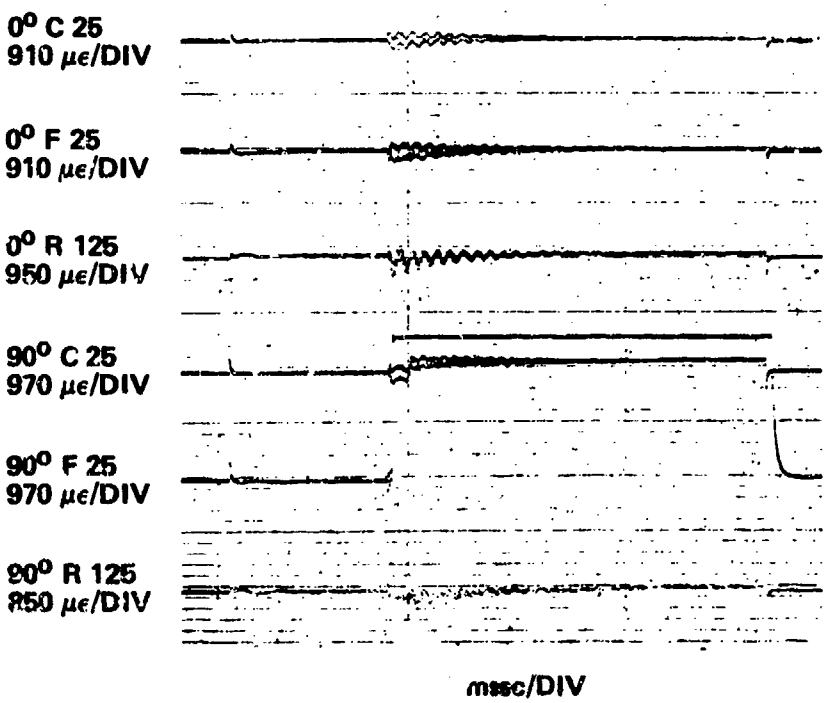

Figure D-13 Strain gauge records for pulse 3847. Gauges in Configuration III.

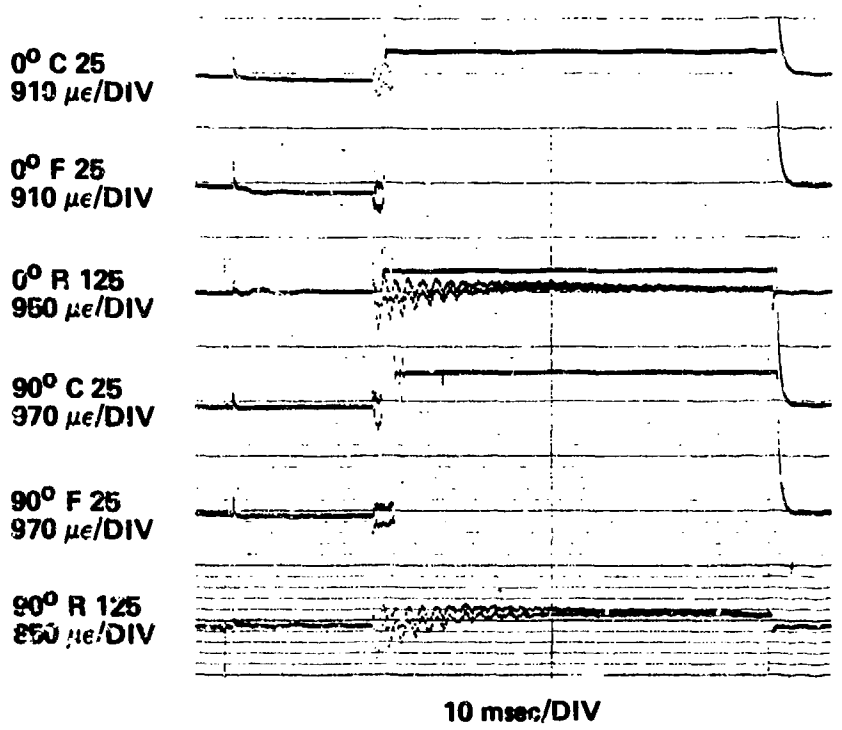

Figure D-14 Strain gauge records for pulse 3489. Gauges in Configuration III.

APPENDIX E

QUARTZ PRESSURE TRANSDUCER RECORDS

VERTICAL SCALE FACTOR: 1 VOLT = 0.86 KBAR

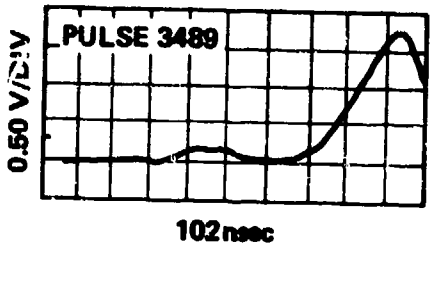
PULSE 3489
0.50 V/DIV
102 nsec

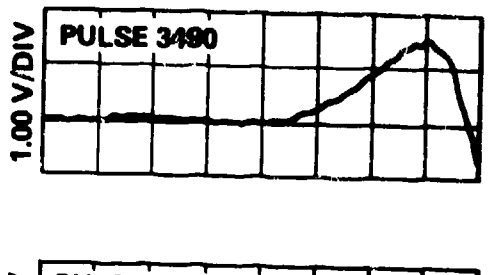
PULSE 3490
1.00 V/DIV

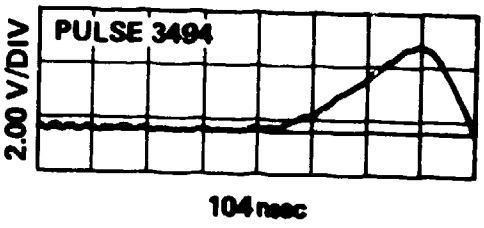
PULSE 3494
2.00 V/DIV
104 nsec

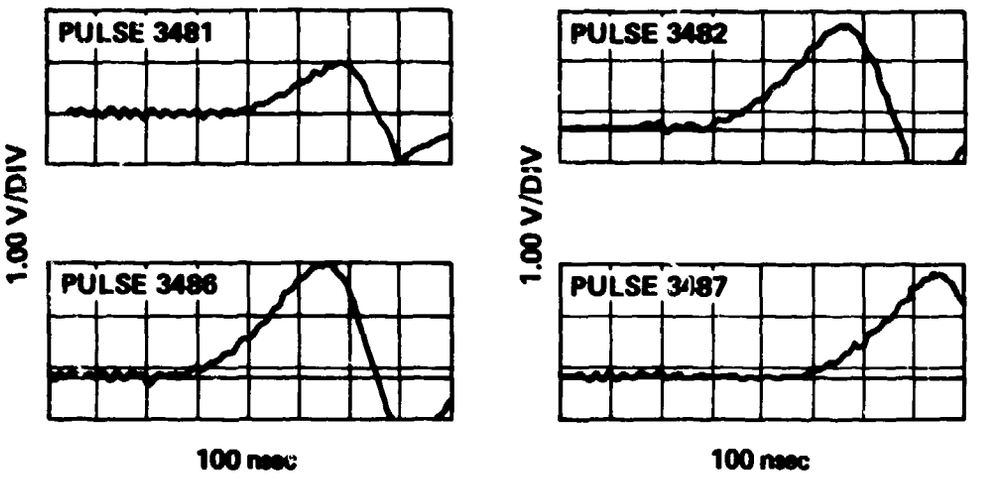
PULSE 3481
PULSE 3482
PULSE 3486
PULSE 3487
1.00 V/DIV
1.00 V/DIV
100 nsec
100 nsec

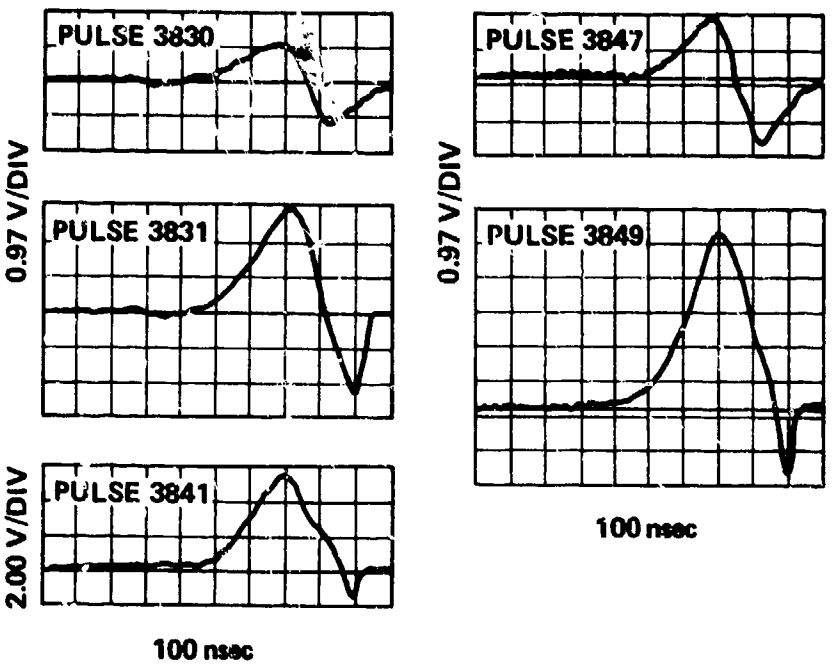
PULSE 3830
PULSE 3831
PULSE 3841
0.97 V/DIV
2.00 V/DIV
100 nsec
PULSE 3847
PULSE 3849
0.97 V/DIV
100 nsec

DISTRIBUTION LIST

DEPARTMENT OF DEFENSE

Director
Defense Advanced Rsch. Proj. Agency
ATTN: Strategic Tech. Office

Defense Documentation Center
Cameron Station
12 cy ATTN: TC

Director
Defense Intelligence Agency
ATTN: DT-2, Wpns. & Sys. Division

Director
Defense Nuclear Agency
ATTN: DDST
ATTN: SPSS
ATTN: TISI, Archives
ATTN: STSP
ATTN: SPTD
ATTN: SPAS
3 cy ATTN: TITL, Tech. Library

Commander
Field Command
Defense Nuclear Agency
ATTN: FCTMD
ATTN: FCPR

Director
Joint Strat. Tgt. Planning Staff
ATTN: JPTM
ATTN: JLTW-2

Chief
Livermore Division, Fld. Command, DNA
Lawrence Livermore Laboratory
ATTN: FCPRL

OJCS/J-5
ATTN: J-5, Plans & Policy Force Planning & Program Div
ATTN: J-5, Plans & Policy Nuc. Div.

Studies Analysis and Gaming Agency
Joint Chiefs of Staff
ATTN: SDEB

Under Secretary of Def. for Rsch. & Engrg.
ATTN: S&SS (OS)

DEPARTMENT OF THE ARMY

Director
BMD Advanced Tech. Center
ATTN: Marcus Whitfield
ATTN: ATC-T, Melvin T. Capps

Program Manager
BMD Program Office
ATTN: DACS-BMZ
ATTN: DACS-BMT, Clifford E. McLain
ATTN: DACS-BMT, John Shea
ATTN: Technology Division
ATTN: DACS-BMZ-D, Julian Davidson

DEPARTMENT OF THE ARMY (Continued)

Commander
BMD System Command
ATTN: BDMSC-TEN, Noah J. Hurst

Dep. Chief of Staff for Rsch. Dev. & Acq.
ATTN: NCB Division

Deputy Chief of Staff for Ops. & Plans
ATTN: Dir. of Nuc. Plans & Policy

Commander
Harry Diamond Laboratories
ATTN: DELHD-NP
ATTN: DRXDO-RBH, James H. Gwaltney
ATTN: DELHD-RC, Robert B. Oswald/D. Schallhorn

Commander
Picatinny Arsenal
ATTN: SARPA-ND-C-T, Donald Miller
ATTN: SARPA-FR-E, Louis Avrami

Director
U.S. Army Ballistic Research Labs.
ATTN: DRXRD-BVL, William J. Schuman, Jr.
ATTN: DRXBR-X, Julius J. Meszaros
ATTN: DRDAR-BLE, J. H. Keefer

Commander
U.S. Army Mat. & Mechanics Rsch. Ctr.
ATTN: DRXMR-HH, John F. Dignam

Commander
U.S. Army Materiel Dev. & Readiness Command
ATTN DRCDE-D, Lawrence Flynn

Commander
U.S. Army Missile Command
ATTN: DRS-RKP, W. B. Thomas

Commander
U.S. Army Nuclear Agency
ATTN: MONA-SA
ATTN: MONA-WE
ATTN: CDC-NYA

Chief
U.S. Army Research Office
ATTN: Technical Library

DEPARTMENT OF THE NAVY

Chief of Naval Material
ATTN: MAT 0323, Irving Jaffe

Chief of Naval Operations
ATTN: OP 62
ATTN: Code 604C4, R. Blaise
ATTN: OP 981

Chief of Naval Research
ATTN: Code 464, Thomas P. Quinn

DEPARTMENT OF THE NAVY (Continued)

Director
Naval Research Laboratory
ATTN: Code 5180, Mario A. Persechino
ATTN: Code 2600, Tech. Library
ATTN: Code 7770, Gerald Cooperstein

Commander
Naval Sea Systems Command
ATTN: Code 0351
ATTN: 0333A, Marlin A. Kinna

Officer-in-Charge
Naval Surface Weapons Center
ATTN: WA501, Navy Nuclear Programs Office
ATTN: Code 2302
ATTN: WR10, Joseph Petes
ATTN: WA07, Carson Lyons

Commanding Officer
Naval Weapons Evaluation Facility
ATTN: Lawrence R. Oliver

Director
Strategic Systems Project Office
ATTN: NSP-273
ATTN: NSP-272

DEPARTMENT OF THE AIR FORCE

AF Materials Laboratory, AFSC
ATTN: MBE, George F. Schmitt
ATTN: MBC, Donald L. Schmidt
ATTN: T. Nicholas

AF Rocket Propulsion Laboratory, AFSC
ATTN: RTSN, G. A. Beale

AF Weapons Laboratory, AFSC
ATTN: DYS
ATTN: NT
ATTN: DYT
ATTN: DYV
ATTN: SUL

Headquarters
Air Force Systems Command
ATTN: SOSF
ATTN: XRTO

Commander
ASD
ATTN: ENFTV

Commander
Foreign Technology Division, AFSC
ATTN: TDFBD, J. D. Pumphrey
ATTN: TDPTN
ATTN: PDBG

Hq USAF/RD
ATTN: RDQSM
ATTN: RD

SAMSO/DY
ATTN: DYS

SAMSO/MN
ATTN: MNNR
ATTN: MNNH

DEPARTMENT OF THE AIR FORCE (Continued)

SAMSO/RS
ATTN: RSS
ATTN: RSMA
ATTN: RSSE

Commander in Chief
Strategic Air Command
ATTN: NRI
ATTN: XOBM
ATTN: XPQM
ATTN: DOXT
ATTN: XPFS

DEPARTMENT OF ENERGY

Division of Military Application
ATTN: Doc. Con. for Res. & Dev. Branch

University of California
Lawrence Livermore Laboratory
ATTN: D. Hanner
ATTN: Joseph E. Keller, Jr., L-125
ATTN: C. Joseph Taylor, L-92
ATTN: Larry W. Woodruff, L-96

Los Alamos Scientific Laboratory
ATTN: Doc. Con. for John McQueen/J. W. Taylor
ATTN: Doc. Con. for Robert Skaggs
ATTN: Doc. Con. for D. Shover
ATTN: Doc. Con. Off. for R. Dingus

Sandia Laboratories
Livermore Laboratory
ATTN: Doc. Con. for T. Gold
ATTN: Doc. Con. for 8131, H. F. Norris, Jr.

Sandia Laboratories
ATTN: Doc. Con. for Clarence R. Mehl, Org. 5230
ATTN: Doc. Con. for Carter Broyles
ATTN: Doc. Con. for M. Cowan, Org. 5230
ATTN: Doc. Con. for R. R. Boade

DEPARTMENT OF DEFENSE CONTRACTORS

Acurex Corporation
ATTN: J. Huntington

Aerospace Corporation
ATTN: W. Mann
ATTN: Robert L. Strickler
ATTN: R. Mortensen
ATTN: W. Barry
ATTN: Richard Crolius, A2-Rm. 1027

Avco Research & Systems Group
ATTN: William Broding
ATTN: Pat Grady
ATTN: John E. Stevens, J100
ATTN: Document Control
ATTN: George Weber, J230
ATTN: John Gilmore, J400

Battelle Memorial Institute
ATTN: Merwyn R. Vanderlinn

The Boeing Company
ATTN: Brian Lempriere

DEPARTMENT OF DEFENSE CONTRACTORS (Continued)

California Research & Technology, Inc.
ATTN: Ken Kreyenhagen

Effects Technology, Inc.
ATTN: Richard Parise/M. Rosen
ATTN: Robert Wengler/R. A. Bick

Ford Aerospace & Communications Operations
ATTN: P. Spangler

General Electric Company
Space Division
ATTN: Phillip Cline
ATTN: Daniel Edelman
ATTN: G. Harrison

General Electric Company
TEMPO-Center for Advanced Studies
ATTN: DASIAC

General Research Corporation
ATTN: Robert E. Rosenthal

Institute for Defense Analyses
ATTN: IDA Librarian, Ruth S. Smith
ATTN: Joel Bengston

Ion Physics Corporation
ATTN: Robert D. Evans

Kaman AviDyne
Division of Kaman Sciences Corp.
ATTN: Ray Rentinick

Kaman Sciences Corporation
ATTN: Ronald C. Sachs/R. O'Keefe
ATTN: Frank H. Shelton
ATTN: Thomas Meagher

Lockheed Missiles & Space Co., Inc.
ATTN: Oliver Burford, Dept. 81-14
ATTN: Richard Walls, Dept. 81-14

Lockheed Missiles and Space Co., Inc.
ATTN: T. R. Fortune

Lockheed Missiles and Space Co., Inc.
ATTN: F. G. Borgardt

Martin Marietta Aerospace
ATTN: Laird Kinnaird

McDonnell Douglas Corporation
ATTN: H. M. Berkowitz
ATTN: L. Cohen
ATTN: J. Peck
ATTN: M. Schneider

DEPARTMENT OF DEFENSE CONTRACTORS (Continued)

Pacific-Sierra Research Corp.
ATTN: Gary Lang

Physics International Company
2 cy ATTN: Doc. Con. for James Shea/V. Buck

Prototype Development Associates, Inc.
ATTN: T. K. McKinley
ATTN: John McDonald
ATTN: Neal Harington

R & D Associates
ATTN: William R. Graham, Jr.
ATTN: Paul Rausch
ATTN: F. A. Field

The Rand Corporation
ATTN: R. Robert Rapp

Science Applications, Inc.
ATTN: W. Yengst
ATTN: Olan Nance

Science Applications, Inc.
ATTN: William R. Seebaugh
ATTN: William M. Layson

Southern Research Institute
ATTN: C. D. Fears

SRI International
ATTN: B. E. Lindberg
ATTN: George R. Abrahamson
ATTN: Donald Curran

SRI International
ATTN: Harold Carey

Systems, Science and Software, Inc.
ATTN: Russell E. Duff
ATTN: G. A. Gurtman

Terra Tek, Inc.
ATTN: Sidney Green

TRW Defense & Space Sys. Group
ATTN: J. Farrel
ATTN: W. W. Wood
2 cy ATTN: Peter K. Dai/D. Jortner

TRW Defense & Space Sys. Group
ATTN: L. Berger
ATTN: V. Blankenship
ATTN: William Polich